DUAL POLARIZED MICROSTRIP ANTENNA ARRAY FOR THE OFF-THE-GRID RADAR

By

Víctor J. Marrero-Fontánez

A thesis submitted in partial fulfillment of the requirements for the degree of

MASTER OF SCIENCE

in

ELECTRICAL ENGINEERING

UNIVERSITY OF PUERTO RICO
MAYAGÜEZ CAMPUS
2007

Approved by:

_____	_____
José Colom Ustariz, PhD Member, Graduate Committee	Date
_____	_____
Lionel Orama Exclusa, PhD Member, Graduate Committee	Date
_____	_____
Rafael Rodríguez Solís, PhD President, Graduate Committee	Date
_____	_____
Esov S. Velázquez Suárez, PhD Representative of Graduate Studies	Date
_____	_____
Isidoro Couvertier Reyes, PhD Chairperson of the Department	Date

ABSTRACT

The design and development of a linear antenna array operating at center frequency of 9.5 GHz is presented in this thesis. A 12 patch center-fed array composed of sub-arrays of series fed antenna array conformed by 6 elements is designed in a multi-layered structure. The patch antennas are located on a foam material with copper cladding (FoamClad by Arlon) and the feed network of the antenna in a different material (Rogers RO 3006). FoamClad material has a permittivity of 1.2 and a thickness of 1.75mm and the RO 3006 material has a permittivity of 6.15 and a thickness of 0.625mm. Two different arrays where considered and studied. One of the arrays has loading chip resistors at the end of the sub-arrays to dissipate the remaining power. The second one, the last element was replaced with a load-radiating element to radiate the remaining power. The results for both configurations are presented and discussed in this thesis.

RESUMEN

En esta tesis se presenta el diseño de un arreglo lineal con frecuencia de operación de 9.5 GHz. Este arreglo, que es alimentado desde el centro, esta compuesto de 12 elementos divididos en sub-arreglos de 6 elementos conectados en serie. Los elementos están diseñados en una estructura multicapa. El parche de la antena esta localizado en un material de espuma (foam) cubierto de cobre por uno de sus lados (FoamClad de Arlon) y la red de alimentación de las antenas en una capa aparte otro material (Rogers RO 3006). El material de FoamClad tiene una permitividad de 1.2 y un espesor de 1.75 mm, y el RO 3006 tiene una permitividad de 6.15 y un espesor de 0.625 mm. Dos tipos de arreglos fueron considerados y estudiados. En uno de los arreglos se usaron cargas resistivas para disipar la potencia sobrante, en el segundo arreglo se substituyo el ultimo elemento con que irradia la potencia restante. Los resultados para ambas configuraciones son presentados y discutidos en esta tesis.

To God, to my mother María Fontánez, my father Víctor M. Marrero, my sister Viviana M. Marrero and my girlfriend Yoreim Virella, for encouraging and believing in me, for all your support and advice over the past years and for always having a listening ear, I love you.

ACKNOWLEDGEMENTS

During the course of my graduate studies at the University of Puerto Rico several persons collaborated directly and indirectly with my research. Without their support it would have been impossible for me to complete my work. That is why I wish to dedicate this section to recognize their support.

I would like to thank the professors of my graduate committee: Dr. Rafael Rodríguez Solís, Dr. José Colom Ustáriz and Dr. Lionel Orama for their contributions to this project. Most importantly I would like to express my endless appreciation to two persons that I would like to refer to them as my mentors, Dr. Rafael Rodriguez Solis and Dr. José Colom Ustáriz for their guidance, motivation and support during the last three years. Dr. Rodriguez Solis, for showing me everything I know about microwave antenna engineering and allowing me to run freely the design and implementation of this project and still watching over me so that I could keep myself focused on the task at hand. Dr. Colom for being there every time that I needed help no questions asked, for that and more a lot more I thank you. But most important thing that I am grateful for is that theses persons, my mentors, they always had a smile on their faces that made the student/professor relation a very comfortable one. It felt like they were colleagues, not superiors. I would like to thank them and Dra. Sandra Cruz-Pol for bringing me into the Radiation Lab. and CASA groups, where I have been able to work in a very interesting research field and made good friends in the process.

I will also like to show my sincere appreciation to Alfredo Moreu from the Physics department, for all the help and time that he gave to the final stage of this project. I learn so much in so little time that I can't find the words to say how grateful I am for you unconditional help.

I feel very lucky to have worked with the current and previous members of the Radiation Laboratory and CASA group. From CASA y would like to express my sincere gratitude to Mauricio Sanchez, for being source of knowledge when I need one and a good friend the rest of the time; Jose Maeso and Jose Morales, for all your help and the good laughs. Juan Torres, you always lent a hand when I needed. Carlos Rodríguez, Jaime Di Cristina, Ricardo Rios, Jose Padovani, Manuel Cruz, Soralis Pimentel, Carlos and Luis Giraldo and Diego Arias, each of whom gave me a lot of help in many aspects and made my time at UPRM enjoyable. Special thanks to Jorge Trabal, Rafael Medina and Jorge Salazar, Eric Knapp and Brian Donovan for their help from UMass.

Very special thanks to my “house-mates” Ronald Ayuso, José E. Del Rosario and Ramon Díaz for their friendship and support. You really made life easier and joyful in the most stressful moments. To Pablo Lozada, because you just don’t know how to say no when I asked for help, for that I thank you my friend. My two very dear friends, Antonio Amador and his wife Silvia Herrera, you were key factors for the completion of this project, because aside from the help and knowledge you provided to me, you were family away from home, I treasure your friendship in my heart. A big thank you to Manuel Vega, your help was invaluable to me, I owe you a lot my friend, and I wish that I had met you earlier. A very special appreciation goes to Madeline Rodríguez for support and encouragement, for listening when I needed to talk to someone, and most of all for being one of the most amazing and wonderful persons that I have ever meet, you are like a big sister to me. It may sound impressive but you can fix anything with a smile.

I would also like to express my gratitude to my close family for encouragement and support given throughout my life. Heartfelt thanks and appreciation goes to my parents and my sister, for their love and continuous support throughout the years.

Last but not least I would like to express my appreciation to my sweetheart, my fiancée, Yoreim Virella, for her love, patience, support and understanding throughout

these difficult and challenging years. Every time that I felt I was falling apart you always knew how to keep me together. I love you with all my heart and I always will.

Table of Contents

Table List

Tables **Page**

Figure List

Figures **Page**

1 INTRODUCTION

1.1 Motivation

The National Science Foundation Engineering Research Center for Collaborative Adaptive Sensing of the Atmosphere (CASA) goal is to explore and develop methods for improving observation, detection and prediction of atmospheric phenomena. The center is focused on developing Distributed Collaborative Adaptive Sensing (DCAS) as a systems technology to improve our ability to monitor the earth's lower troposphere. Improving today's weather monitoring and forecasting requires an increase in both the resolution and volume coverage of observations in the lowest kilometers of the atmosphere. The DCAS system will be created with a network of X-band polarimetric radars with those previous conditions in mind. The center is comprised of four partners: University of Massachusetts, Colorado State University, University of Oklahoma and University of Puerto Rico, Mayagüez.

Current approaches to sampling the first three kilometers of atmosphere are physically limited in their ability to provide the required resolution and coverage. These radars are used to cover distances up to 240km, as in the case of the WSR-88D (referred to as NEXRAD), introducing limitations due to the earth's curvature. As the range increases away from the radar, the earth's surface curves away under the radar beam creating an inability to observe the atmosphere close to the earth's surface. Atmospheric phenomena can go unobserved, literally lying "under the radar". In addition, as the radar range increases there is a corresponding degradation of the radar resolution. The radar beam spreads proportionally to the sine of the antenna's beamwidth, causing long-range cross-resolution to degrade. Finally, radar suffers from terrain blockage. Obstacles such as mountain ranges also block the radar beam preventing observation of events beyond the obstacle. A network of X-band radars located at closer range (~25 Km) will overcome the issues mentioned above.

Satellites in orbit above a storm are unable to observe precipitation below the cloud tops, ground sites are located in densities unable to measure the variability of the storm, while radar is unable to observe phenomena lying under the beam at long ranges. This provides an incomplete picture of the state of the atmosphere, hampering forecasting and warning of severe weather. To achieve a DCAS system, a series of technology and full-system testbeds are created and distributed throughout different collaborators. An innovative approach of the center is to integrate students from the four different campuses in a unique research experience under a Student Led Test-bed (SLT).

The SLT main goals are to establish a Quantitative Precipitation Estimation (QPE) sensing network starting at the western end of the island taking into consideration coverage gaps from NEXRAD in this part of Puerto Rico. NEXRAD is located in the northeast section of the island. QPE provides an estimation of rainfall and is a key tool in the construction of flash flooding forecasts. It is expected in the future, that with more coverage, and better resolution a significant improvement in precipitation estimates for western Puerto Rico will be achieved.

Due to the mountainous terrain and topography of the Island, an"off-the-grid" radar with portability characteristics has been proposed for the SLT. Because there is limited reliance on existing infrastructure and constrained power capabilities to be using high power radars, students from the SLT came with the concept of "Off-The-Grid" (OTG) radar. The idea is to relax some systems design parameters and develop a self powered portable X-band radar. Batteries and a photovoltaic panel will power the radar. Its name "Off-the-grid" refers to off the grid from the main electrical grid system. The basic idea is to build a solid-state radar with 15 Km range that will be operational under severe weather conditions.

In present-day radar systems, the need for antennas of small size and high efficiency has generated much attention in the study of compact microstrip antennas.

These antennas exhibit low profile and lightweight properties as well as low cross polarization radiation in some designs.

The interest here is to design and develop a light and compact antenna. This antenna will be a multi-layer flat panel printed circuit. It should have the same phase center for both polarizations and the scanning will be made mechanically in both azimuth and elevation.

1.2 Objectives

The main objective of this research is to design a dual polarization antenna operating at 9.5 GHz for the Off-the-Grid radar that meets the specifications needed for QPE. Each patch are coupled-fed to minimize cross-polarization. Finally, the simulated results need to be validated by the construction and measuring of antenna prototypes using the UPRM Radiation Laboratory facilities.

1.3 Project Description

Aperture Couple Antennas have the advantage of separating the radiating element (patch antenna) from the feed network. This allows using high dielectric constant substrate for the feed and a thick, low dielectric constant substrate for the antenna. Because the ground plane separates the antenna from the feed, the spurious radiation from the feed interfering with the antenna pattern or polarization purity is eliminated, making them attractive for dual polarization antennas with high cross-polarization levels (greater than 20 dB). An important aspect of the aperture-coupled patch is the fact that the aperture is usually smaller than resonant size, so the backlobe radiated by the slot is typically 15-20 dB below the forward main beam [1].

A series-fed aperture-coupled antenna array will be design using a substrate with a permittivity of 1.2 and a thickness of 1.75mm for the patch antenna. A substrate with a

permittivity of 6.15 and a thickness of 0.625mm will be used for the feed lines. The array will be design to achieve a sidelobe level lower of 20 dB and a cross-polarization lower than 25 dB

1.4 Work Organization

The theory of Microstrip Antennas, Aperture-Coupling Slots, Aperture Coupled Antennas, and linear arrays, as well as a review on previous publications on different aspects of aperture-coupled antennas and their applications in arrays is described in Chapter 2. Chapter 3 explains the methodology used to design the aperture coupled antenna array. The results are presented in Chapter 4 along with an explanation of those results. Finally, the conclusions and recommendations for future work are presented in Chapter 5.

2 LITERATURE REVIEW

2.1 Micriostrip Antennas

Microstrip antennas are one of the most innovative developments in antenna theory and design in recent years, and are increasingly finding application in a wide range of modern microwave systems [1].

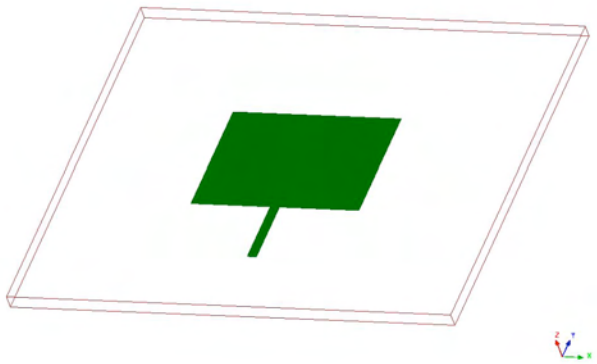

Figure 2.1 A rectangular microstrip antenna with microstrip line feed.

The idea of the microstrip antenna dates back to the 1950's, but it was not until the 1970's that serious attention was given to this particular element. As shown in Figure 2.l, the basic configuration of a microstrip antenna is a metallic patch printed on a thin, grounded, dielectric substrate. The microstrip antenna radiates a relatively broad beam broadside to the plane of the substrate. A few of the features that make this type antenna attractive are that it can be made conformable, and potentially at low cost, easy fabrication into linear or planar arrays, and easy integration with microwave integrated circuits. Since the original configuration was proposed, dozens of variations in patch shape, feeding techniques, substrate configurations, and array geometries have been developed by researchers throughout the world. The variety of designs that are possible with microstrip antennas probably exceeds that of any other type of antenna element [1].

Basic properties, analytical models, and design techniques for microstrip antennas, can be found in [1], [2] and [3].

To a large extent, the development of microstrip antennas has been driven by systems requirements for antennas with low-profile, low-weight, low-cost, easy integration into arrays or with microwave integrated circuits, or polarization diversity.

Some disadvantages of the original microstrip antenna configurations include narrow bandwidth, spurious feed radiation, poor polarization purity, and limited power handling. Much of the research work in microstrip antennas has thus gone into trying to overcome these problems, in order to satisfy increasingly rigorous systems requirements. This effort has produced the development of novel microstrip antenna configurations, and the development of accurate and versatile analytical models for the understanding of the inherent limitations of microstrip antennas, as well as for their design and optimization [1].

2.2 Definition of Aperture-Coupled Antennas

An aperture coupled microstrip antenna is a non-contacting feed type antennas. As shown in Fig. 2.2, this configuration uses two parallel substrates that share a common ground between them. A microstrip feed line on the bottom substrate is coupled through a small aperture, typically a narrow rectangular slot in the ground plane to a microstrip patch on the top substrate. By using this configuration, the designer has the advantage of using high dielectric constant substrate for the feed and a thick, low dielectric constant substrate for the antenna. Because the ground plane separates the antenna from the feed, the spurious radiation from the feed interfering with the antenna pattern or polarization purity is eliminated. An important aspect of the aperture coupled patch is the fact that the aperture is usually smaller than resonant size, so the backlobe radiated by the slot is typically 15-20 dB below the forward main beam [1].

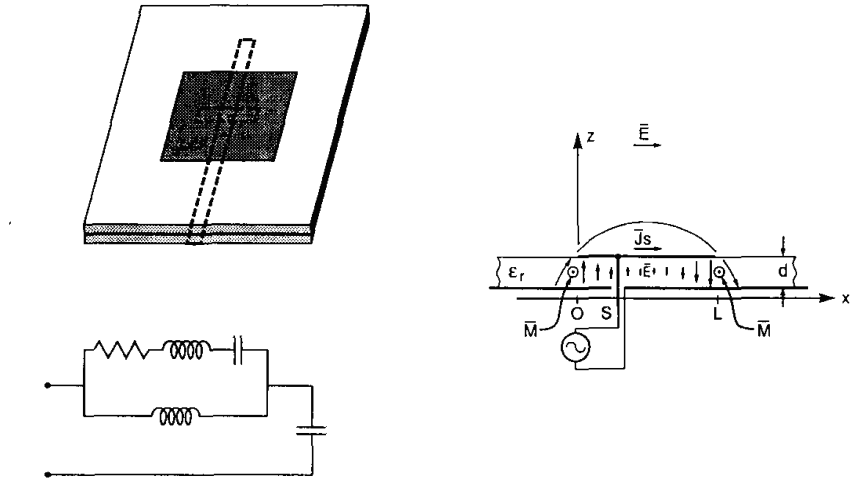

Figure 2.2 Patch aperture coupled to a microstrip feed line and its equivalent circuit from [1].

This geometry has at least five degrees of freedom: the slot size, the slot position, the feed substrate parameters, antenna substrate parameters and the feed line width. Impedance matching is performed by adjusting the size (length) of the coupling slot, together with the width of the feed line, which is usually terminated in an open-circuited tuning stub. Coupling occurs due to magnetic polarization in the slot, making the equivalent magnetic current M_y in the aperture to the dominant H_y, field of the patch [1]:

$$\text{Coupling} \sim \int_v M_y H_y dv \sim \sin\frac{\pi s}{L} \qquad (1)$$

where L is the length of the patch and s is the feeding point along the E plane in the patch. Equation (1) shows that maximum coupling occurs when the aperture is centered below the patch ***(s = L/2),*** where the magnetic field is maximum.

The equivalent circuit of an aperture coupled microstrip antenna is shown in Fig. 2.2. The patch resonator now appears as a series *RLC* network (since a series-type feed at the center of the patch is λ/4 away from a shunt-feed at the edge of the patch, resulting in

an admittance inverter effect), with a shunt inductance representing the coupling slot [1]. This network allows the possibility of double tuning for increased bandwidth. Aperture coupled antennas are analyzed in detailed in [4] to determine the input impedance based on the antenna configuration proposed by Pozar [5].

2.3 Design parameters of Aperture-Coupled Antennas

Figure 2.3 shows the geometry of the basic aperture coupled patch antenna. The radiating microstrip patch element is etched on the top of the antenna substrate, and the microstrip feed line is etched on the bottom of the feed substrate. The thickness and dielectric constants of these two substrates may thus be chosen independently to optimize the distinct electrical functions of radiation and circuitry. Most aperture coupled microstrip antennas now use rectangular slots, or variations, such as “dogbones” or H-shaped apertures proposed in [6], bow–ties, etc.

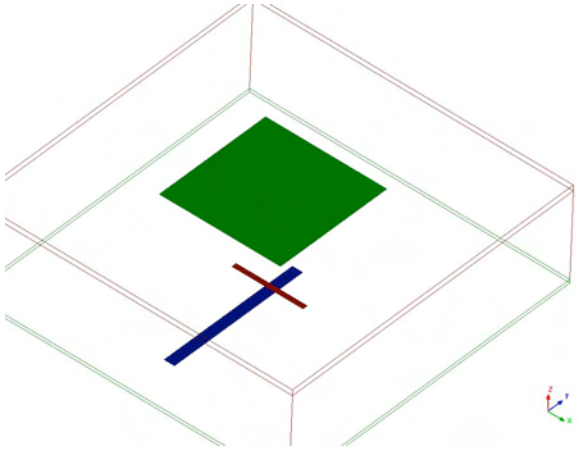

Figure 2.3 Geometry of the basic aperture coupled microstrip antenna.

The aperture coupled microstrip antenna involves over a dozen material and dimensional parameters, and Pozar summarized in [7] the basic trends with variation of these parameters. These parameters are presented below:

- *antenna substrate dielectric constant:*

  Affects the bandwidth and radiation efficiency of the antenna. Lower permittivity gives wider impedance bandwidth and reduced surface wave excitation.
- *antenna substrate thickness:*

  Affects bandwidth and coupling level. A thicker substrate results in wider bandwidth, but less coupling for a given aperture size.
- *microstrip patch length:*

  Determines the resonant frequency of the antenna.
- *microstrip patch width:*

  Affects the resonant resistance of the antenna, with a wider patch giving a lower resistance. Square patches may result in the generation of high cross polarization levels, and thus should be avoided unless dual
  or circular polarization is required.
- *feed substrate dielectric constant:*

  This should be selected for good microstrip circuit qualities, typically in the range of 2 to 10.
- *feed substrate thickness:*

  Thinner microstrip substrates result in less spurious radiation from feed lines, but higher loss. Thickness of 0.01λ to 0.02λ is usually good.
- *slot length:*

  The coupling level is primarily determined by the length of the coupling slot, as well as the back radiation level. The slot should therefore be made no larger than it is required for impedance matching.
- *slot width:*

  Affects the coupling level, but to a much less degree than the slot width. The ratio of slot length to width is typically 1/10 λ_o (up to 1/100 λ_o).
- *feed line width:*

  Besides controlling the characteristic impedance of the feed line, the width of the feed line affects the coupling to the slot. To a certain degree, thinner feed lines couple more strongly to the slot.

- *feed line position relative to slot:*

  For maximum coupling, the feed line should be positioned at right angles to the center of the slot. Skewing the feed line from the slot will reduce the coupling, as will positioning the feed line towards the edge of the slot.
- *position of the patch relative to the slot:*

  For maximum coupling, the patch should be centered over the slot. Moving the patch relative to the slot in the H-plane direction has little effect, while moving the patch relative to the slot in the E-plane (resonant) direction will decrease the coupling level.
- *length of tuning stub:*

  The tuning stub is used to tune the excess reactance of the slot coupled antenna. The stub is typically slightly less than $\lambda_g/4$ in length; shortening the stub will move the impedance locus in the capacitive direction on the Smith chart.

2.3.1 Aperture-Coupled Slot

For the rectangular slot, the transverse electric field must vanish at the slot ends, and because the slot length is less than $\lambda_g/2$ the field must have a variation similar to a half sinusoid as shown in figure 2.3 (a). Lets say that an H aperture is composed of one horizontal slot loaded at its ends with a vertical slot at each end. If the length of the horizontal slot is S, then a common design is to make the loading slots of length S/2. For the H aperture, the transverse electric field must still vanish at the far ends of the slot, but the *S/2* length of the loading slots causes an increase in the effective moment of these areas of the aperture. As shown in figure 2.3 (b), this has the effect of increasing the field level at the ends of the central portion of the H aperture, making the field variation more uniform than that of the rectangular slot [6].

In aperture coupling to a microstrip antenna, how the magnetic field polarize is the dominant mechanism for an aperture near the centre of the patch. Because the

polarisabilities depend on the shape and size of the aperture, it is desirable to use a shape that provides the greatest polarization for a given size. This allows the antenna to be impedance matched with the smallest possible aperture, resulting in the following advantages [6]:

(1) Smaller aperture area results in a lower back radiation level, leading to improved efficiency and less spurious radiation in the back region.

(2) Smaller aperture size eases positioning constraints in dual or circularly polarized antenna designs that use two orthogonal coupling apertures.

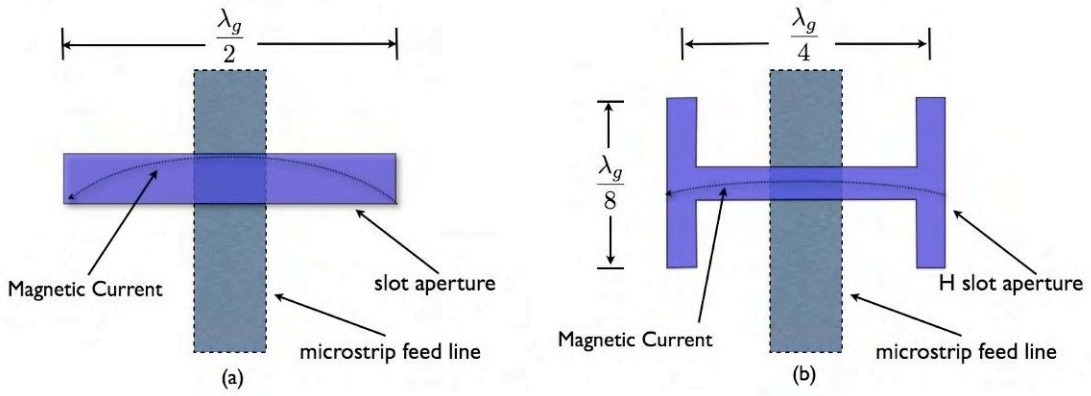

Figure 2.4 (a) Basic configuration of a rectangular coupling slot, and (b) common configuration of an H-shaped coupling slot.

An H-shaped slot can give an increase of more than three in the input impedance of an aperture coupled microstrip antenna, as compared with a rectangular slot of the same length. This allows the use of smaller coupling apertures for this antenna, which will reduce the back radiation as well as ease positioning constraints for antennas with multiple aperture feeds. Probably the only disadvantage with this technique is that the H-shape complicates the theoretical analysis of the antenna [6].

2.4 Arrays

2.4.1 Microstrip Arrays

One of the best features of microstrip antennas is the ease with which they can be formed into arrays, and a wide variety of series-fed, corporate-fed, scanning, and polarization-agile arrays have been designed using microstrip elements [2], [8].

Microstrip arrays are limited in that they tend to radiate efficiently only over a narrow band of frequencies and their feed lines cannot operate at the high power levels of waveguide, coaxial line, or even stripline. Microstrip transmission line circuits provide phase control and power distribution to the array elements. When these circuits are on the same surface as the array face, the array is termed a monolithic array. These functions can also be performed either in the plane of the ground screen or in successive layers behind that plane, making a multilayered array.

A corporate feed can be very useful to efficiently distribute the current throughout the antenna. Another important issue is the consideration of losses in the corporate feed. The general conclusions in [9] concerning the losses in a corporate feed are as follow:

- The desire to minimize radiation and surface wave losses suggests that high characteristic impedances should be chosen, because these losses are proportional to 1/Zo.
- For a microstrip line given length and characteristic impedance, the radiation loss increases with $(h\sqrt{\varepsilon_r}/\lambda_o)^2$ and the surface wave loss increases with $(h\sqrt{\varepsilon_r}/\lambda_o)^3$. Thus the desire to decrease radiation losses dictates low values of $(h\sqrt{\varepsilon_r}/\lambda_o)$.
- For a microstrip line with given thickness and characteristic impedance, the radiation loss depends on the line length as follows: in the range of $0 < L < \lambda_o$ the loss grows with $(L/\lambda_o)^2$. For $L \geq 3\lambda_o$ they are not sensitive to

the length. The behavior of the surface wave loss as a function of the line's length is oscillatory.

- The radiation losses are higher in end-fed microstrip lines than in center-fed lines. The surface wave losses are almost the same for end-fed and center-fed lines.

From the above discussion, it can be said that typical losses in microstrip lines are inversely proportional to the impedance, proportional to the square of the thickness and not sensitive to the length.

It soon became apparent, however, that the one sided board, although a direct outgrowth of the early microstrip antenna technology which promised simple microstrip fabrication, introduced problems. For example, feed networks in microstrip are too lossy for many high gain or large phased array requirements. Waveguide (and sometimes coaxial cable feeds) are necessary and, because of space restrictions, the feed network must be placed either on the backside of the element board or on an entirely separate board [2], [10].

The experience of a number of workers who have been designing and testing microstrip arrays in recent years has led to the conclusion that feedline radiation from series or corporate feeds is an unavoidable problem that sets a lower limit on cross-polarization and side lobe levels. Depending on the substrate thickness and the topology of the feed network, these levels may range from -15 to -25 dB. Achievement of better cross-polarization or side lobe levels requires that the feed network be isolated by a ground plane from the radiating face of the array, and coupled to the radiating elements with either feed-through probes or by aperture coupling. This and other factors were considered in a study of low side lobe microstrip arrays [10], where an array with a -35 dB (-19 dBi) side lobe level was demonstrated.

2.4.2 Linear Array Theory

In many applications, it is desired to design antennas with very high gains, and narrow beam-widths, (like in high resolution radar systems). By increasing the gain of the antenna the directivity increases, therefore the beam-width becomes narrower. The mathematical expressions that relate these antenna properties are well explained in [11].

To achieve high gains from a radiating element, the electric size must be increased. This can be accomplished by either enlarging the radiating element or by forming an ensemble of antennas in space. The mechanical problem that brings the option of enlarging a single element, like manufacture cost, installation cost, operation and maintenance, are traded for electrical problems of feeding several small antennas in the ensemble option. The ensemble approach, that from this point on we will refer to it as an antenna array, gives more degrees of freedom for enlarging the electrical size of the array, thus more control of the beam the single large element approach. In most of the cases the antenna elements are identical and for the rest of the discussion we will assume they are.

The total radiated field intensities of an array are determined by the vector addition of the radiated field intensities of the individual elements. In an array of identical elements, there are at least five controls that can be used to shape the overall pattern of the array. These are:

- Geometrical configuration of the overall array
- Spacing between elements
- Excitation amplitude of the individual elements
- Excitation phase of the individual elements
- Relative pattern of the individual elements

Arrays offer the unique capability of electronic scanning of the main beam. This is accomplished by changing the relative excitation phase between elements. Also the

pattern can be shaped by changing the relative excitation amplitude between the elements [12], [13].

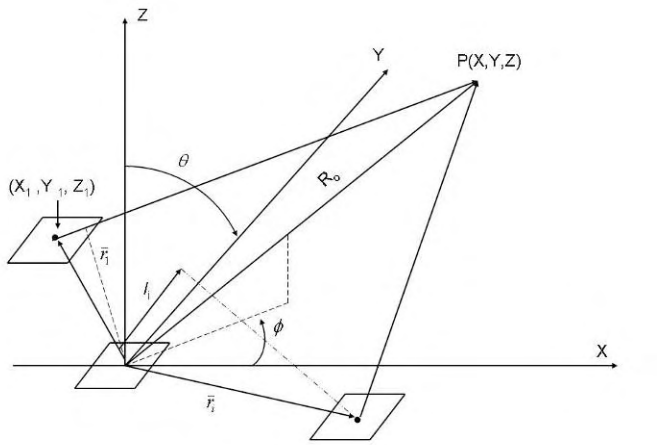

Figure 2.5 Generalized array configuration from [13].

Figure 2.5 shows a generalized distribution of array elements. Each element radiates a vector directional pattern that has both angle and radial dependence near the element. For distances far from the element, the radiation has the *[exp(-jkR)]/R* dependence of a spherical wave multiplied by a vector function of angle $f_i(\theta,\varphi)$, called the element pattern. Although this vector function $f_i(\theta,\varphi)$ depends on the kind of element used, the far field of any *i*th element can be written as:

$$E_i(r,\theta,\phi) = f_i(\theta,\phi)\frac{e^{-jkR_i}}{R_i} \qquad (2)$$

for

$$R_i = \sqrt{(x-x_i)^2 + (y-y_i)^2 + (z-z_i)^2}$$

where $k = 2\pi/\lambda$ is the wave number of frequency *f*.

If the pattern is measured at a distance very far from the array, then the exponential above can be approximated by reference to an exponential distance R measured from an arbitrary center of the coordinate system. Since $R_i \approx R - \hat{r} \cdot r_i$, then

$$\frac{e^{(-jkR_i)}}{R_i} = \frac{e^{(-jkR)}}{R} e^{(jkr_i \cdot \hat{r})}$$

for r_i, the position vector of the ith element to the center of the chosen coordinate system, and $\hat{r}$, a unit vector in the direction of any point in space (R, θ, ϕ). The vectors are written:

$$r_i = \hat{x}x_i + \hat{y}y_i + \hat{z}z_i \qquad (3)$$

$$\hat{r} = \hat{x}u + \hat{y}v + \hat{z}\cos\theta \qquad (4)$$

where $u = \sin\theta\cos\phi$ and $v = \sin\theta\sin\phi$ are directional cosines. The required distance R for which one can safely use the far-field approximation depends on the degree of fine structure desired in the pattern. Using the distance

$$R = \frac{2L^2}{\lambda} \qquad (5)$$

for L the largest array dimension, is adequate for many pattern measurements. For measuring extremely low sidelobe patterns or patterns with deep nulled regions, it may be necessary to use

$$R = \frac{10L^2}{\lambda} \qquad (6)$$

or greater distances. For now on far-field expressions will be used throughout this discussion.

For an arbitrary array,

$$\overline{E}(r) = \frac{e^{(-jkR)}}{R} \sum_i a_i \hat{f}_i(\theta,\phi) e^{(jkr_i \cdot \hat{r})} \qquad (7)$$

The expression above is very general in form because it is written in terms of the unknown element patterns for each element in the presence of the whole array. The coefficient a_i are the applied element weights (currents) of the incident signal. In general, the vector element patterns are different for each element in the array, even in an array of equal elements. The difference is usually due to the interaction between elements near the array edge. However, throughout the rest of the discussion, it will be assumed that all patterns in a given array are the same. That said, equation 7 can be re-written as

$$\overline{E}(r) = f(\theta,\phi) \frac{e^{(-jkR)}}{R} \sum_i a_i e^{(jkr_i \cdot \hat{r})} \qquad (8)$$

Because the pattern is usually described or measured on a sphere of constant radius, it is customary to remove the normalizing factor constant exp(-jkR)/R.

Les us ensemble an array of $N + 1$ number of equal elements of far-field pattern given by $f(\theta,\varphi)$ as shown in Figure 2.6. Considering the weight number or amplitude and phase of each element the far-field of the array is:

$$E_T(\theta) = f(\theta) \sum_i a_i e^{(j\beta_i)} \frac{e^{(-jkR)}}{R} \qquad (9)$$

If the array elements are closely spaced, mutual coupling will cause disrupted current distributions between neighboring elements. For a broadside radiating array the current distribution on the elements will be a function of the element position on the array, making the assumption above a fair approximation for separations larger than λ/2. For a scanning array this assumption is an erroneous one, thus coupling must be accounted for.

If we measure the field produced by the array in a very remote distance in space($R>>d$), we could assume that

$$R_1 = R - d\cos\theta$$

$$R_{-1} = R + d\cos\theta$$

And if the elements are fed with the same amplitude and the relative phase between elements is progressive ($\beta_n = n\beta_o$). The total field of the array can be written as

$$E_T(\theta) = af(\theta)\sum_{n=-N/2}^{N/2} e^{jn(kd\cos\theta+\beta_o)} \qquad (10)$$

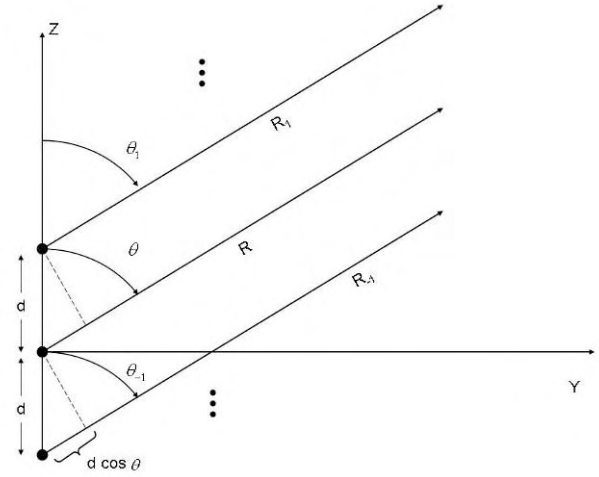

Figure 2.6 Geometry of array positioned along the z-axis.

Note that the total field is the product of two factors, the element factor and the array factor. The element factor is only a function of the element pattern and the distance between the array center and the observation point. The array factor is only function of the number of elements, the separation between them and relative phase between the elements [13].

Normalizing the array factor the summation reduces to

$$AF(\theta) = \frac{\sin\left[\frac{M}{2}\left(kd\cos\theta + \beta\right)\right]}{M\sin\left[\frac{1}{2}\left(kd\cos\theta + \beta\right)\right]}; \quad \text{M = N + 1} \tag{11}$$

The function above is periodic and the maxima of the function occurs when

$$\frac{\psi}{2} = \frac{kd\cos\theta + \beta}{2}\Bigg|_{\theta=\theta_m} = \pm m\pi \tag{12}$$

$$\theta_m = \cos^{-1}\left[\frac{1}{kd}\left(-\beta \pm 2m\pi\right)\right]; \qquad \text{m = 0,1,2,…} \tag{13}$$

The nulls of the function occur when $\sin(M\psi/2) = 0$. This occurs when $M\psi/2\big|_{\theta=\theta_o} = \pm m\pi$, therefore

$$\theta_n = \cos^{-1}\left[\frac{1}{kd}\left(-\beta \pm \frac{2n\pi}{N}\right)\right] \qquad \begin{matrix} n = 1,2,2,... \\ n \neq N,2N,3N,... \end{matrix} \tag{14}$$

The half power points, better known as the 3dB beamwidth, of the function are found by

$$\frac{\sin\left(\frac{M}{2}\psi\right)}{M\sin\left(\frac{\psi}{2}\right)} = \frac{1}{\sqrt{2}} \tag{15}$$

For an array scanned to θ_o, the 3dB beamwidth, θ_{3dB}, is given by

$$\theta_{3dB} = \sin^{-1}\left(\sin\theta_o + .4429\frac{\lambda}{Md}\right) - \sin^{-1}\left(\sin\theta_o - .4429\frac{\lambda}{Md}\right) \tag{16}$$

For large values of M

$$\theta_{3dB} = \frac{.8858\lambda}{MD\cos\theta_o} \tag{17}$$

The directivity of an antenna is defined by the *IEEE Standard Definitions of Terms for Antennas* as "the ratio of the radiation intensity in a given direction from the antenna to the radiation intensity averaged over all directions. The general expression for the directivity can be written as [11]

$$D(\theta,\phi) = 4\pi \frac{f(\theta,\phi)}{\int_0^{2\pi}\int_0^{\pi} f(\theta,\phi)\sin(\theta)d\theta d\phi} \tag{18}$$

where $f(\theta,\varphi)$, as mentioned before is the far-zone electric field.

For linear array, the scan loss also depends on the directive gain in the plane orthogonal to the scan plane [13]. Robert Mailloux discusses in [13] what Elliot demonstrated in [14]. Elliot stated that the directivity is independent of scan angle and is given by

$$D_o = \frac{\left|\sum a_n\right|^2}{\sum \left|a_n\right|^2} \tag{19}$$

Increasing array mismatch due to element mutual coupling negates this possibility, even for omnidirectional elements. An array with element patterns narrowed in the plane orthogonal to scan suffers substantially increased losses when scanned to wide angles. Since maximum value of equation 19 is equal to N and occurs when all a_n values are the same, it is convenient to define a taper efficiency ϵ_T such that the above results for half-wavelength-spaced isotropic elements is [11]

$$D_0 = N \epsilon_T \tag{20}$$

where

$$\epsilon_T = \frac{1}{N}\frac{\left|\sum a_n\right|^2}{\sum |a_n|^2} \tag{21}$$

2.4.3 Series-fed Arrays

Series array configurations offer unique advantages to the microstrip antenna designer as shown in [8]. First, feed line lengths are inherently minimized, thus reducing line radiation and dissipation losses, which decrease array efficiency. Further, in large arrays high-power feed lines are decoupled from elements radiating low-power levels. This permits tighter control of aperture distributions. Steered beams can be easily achieved, and the series configuration is particularly applicable when frequency scanning with single or dual polarization is desired as demonstrated in [15], [16] and [17].

In microstrip series-fed arrays both radiation and ohmic losses from the feed network are minimized and antenna efficiency come to be noticeably improved [8]. Such kind of arrays may be designed as either resonant or traveling wave arrays [18]. Traveling wave arrays can be used to obtain quite large bandwidth, although the use of terminal dissipative matched loads to prevent reflections from the feed ends counteracts the efficiency increase associated with series feed configurations. A way to improve this problem is to use a loading radiating element instead of the terminal loads. A good example of this can be seen in [17].

As mentioned before, polarization agility with low cross-polarization can be achieved by aperture coupled patch technology, which provides better control of the cross-polarization level [1]. In the last decade or so, polarization-agile series-fed

microstrip arrays have been proposed along with a design procedure based on the image parameter method for network synthesis [15], [19].

2.4.4 Aperture-Coupled Arrays

Arrays using proximity coupled elements have the advantages of improved bandwidth and reduced spurious radiation over microstrip line-fed elements, but feed radiation is still high enough so that cross-polarization or side lobe levels better than about 20 - 25 dB are unlikely to be obtained. This is not a problem with aperture coupled patch arrays, since the feed lines are shielded by the ground plane [1].

For series-fed aperture coupled patch arrays, design flexibility can be greatly enhanced by simply varying the size of the coupling slots so as to properly excite the corresponding patches on the line. Slot size clearly affects both the transmission characteristics and the amplitude of the current excited on the patch giving a degree of freedom for tapering more efficiently.

2.5 Aperture-Coupled Antennas Applications

In the last 10 years or so, passive and active phased array antennas employing electronic beam scanning and polarization agility have been widely used for space and terrestrial applications, such as in synthetic aperture radar (SAR), personal communication networks (PCN), wireless local area networks (WLAN) and millimeter-wave sensors (MWS) and for global positioning systems (GPS). In this section a few examples of previous works will be mention in order to understand the scope of this kind of structure.

An aperture-coupled series-fed array was presented in [15] at a frequency of 2.45 GHz. Image parameter analysis was employed for the design of the basic element. Similar structures have been developed for dual-polarization and dual-band in [17] and [20]. Figure 2.7 shows the array proposed in [20] to operate at L-band and C-band. The whole array layout is obtained by mirroring with respect to the vertical plane.

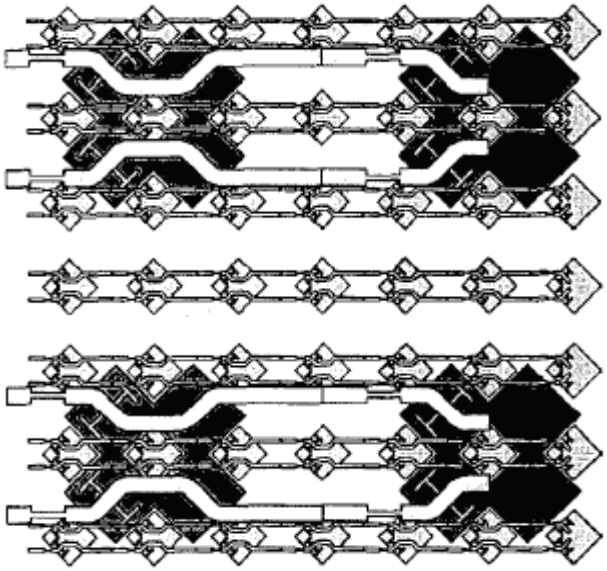

Figure 2.7 Sample geometry for one half of the DBDP array antenna. A 4 x 2 L-band array is interleaved with a 14 x 7 C-band array from [20].

The work in [21] describes the design and testing of an aperture-coupled circularly polarized antenna for global positioning satellite (GPS) applications. The antenna operates at both the L1 and L2 frequencies of 1575 and 1227 MHz, which is required for differential GPS systems in order to provide maximum positioning accuracy. A broadband dual polarization patch antenna double fed by an L-shaped probe and a near-resonant aperture is presented in [22]. The proposed antenna achieves a 1.5:1 standing wave ratio bandwidth greater than 20% at the two ports. Input isolation exceeding 25 dB has been obtained in the wide bandwidth. Thus, it can potentially be used as a base station antenna for cellular-phone networks. Figure 2.8 shows the configuration proposed.

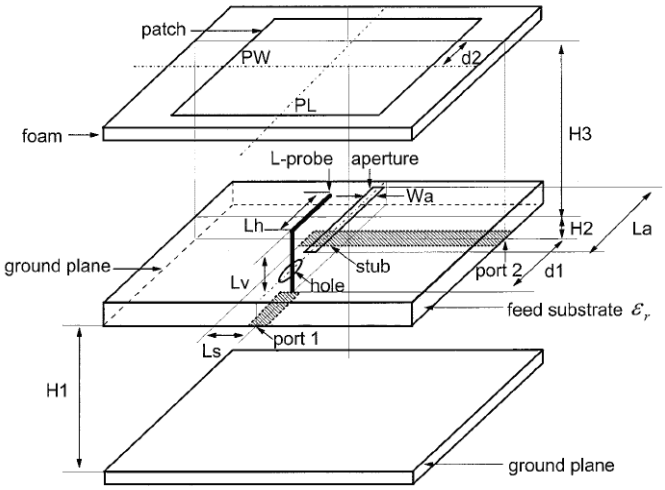

Figure 2.8 Geometry of antenna proposed for cellular phone-base stations from [22].

A dual-feeding technique for a broadband circularly polarized aperture-coupled microstrip antenna operating in a 2.45 GHz system is presented in [23]. Figure 2.9 shows how the dual feeds are placed in orthogonal directions, and are connected to a Wilkinson power divider with a 90º phase shift between its two output feedlines. The isolation achieved between its ports is around -40 dB, and a purity of circular polarization is obtained. A broad impedance bandwidth (VSWR<2) of about 54.7% and a 1 dB axial-ratio bandwidth of about 9.8% were achieved.

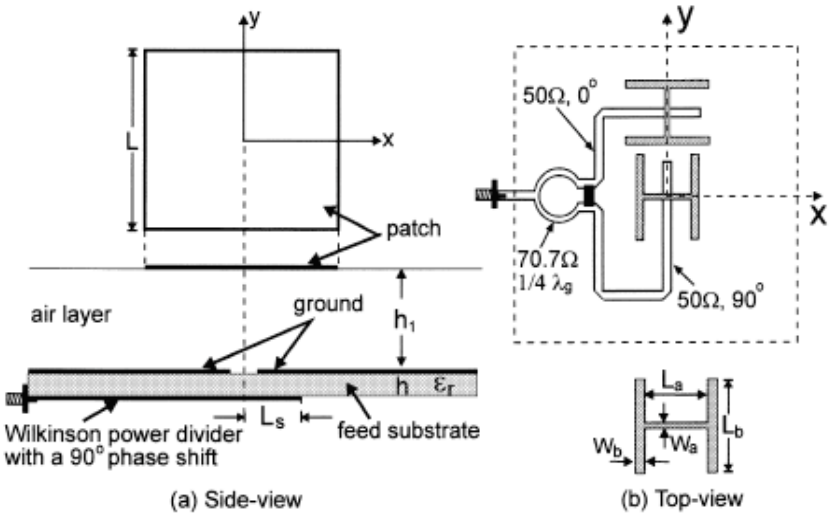

Figure 2.9 Geometry of the single-layer, broadband circularly polarized aperture-coupled microstrip antenna from [23].

Figure 2.10 shows an aperture-coupled micromachined microstrip antenna operating at 94 GHz proposed in [24]. The design consists of two stacked silicon substrates: the top substrate, which carries the microstrip antenna, is micromachined to improve the radiation performance and the bottom substrate, which carries the microstrip feed line and the coupling slot. The measured return loss is -18 dB at 94 GHz for a 10 dB bandwidth of 10%. The radiation patterns show a measured front-to-back ratio of -10 dB at 94 GHz. The measured mutual coupling presented is below -20 dB in both E- and H-plane directions due to the integration of small 50 μm silicon beams between the antennas. The micromachined microstrip antenna is an efficient solution to the vertical integration of antenna arrays at millimeter-wave frequencies [24].

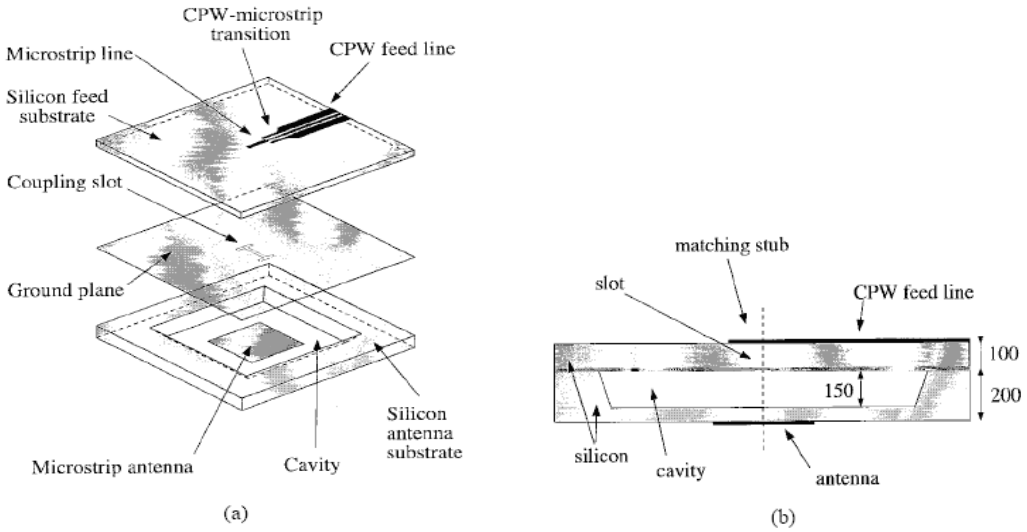

Figure 2.10 (a) Perspective view and (b) cross section of the aperture-coupled micromachined microstrip antenna. All dimensions are in microns from [24].

The development of wireless indoor communication in the millimeter-wave domain at 60 GHz requires antenna arrays with specific performances. Microstrip technology is attractive at these frequencies if one uses material with weak losses and a low-cost technology. PTFE, commercially available as RT/D Duroid 5880, or polymethyl-pentene, commercially available as TPX, are good candidates. The effect of

spurious radiation due to the feed network often increases the cross-polarization component and the sidelobe levels, a solution to reduce these problems is presented in [25]. In order to obtain a pencil beam, a two-dimensional (6 x 6) antenna array with 36 aperture-coupled patches was designed. The feed network was design with identically tapered in amplitude in both the *E*- and *H*-planes to reduce the sidelobe level. Figure 2.11 show a slot-coupled printed antenna array, with radiating elements that are separated from the feeding lines by the ground plane.

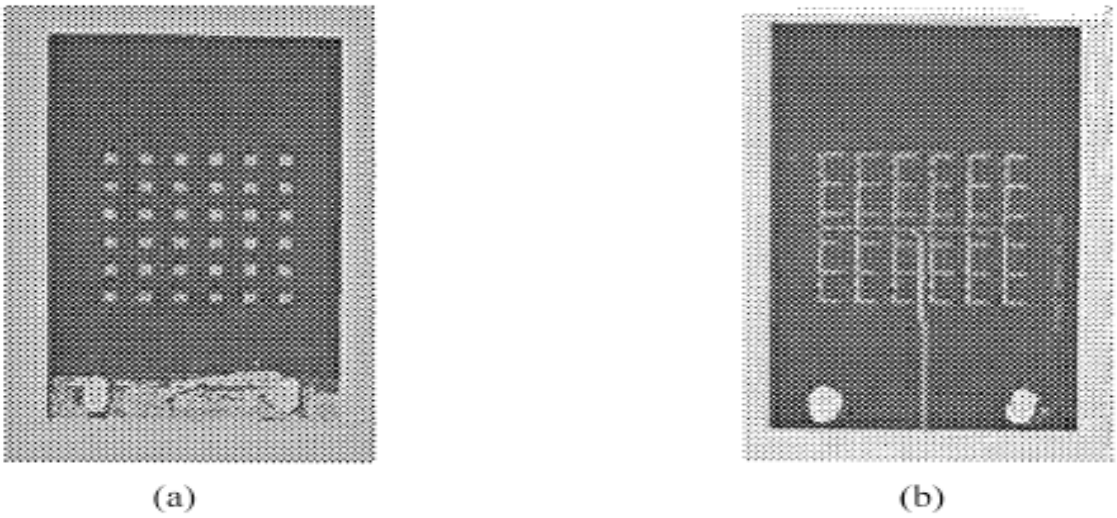

Figure 2.11 (a) radiating elements of the array and (b) feed network from [25].

A design method for an aperture-coupled microstrip patch antenna with a single feeding structure is proposed for dual resonance frequencies with mutually perpendicular polarizations in [23]. A type of square patch with double notches is used as a radiator, and the crossed slot and bended microstrip feed are adopted for the dual polarizations in the aperture-coupled structure. The characteristics of this antenna were experimentally investigated for generalizing the dual-frequency behavior. Figure 2.12 shows a Ku-band Tx/Rx 2 x 2 sub-array antenna that was designed and manufactured to examine the applicability as a ground terminal antenna for satellite communications [26].

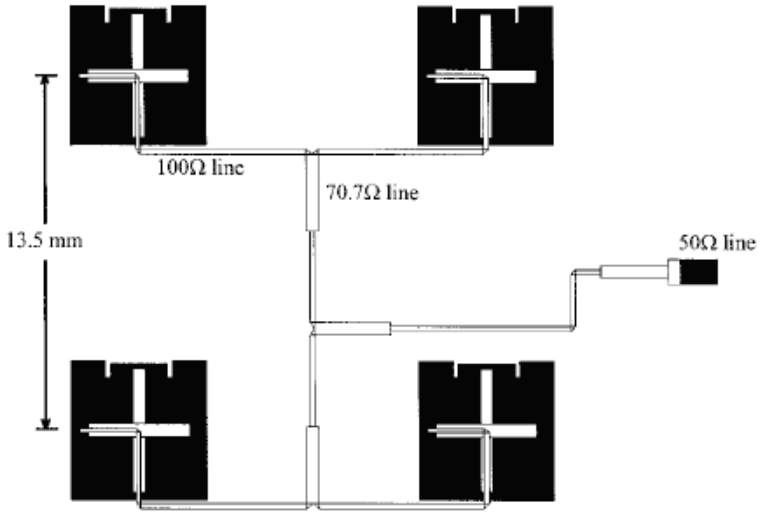

Figure 2.12 Configuration for Ku band 2 x 2 array antenna from [26].

The millimeter-wave (mm-wave) wireless market is expeditiously growing due to the high worldwide demand for rapidly deployable cellular telephone networks and also broadband wireless access networks. For the former application, point-to-point (PTP) mm-wave radio links between cellular base stations are being utilized as an alternative to more expensive wired solutions, while in the latter systems, point-to-multipoint (PMP) mm-wave communications have been proposed to provide high-quality multimedia applications and the Internet. Central to both PTP and PMP systems is the need for unobtrusive antennas that can be easily connected to the mm-wave radio front ends [27].

Although most PTP and PMP mm-wave applications require relatively narrow bandwidths, typically l0%, there are several advantages in incorporating a broadband antenna element into these systems. First of all, broadband printed antenna elements tend to be less susceptible to manufacturing/fabrication error. This is important for providing low cost solutions that do not require accurate fabrication facilities. In addition, if the bandwidth of the antenna is large enough, then perhaps the one radio hub can provide multiple services, for example LMDS at 28 GHz and broadband wireless access networks at 38 GHz, thereby sharing some of the hub hardware and reducing the overall cost of the radio networks [27]. In figure 2.13 a linear array of ASP elements proposed in [27] is

shown. Both printed antennas operate presented in [27] over the entire Ka-band (26 - 40 GHz).

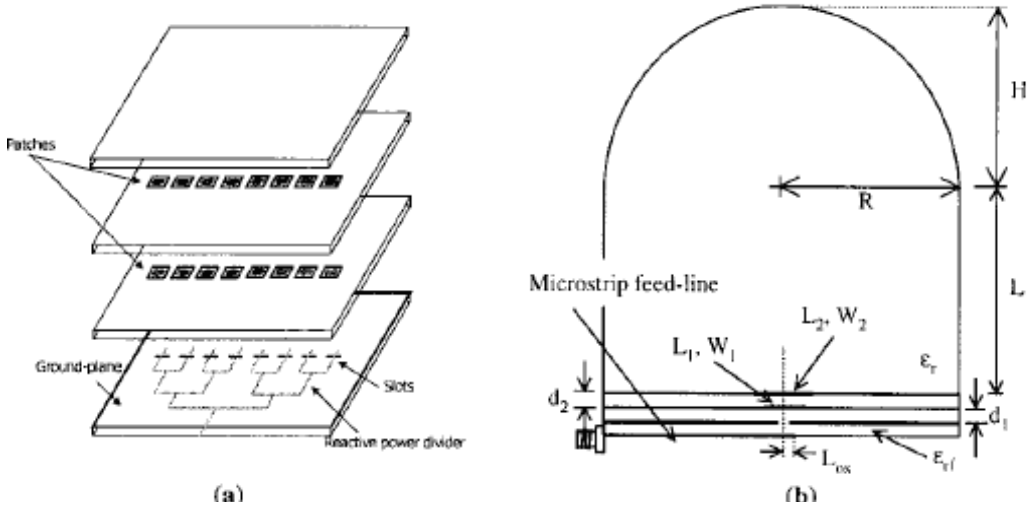

Figure 2.13 Schematic diagrams of (a) linear ASP Array and (b) lens coupled ASP from [27].

In [28] the design and testing of a prototype dual-band dual-polarized planar array operating at L and X-bands is presented. The design presents an antenna with dual-band and dual-polarization capability in a shared aperture, featuring low mass, high efficiency, and limited beam scanning. The design of a prototype planar microstrip array of 2 x 2 L-band elements interleaved with an array of 12 x 16 X-band elements that meets these requirements is discussed in detail and measured results are presented in [28]. The array is modular in form and can easily be scaled to larger aperture sizes. Figure 2.14 show the X-Band feed network (right) and the L-Band feed network with the radiating elements (left).

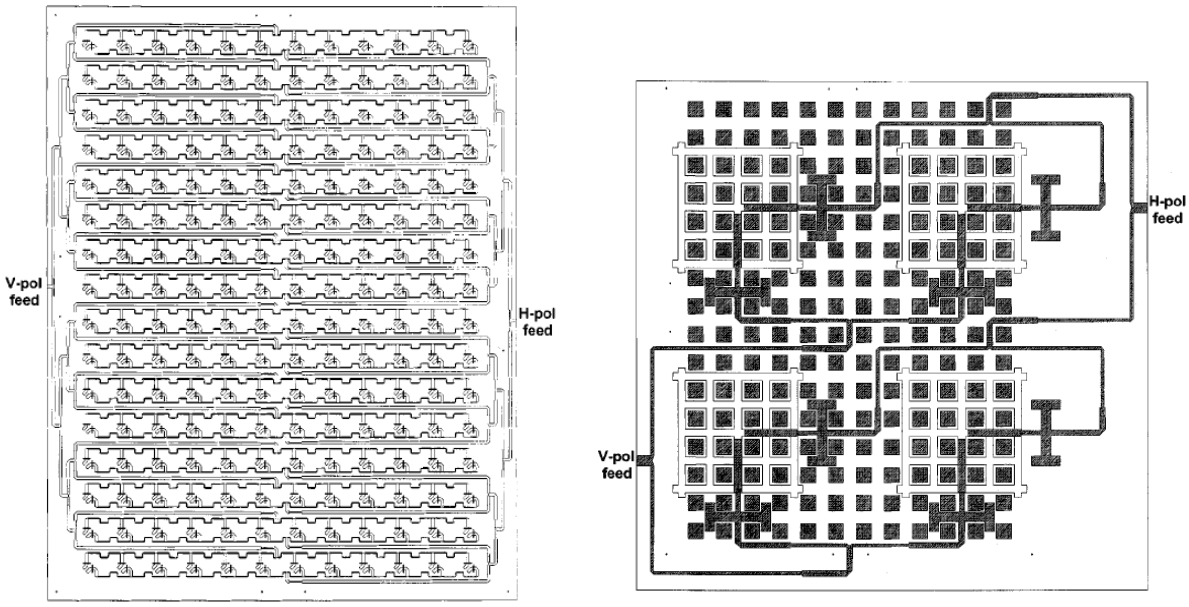

Figure 2.14 Aperture feedline for the 12 x 16 X-band dual polarized array patches and layout of the L-band fed network, L-band patches and X-band parches from [28].

A design of a dual-polarized microstrip series-fed linear traveling-wave array is described in [17]. The array is composed of two identical sub-arrays formed by cascading an equal number of four-port aperture-coupled cross-patch elements and terminated on a two-port radiating matched load. By properly exciting the array, dual linear or circular polarization can be accomplished and by virtue of the symmetric arrangement of the antenna cross-polarization is eliminated. Figure 2.15 shows one half of the polarization agile series-fed array of 14 identical elements. The coupling slots of the iterated four-port antenna element are 0.15λ (36 mm) long; the length of the terminal RML slots is 0.1625λ (39 mm), as required for impedance matching the element.

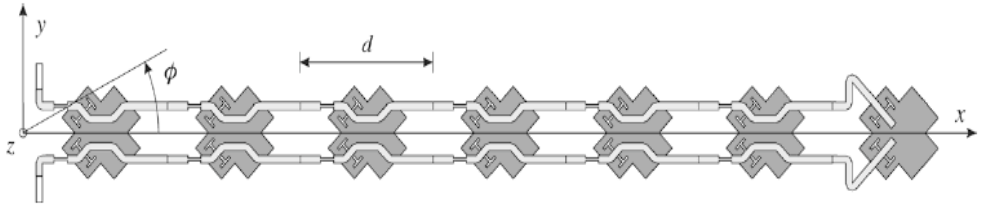

Figure 2.15 Half of the polarization agile series-fed array of 14 identical elements from [17].

3 METHODOLOGY

3.1 Purpose

The main goal of this project is to design a dual polarized printed antenna for the OTG Radar. It is desired to minimize the cost of the antenna to keep the overall cost of the radar as low as possible. To achieve that, different designs with different materials were used to study the tradeoff between configurations.

A single polarized array was first designed to use it as a control variable. The material selected for the dual polarized and the single polarized designs was Rogers RT Duroid 5880. The first dual polarized antenna would use via holes to connect the feed network for one polarization. As the project evolved, the vias were eliminated and the substrate was changed. In the end, two different materials were used, Foam Clad from Arlon for the antenna and RO 3006 for the feed network.

The specifications for this antenna are:

- Half-Power Beamwidth (HPBW) around 6º
- Bandwidth (BW) around 250 MHz
- Sidelobe level (SLL) below -20 dB
- Cross-Polarization below -30 dB
- Front-to-back ratio below -13 dB

3.2 Simulation Software

3.2.1 Ansoft Designer

Designer is a software based on Method of Moments and use full wave electromagnetic functions for planar analysis based on Maxwell's equations. It computes the input impedance and radiation characteristics for arbitrary shape antennas. Designer can produce three types of meshes, an adaptive mesh, which is a more accurate mesh and more time and memory consuming, an edge mesh and a simple mesh, which is the least accurate of the three options. The mesh is simply made of triangles and rectangles created over the structure under test to calculate the E fields in each and every one of them. How the structure is meshed depends on the adaptive or static selection.

The static mesh (normal or edge mesh) depends on the meshing frequency; the adaptive mesh will be denser until a particular response converges. If both meshes provide an accurate response, the adaptive one would most likely be less dense than the static one, but as the structure grows more complex the adaptive mesh estimation becomes more time consuming than the static one. Discontinuities and overlapping in the drawing will cause the mesh to have more polygons in these areas causing more time and memory consuming simulation. Static mesh, the mesh used for the simulations, has a trade off, the higher the frequency the more precise the final mesh will be, but the more time consuming it will be. Creating a mesh at a frequency lower than the resonant frequency will produce inaccurate results. Figure 3.1 shows an example a microstrip line with edge mesh and simple mesh.

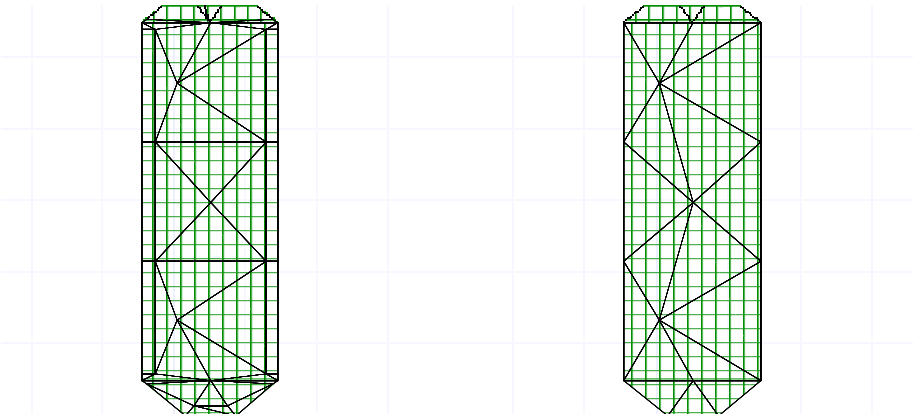

Figure 3.1 Edge Mesh on a microstrip line (left) and simple mesh (right).

3.3 Procedure

A single polarization antenna array will be designed for the OTG Radar on a substrate with permittivity of 2.2 and thickness of 0.787mm, and fed with a corporate feed for the purpose of testing the OTG Radar and comparing the results provided by Designer [29] and the results obtained at the anechoic chamber at UPRM. This antenna is a starting point for the design of the OTG Radar antenna.

A square patch was designed following the Cavity model for a resonant frequency of 9.38 GHz with an input impedance of 100 Ω. A Matlab program was developed to calculate de initial dimensions of the patch antenna and Designer was used to simulate the Matlab results and optimize the dimensions for the microstrip antenna (MSA) to resonate at the desired frequency. Figure 3.2 shows a layout with the MSA dimensions and the results of input impedance provided by Designer. Figure 3.3 shows the patch impedance at the resonant frequency. Figures 3.4 show the radiation pattern of the single polarization MSA.

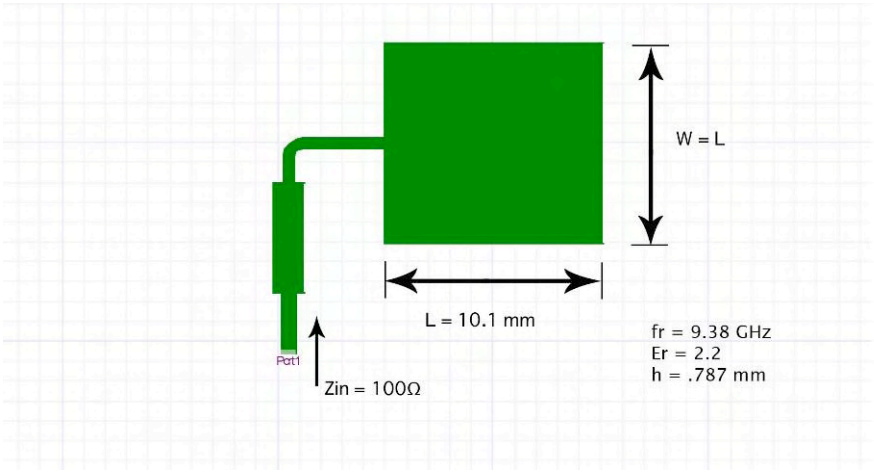

Figure 3.2 Patch dimensions and input impedance.

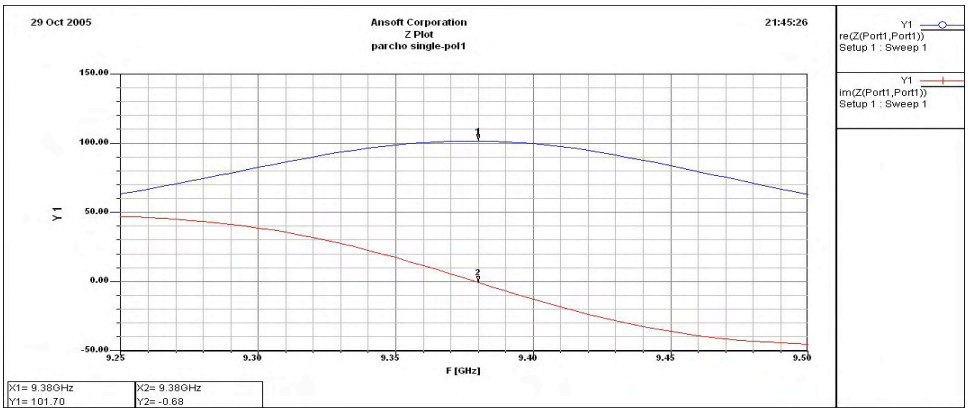

Figure 3.3 Patch Input Impedance.

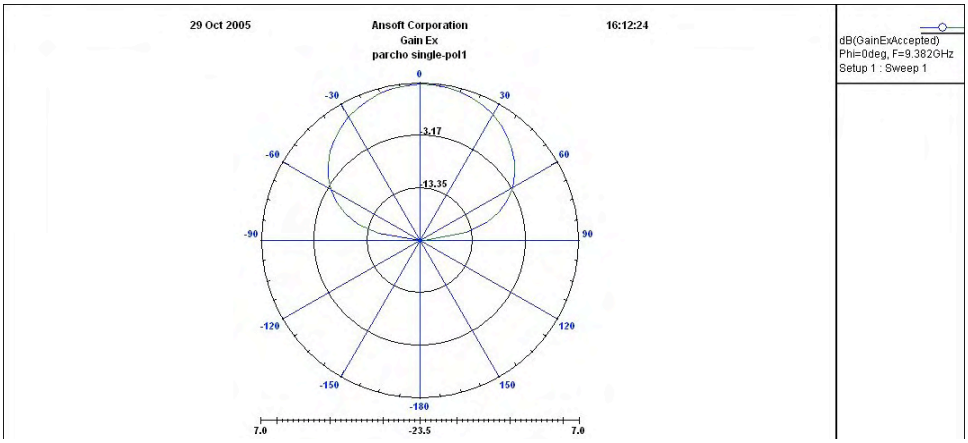

Figure 3.4 Radiation Pattern in Ex plane with 5º of resolution in θ.

For the calculation of the number of elements needed for the array, given the separation between elements, to achieve a Half Power Beam Width (HPBW) of 4º, the Matlab program from [30] was modified. Given the size of the array and the separation of the radiating elements the original program calculates the weighing for each MSA for the array for digital beam forming. Assuming that we have a corporate feed with no losses and uniform weighing for each MSA of the array the modified program estimates the radiation pattern of the array and indicates the HPBW of the array. Without taking into account the polarization, with an array of 16 by 16 elements, the HPBW was of 4º as seen in Figures 3.5 and 3.6.

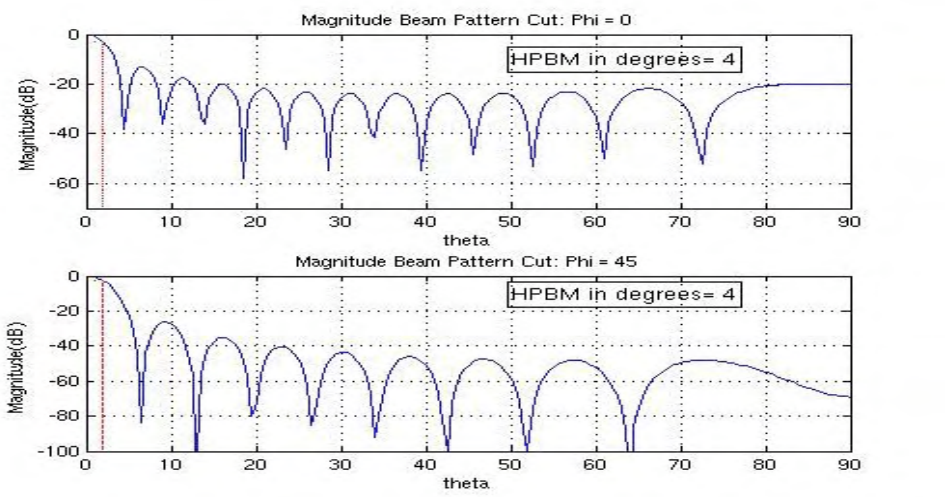

Figure 3.5 HPBW for a 16 x 16 array for φ = 0º and φ = 45º.

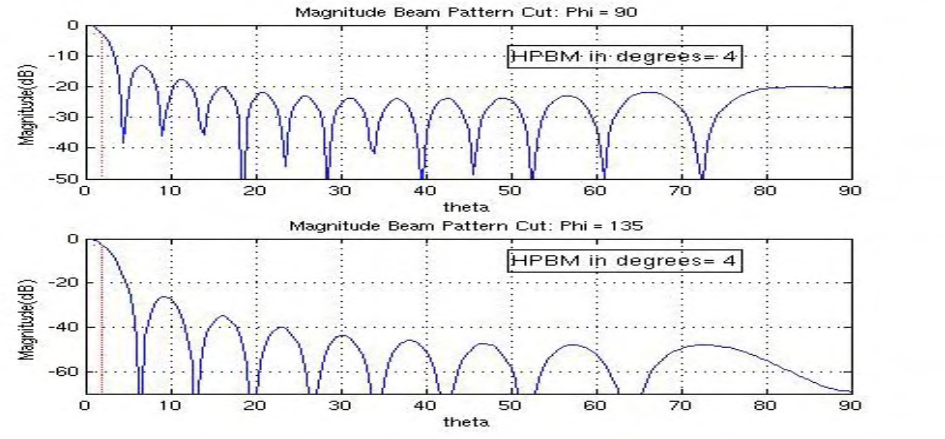

Figure 3.6 HPBW for a 16 x 16 array for φ = 90º and φ = 135º.

Also, this program shows a 3-D image of the radiation pattern and a top view of the beam for the 16 by 16 array shown in Figure 3.7 and Figure 3.8. Figure 3.8 is a top view of the radiation pattern produced by the program for the given array and a scale of power intensity for the pattern. In the center of the plot is where the main beam is located, thus where the more intense the color red is. As you move away from the center you can see where the side lobe will be located by the color spots (power levels) of the array. The degrees shown in the plot are a sweep from 0º to 360º in Φ.

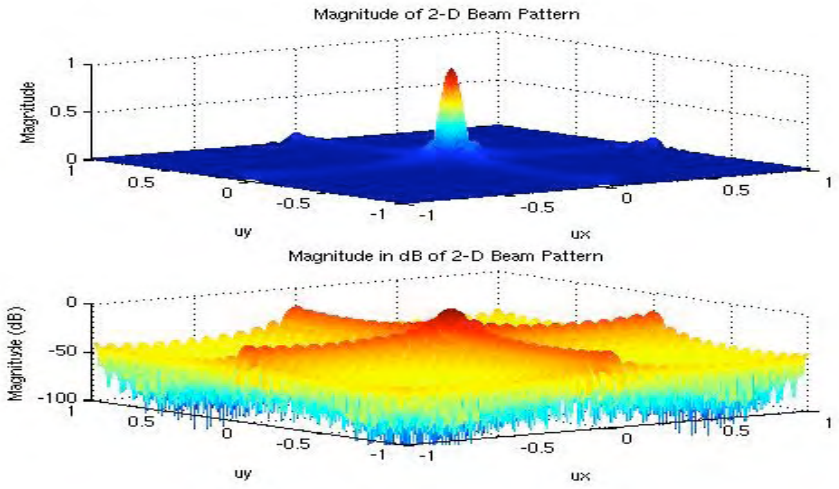

Figure 3.7 Radiation Pattern with linear amplitude normalized (top) and dB normalized (bottom) for a 16 x 16 array.

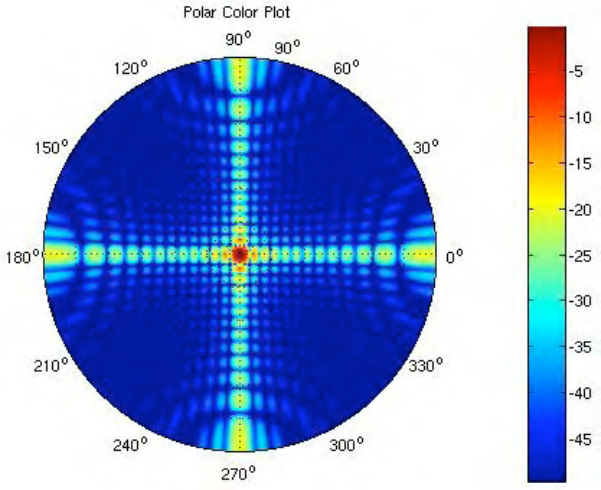

Figure 3.8 Top View of the Radiation Pattern.

Because of computational limitations and the size of the array, the 16 by 16 element array was simulated in Designer just at the resonant frequency and using a simple mesh. As mentioned before, this causes a poor resolution in the mesh created by Designer. The feed point for each patch of the array lies in the X-axis. To calculate the cross-polarization of the array, the Gain of the antenna is divided in two components, the one in the X-axis (Gain Ex), where the feed point is, and the gain in the Y axis (Gain Ey). For a pure polarization, the E field should be in the direction of the feed point of the MSA, with no perpendicular component. Figure 3.9 and Figure 3.10 shows Gain in Ex plane and Ey plane, where the single polarization array has a cross polarization of approximately 17 dB, which is lower than expected (30 dB). Figure 3.11 shows a 3-D pattern of the single polarization array simulated in Designer and Figure 3.12 shows in a Smith Chart the input impedance for this array.

Various factors in the simulation need to be revised, like the mesh of the simulation. Because of the size of the array, a simple mesh and not an "edge-mesh", which has a better resolution, was used. By comparing the simulation with the measurements provided by the anechoic chamber, we could estimate how accurate the simple mesh is.

The following figures show the results provided by Designer for the 16 x 16 single polarization MSA with a 50 Ω impedance port and frequency of 9.385 GHz.

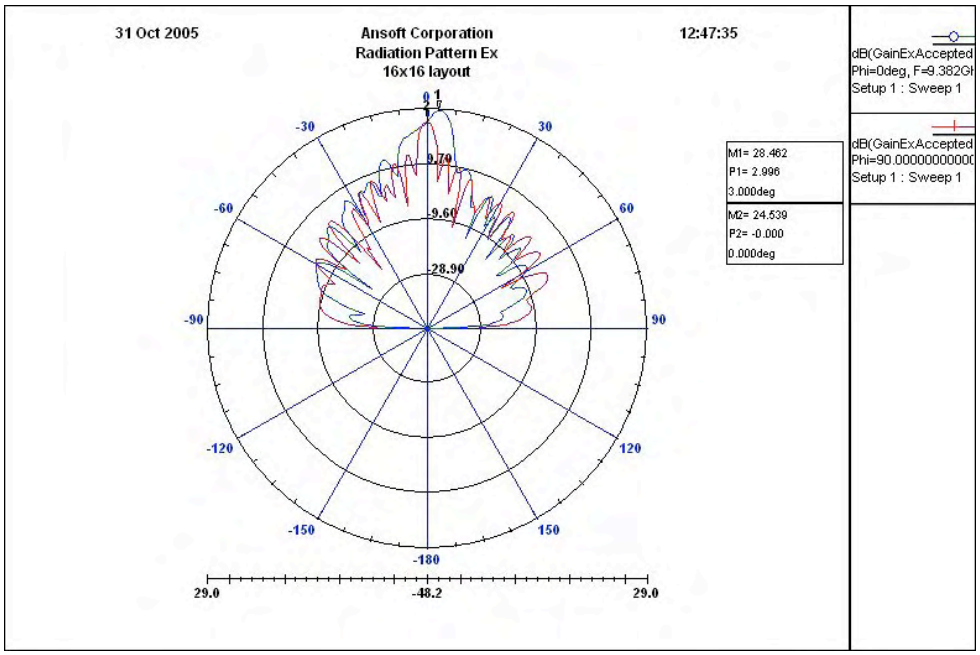

Figure 3.9 Gain Ex field for 16 x 16 single polarization MSA array.

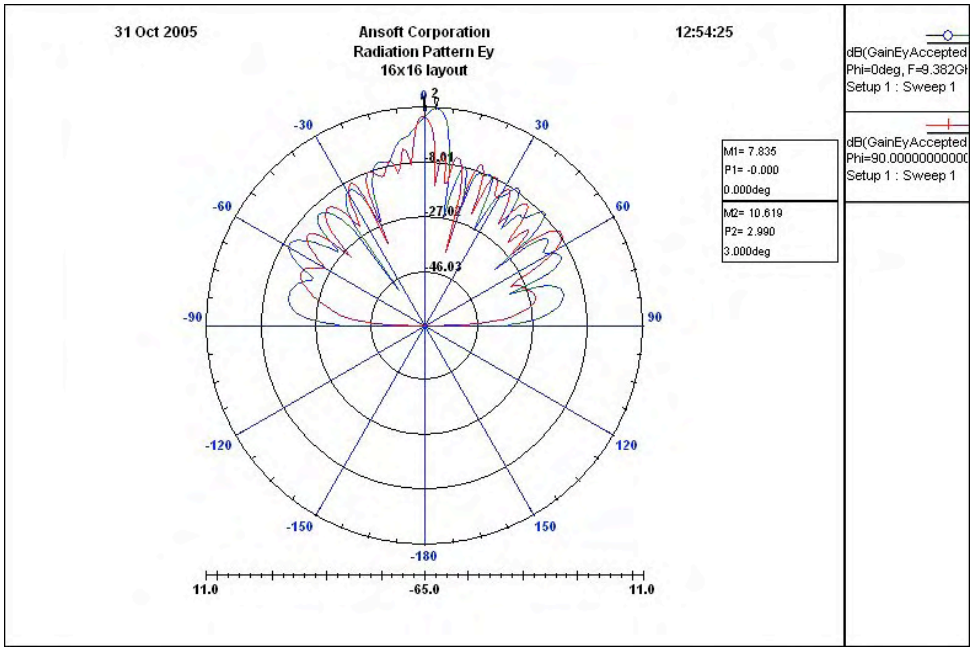

Figure 3.10 Gain Ey field for 16 x 16 single polarization MSA array.

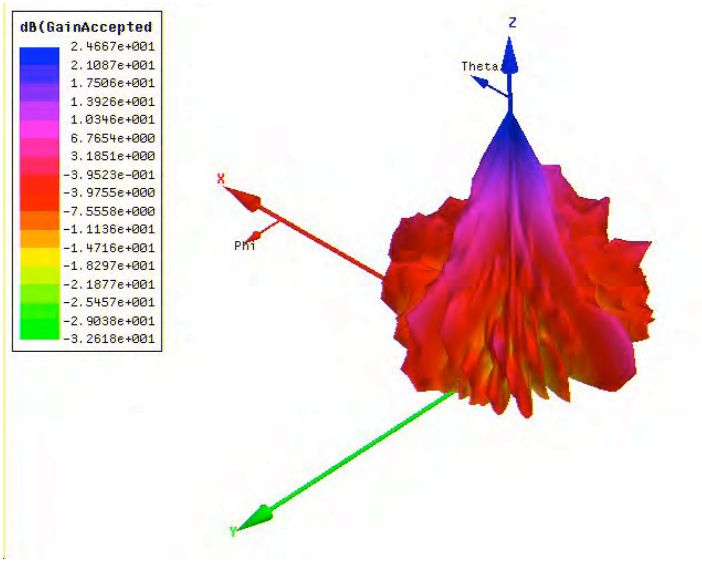

Figure 3.11 3-D Gain Plot of the 16 x 16 single polarization MSA array.

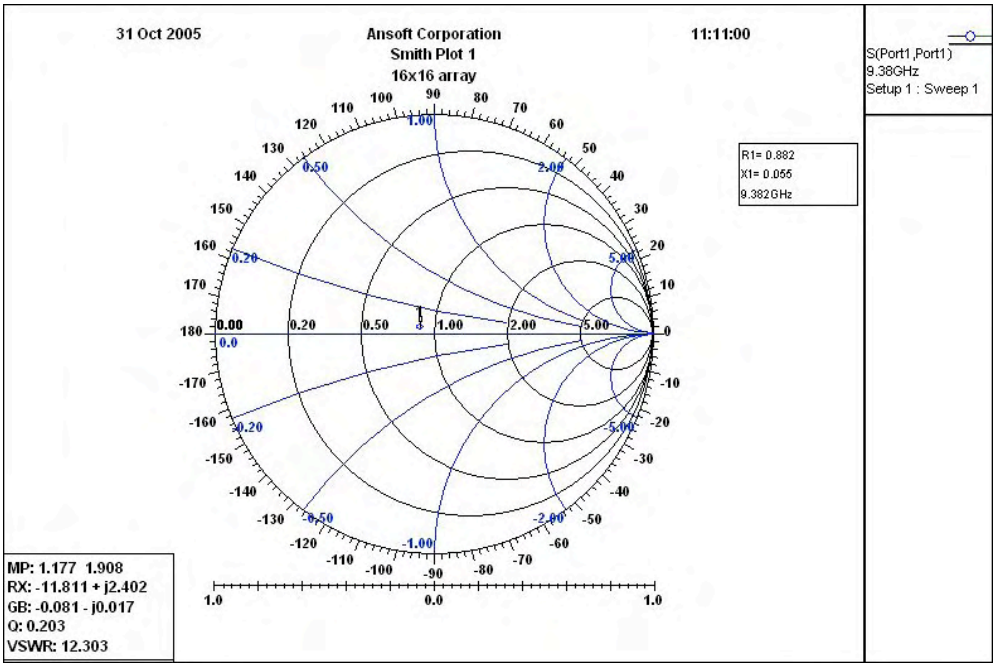

Figure 3.12 Input Impedance viewed in a Smith Chart for 16 x 16 single polarization MSA array.

The second stage consists in the design of a dual polarization antenna array on a substrate with permittivity of 2.2 and thickness of 0.787mm, and fed with a corporate

feed for each of its polarizations. This causes the antenna architecture to be a multi-layer configuration having the MPAs and a corporate feed on the upper layer for one polarization and the other corporate feed in the bottom layer for the other orthogonal polarization. This way the OTG antenna will have one patch for both polarizations. The ground plane will be placed in the middle, separating both feeds minimizing the coupling that could result between them.

Next, some of the different configurations simulated are presented. Tables 3.1, 3.2 and 3.3 shows different configurations tried for the dual-polarized antenna array. The first material configuration shown in table 3.1 is using the same material as the single polarized antenna array proposed before. Figures 3.13 through 3.16 shows different single patch antennas, their input impedance and radiation pattern. This configuration provided poor cross polarization, and aperture coupling became a way to overcome this problem. Figure 3.17 shows the layout of a single antenna with one polarization fed with an aperture coupled slot and its input impedance. Figure 3.18 shows the radiating pattern of such antenna.

Table 3.2 shows another material configuration that was considered. This configuration intended to eliminate all the feed lines from the layer where the patch antennas are located, thus using aperture coupling slots for both polarizations. Because of the complexity of the corporate feed, the feed line of the two polarizations cannot be placed in the same layer, therefore, each polarization was placed on different layers. Figure 3.19 to 3.20 shows a single radiating element with its input gain and radiation pattern. Figure 3.22 shows two designs considered for this material configuration.

Table 3.1 First material configuration.

Type	Material	Thickness
patch antenna	copper	0 mm
dielectric	Duroid 5880	0.787 mm
slots/GND	copper	0 mm
dielectric	Duroid 5880	0.787 mm
feed	copper	0 mm

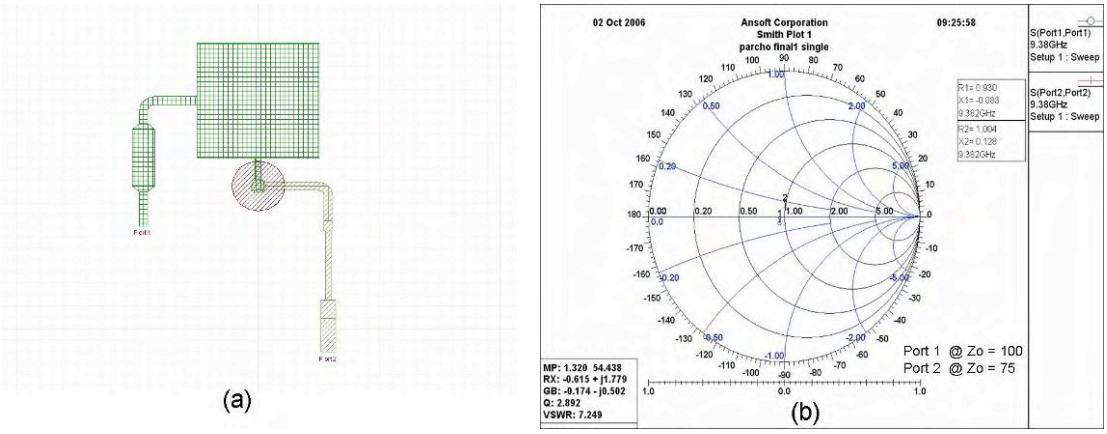

Figure 3.13 (a) A dual-Polarized patch antenna and (b) it input impedance shown in a Smith Chart.

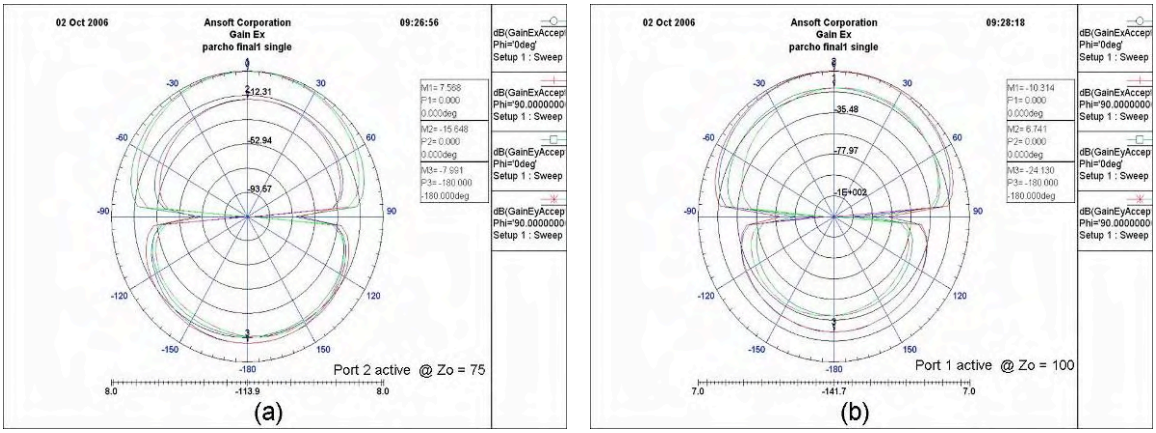

Figure 3.14 (a) Radiation pattern of antenna Port 2 active and (b) Port 1 active.

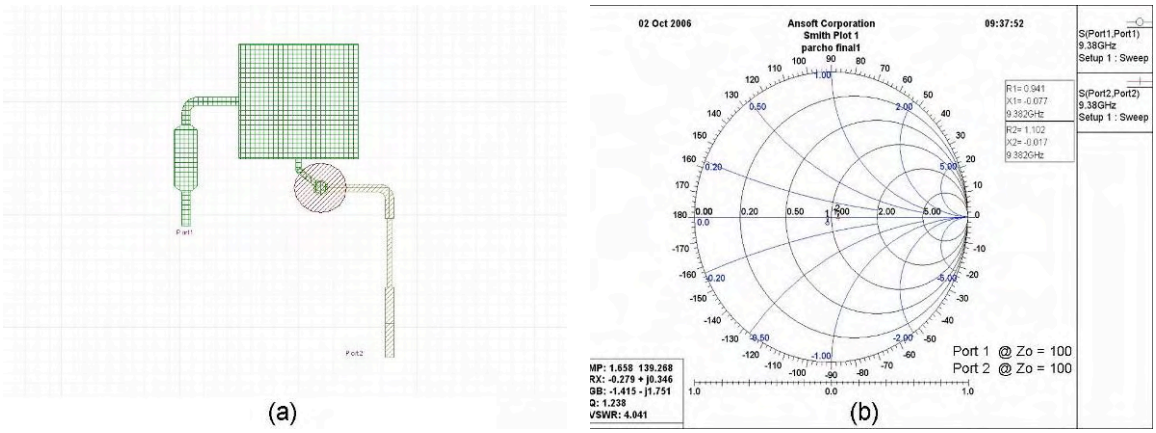

Figure 3.15 (a) A dual-Polarized patch antenna and (b) it input impedance shown in a Smith Chart.

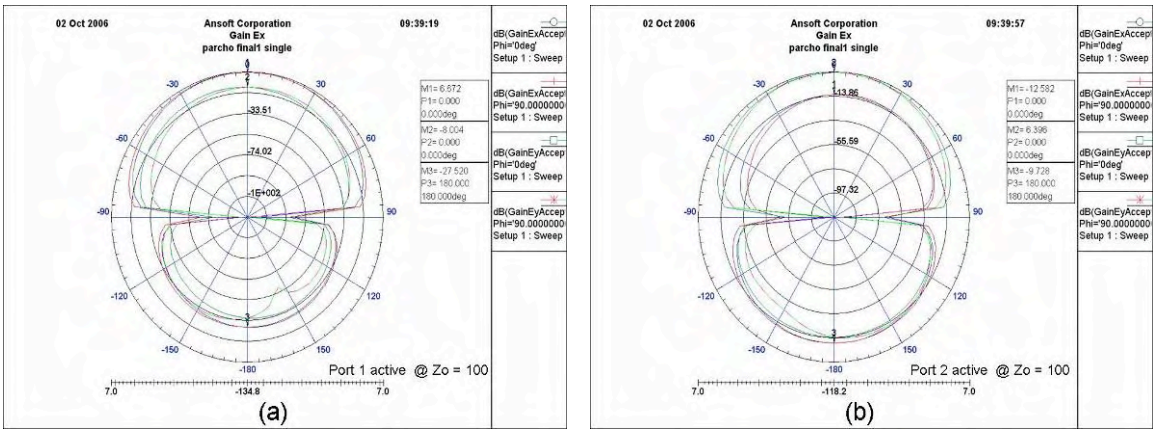

Figure 3.16 (a) Radiation pattern of antenna Port 1 active and (b) Port 2 active.

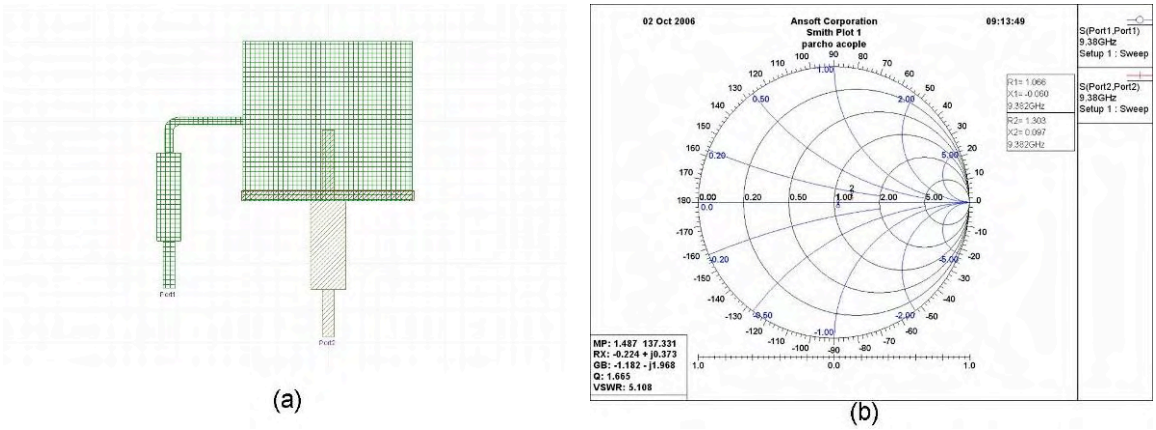

Figure 3.17 (a) A dual-Polarized patch antenna and (b) it input impedance shown in a Smith Chart.

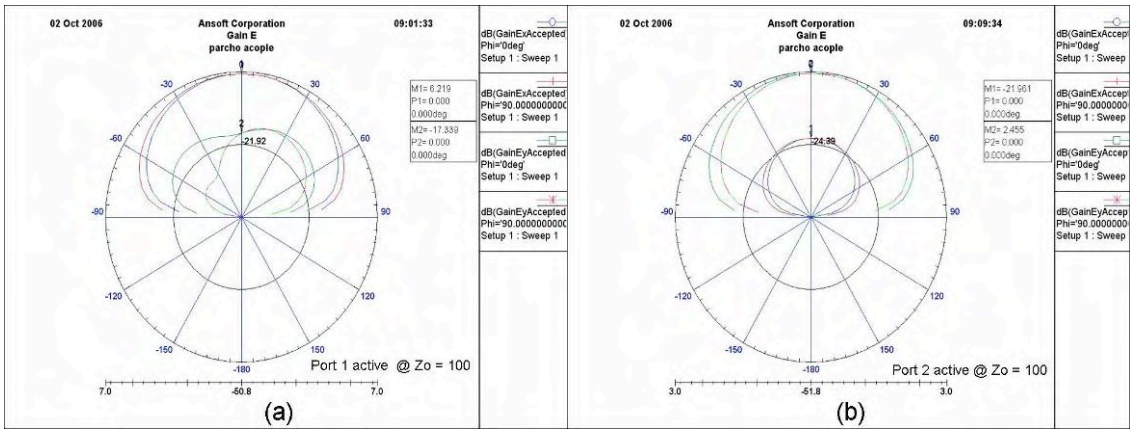

Figure 3.18 (a) Radiation pattern of antenna Port 1 active and (b) Port 2 active.

Table 3.2 Second material configuration.

Type	Material	Thickness
patch antenna	copper	0 mm
dielectric	Duroid 5880	0.787 mm
slots/GND	copper	0 mm
dielectric	RO 4003	1.525 mm
feed	copper	0 mm
dielectric	RO 4003	1.525 mm
slots/GND	copper	0 mm
dielectric	RO 4003	1.525 mm
feed	copper	0 mm
air	air	7.9 mm
GND	copper	0 mm

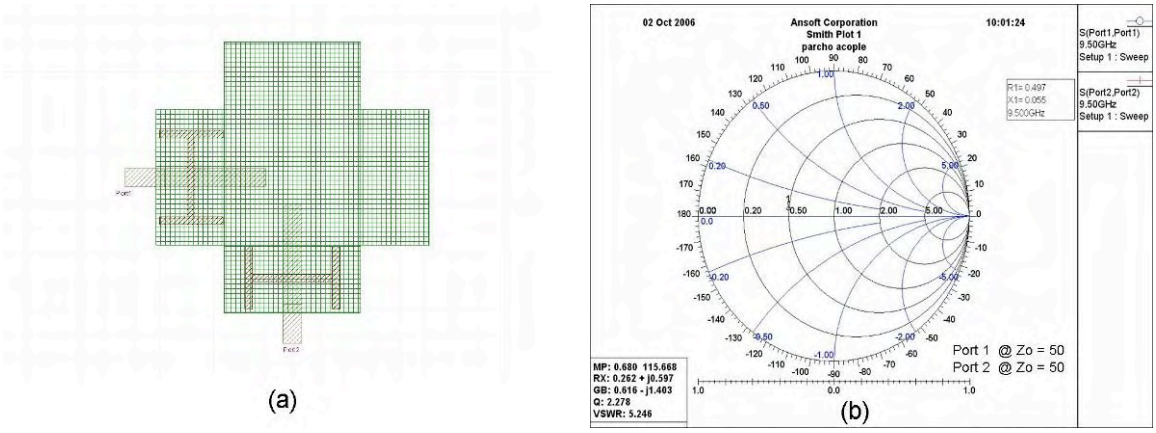

Figure 3.19 (a) A dual-Polarized patch antenna and (b) it input impedance shown in a Smith Chart.

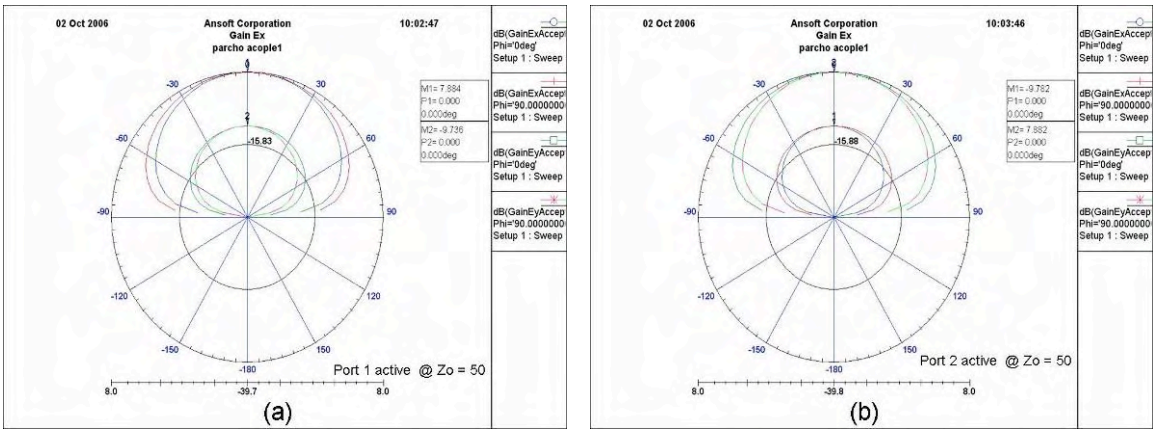

Figure 3.20 (a) Radiation pattern of antenna Port 1 active and (b) Port 2 active.

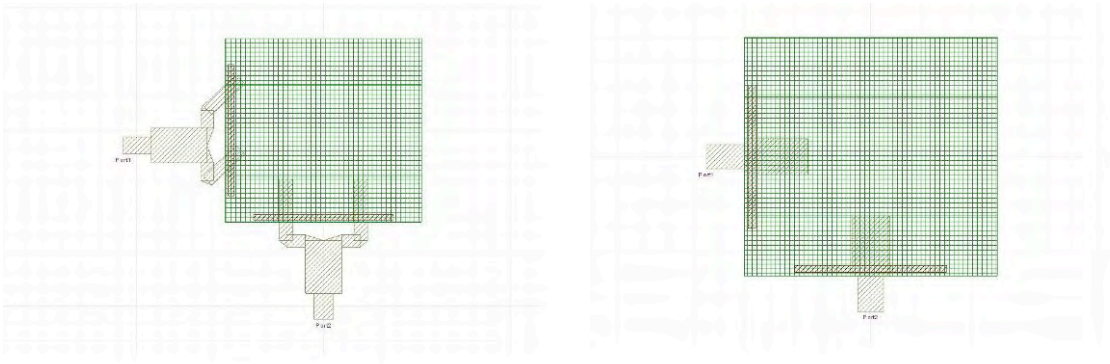

Figure 3.21 Two configurations considered using aperture coupling.

Using the method shown by [17] at a center frequency of 1.25 GHz, a new configuration for the aperture-coupled antenna was proposed. This configuration, based in the guidelines mentioned by Pozar in [7] new materials was selected. Just as in [17] a four-port patch antenna was design, but using different types of slot apertures. A patch load was also design to use it as the last element of the array. After a few shuffles with the materials that will be used for the antenna, the final configuration selected is presented in Table 3.3. The design in [17] allows having most the feed lines of the two polarizations in the same layer. Figures 3.22 to 3.27 shows some single patch antenna configurations using U aperture coupled slots and their input impedance at resonant

frequency. Even though the antennas presented show U slots for coupling, different shapes were tried. At the end an H shaped aperture coupled was used and this configuration is discuss in the following sections.

Table 3.3 Final material configuration.

Type	Material	Thickness
patch antenna	copper	0 mm
dielectric	FoamClad	1.75 mm
slots/GND	copper	0 mm
dielectric	RO 3006	0.625 mm
feed	copper	0 mm

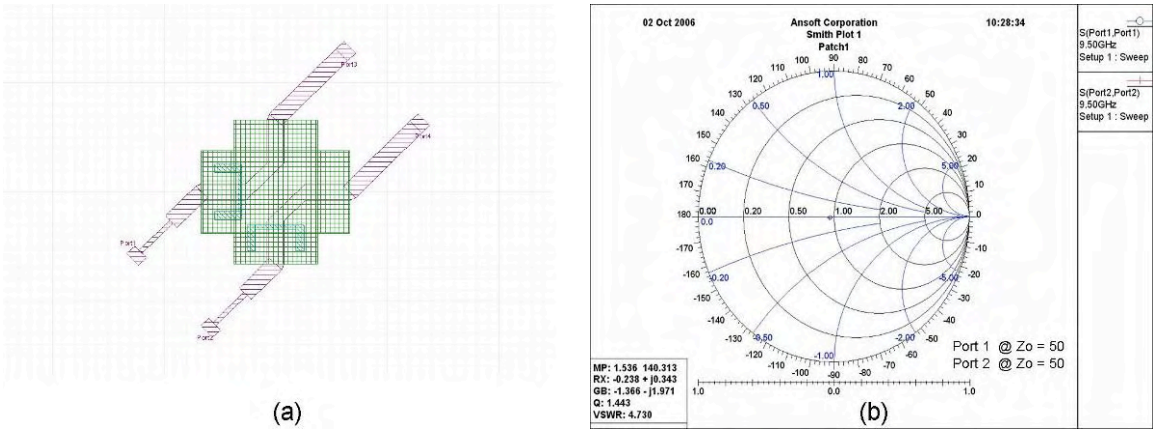

Figure 3.22 (a) A dual-Polarized patch antenna and (b) it input impedance shown in a Smith Chart.

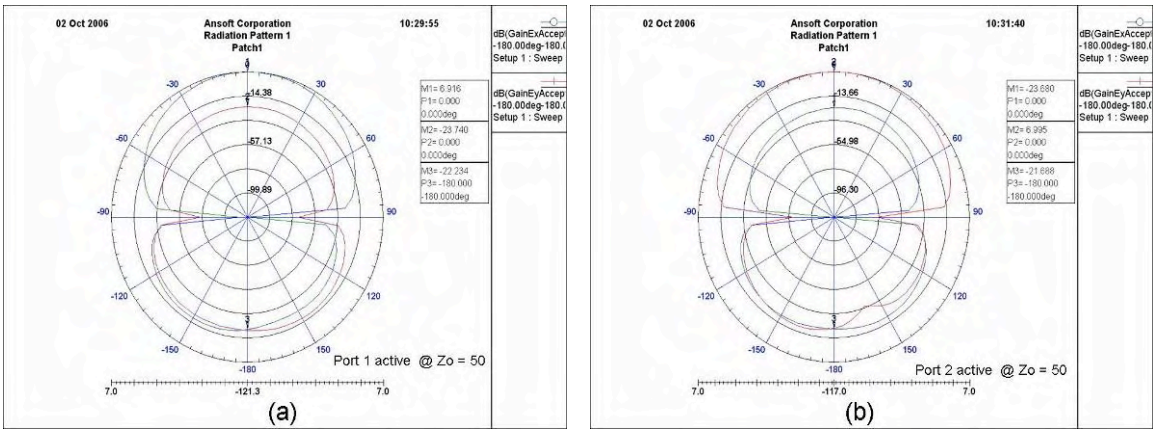

Figure 3.23 (a) Radiation pattern of antenna Port 1 active and (b) Port 2 active.

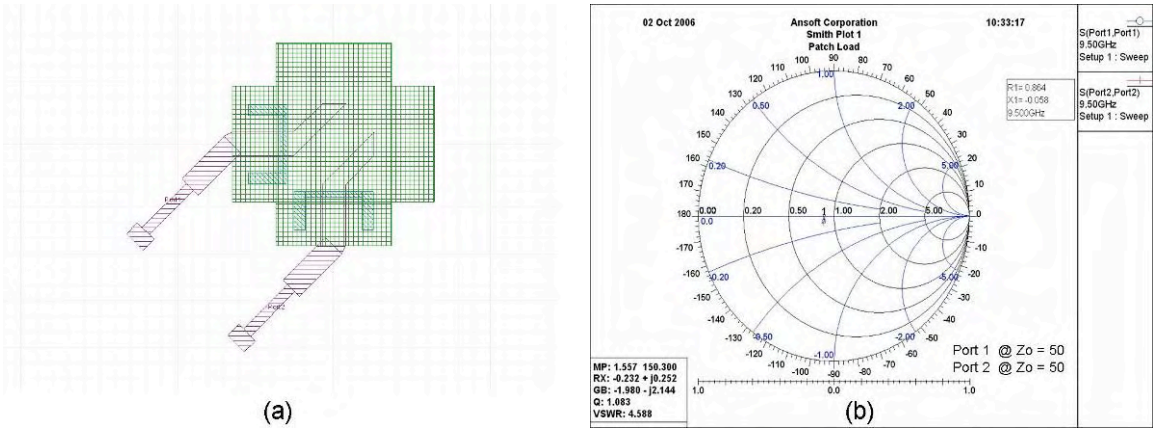

Figure 3.24 (a) A dual-Polarized patch antenna and (b) it input impedance shown in a Smith Chart.

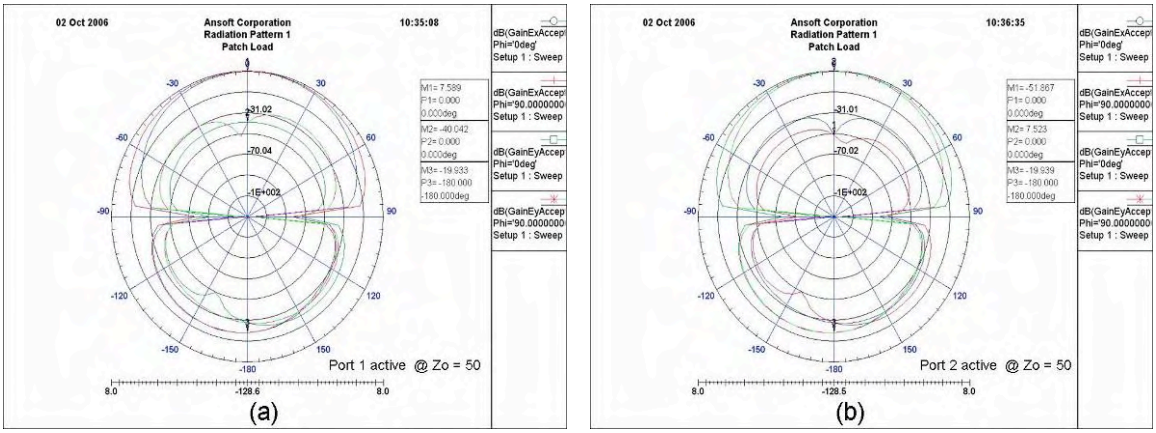

Figure 3.25 (a) Radiation pattern of antenna Port 1 active and (b) Port 2 active.

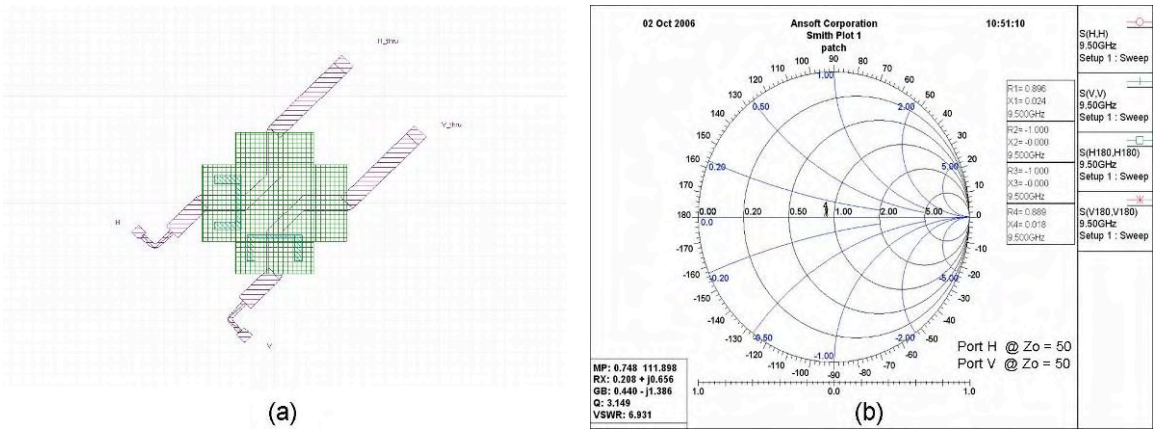

Figure 3.26 (a) A dual-Polarized patch antenna and (b) it input impedance shown in a Smith Chart.

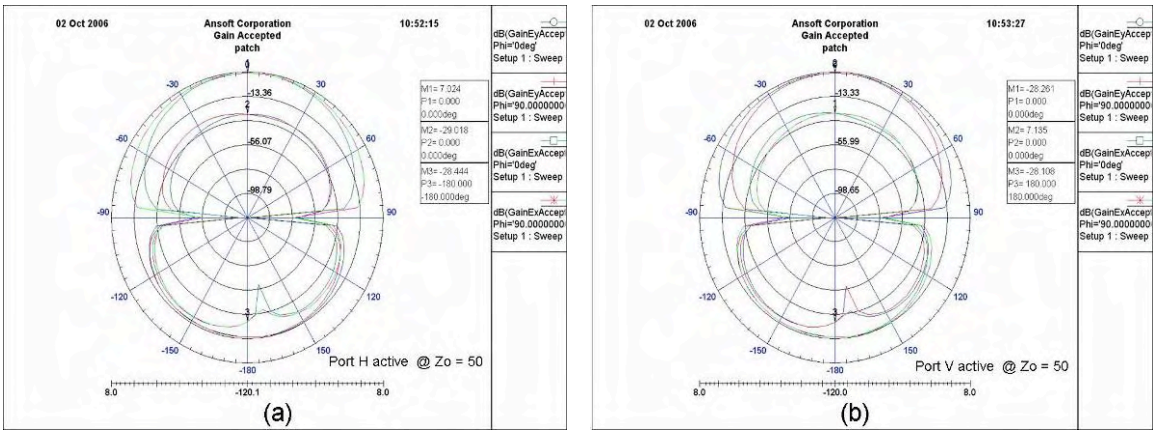

Figure 3.27 (a) Radiation pattern of antenna Port 1 active and (b) Port 2 active.

In the following section a more detailed procedure is presented for the four-port and the load radiating elements.

3.4 Design of Single Radiating Element

Because of the problems of cross polarization presented by the first configuration, an aperture coupled patch antenna was proposed. A new set of materials were chosen keeping in mind cost considerations and the parameters of this kind of antenna proposed in [7]. FoamClad who has a low dielectric constant (ε_r = 1.2) was used for the antenna

and RO 3006 who has a relatively high dielectric constant (ε_r = 6.15) for the feed lines. The way these elements are design allows them to be aligned in series, reducing the size on the feed network, thus reducing losses due to the feed lines.

3.4.1 4-Port Radiating Element design

The four-port antenna element consist of a cross patch, printed on a FoamClad sheet, with two offset orthogonal non-resonant H-shaped apertures etched on the middle ground plane coupling the patch to two parallel 50-Ohm microstrip lines running on the exterior side of the RO 3006 layer.

First, the radiating aperture is designed and simulated making its resonant frequency a few Mhz lower than the desired resonant frequency as seen in the Smith Chart in Figure 3.28. At 9.4 GHz the input impedance of the slot is around 220 Ω. The dimensions of the H aperture coupled slot where chosen using the following equations:

$$S = \frac{\lambda_g}{4} \qquad (1)$$

$$S_{Total} \approx \frac{\lambda_g}{2} \qquad (2)$$

where S is the length of the center slot.

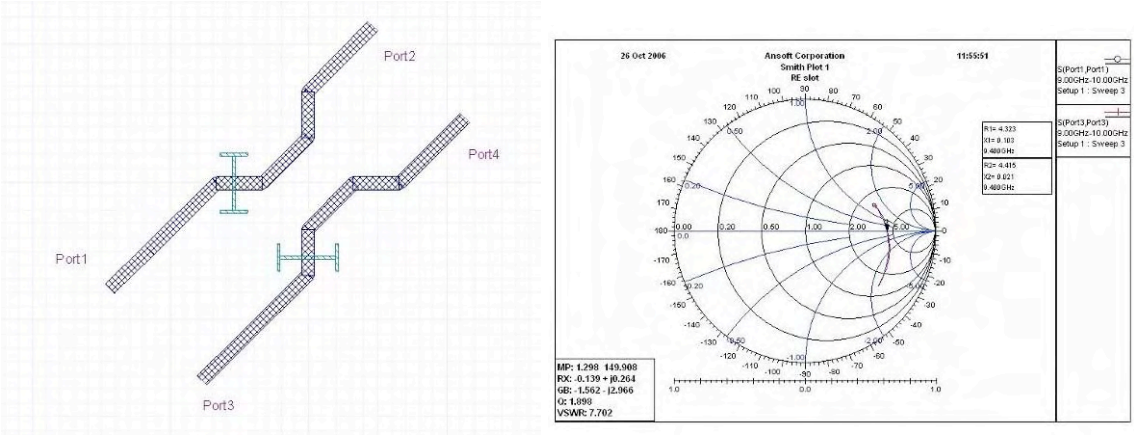

Figure 3.28 layout of feed line and aperture coupled slot (left) and return loss (rigth) for an input impedance of 50 Ω.

Then, the patch antenna is added on top of the slot and adjusted to resonate at 9.5 GHz, which is the desired operating frequency. For the design of the coupling aperture an H shape slot was used. H-shaped slots provide increased coupling and reduced backward radiation with respect to a rectangular slot of the same length [6]. Thus, the slot length required to obtain the desired coupling level is diminished, which is helpful in improving the isolation between the feeding ports. Figure 3.29 shows the basic geometry of the 4-port radiating element. Common values for the width of the slot (W_S) ranges from $\lambda_o/100$ to $\lambda_o/20$. For the design Ws = $\lambda_o/35$ was used. This width was selected to give a good front-to-back ratio and to lie between the fabrication limits of the milling machine that will be used at UPRM.

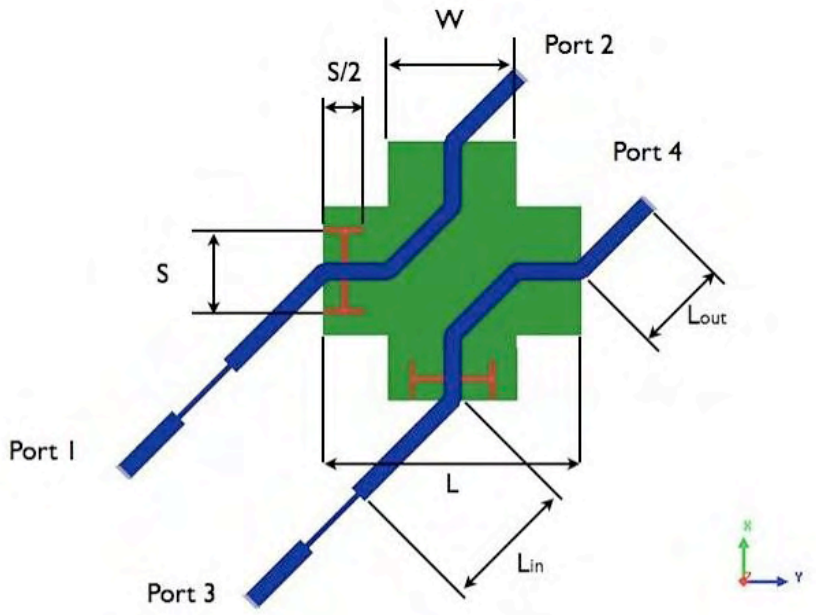

Figure 3.29 Geometry of the basic four-port H-shaped slot-coupled cross-patch element.

The size of the patch was first estimated using the cavity model method for a square patch. For optimization, the physical size of the patch was changed to a value in terms of λ_o, and its square shape changed to a cross-shape patch. Following the same patch design used in [10], the width of the cross arms equals half of the length (W = L/2). After optimization, the length of the patch, L, was set to $0.425\lambda_o$. The configuration provides three degrees of freedom, position of the aperture couple slot (ds) with respect to the center of the patch, length of the output feed lined (L_{out}) and the length of the input feed lines (L_{in}). The position of the aperture controls the coupling intensity, thus the input impedance. Maximum coupling is achieved when the slot is beneath the patch, and decreases significantly as it is moved to the edge of the patch, as explained in [4]. By selecting an appropriate position, the designer can control how much of the energy the patch will radiate and how much will it pass to the next element. The length of the port sections can be stretched or shrunk at their ends to adjust the phase of the four-port cross-patch transmission coefficient. L_{in} is used to eliminate the imaginary part of the input

impedance. Adjusting its length will make the S_{11} move in the Smith Chart as shown in Figure 3.30. By adjusting L_{out}, the designer controls the output phase angle so that when put the elements in series all of them have the same progressive phase.

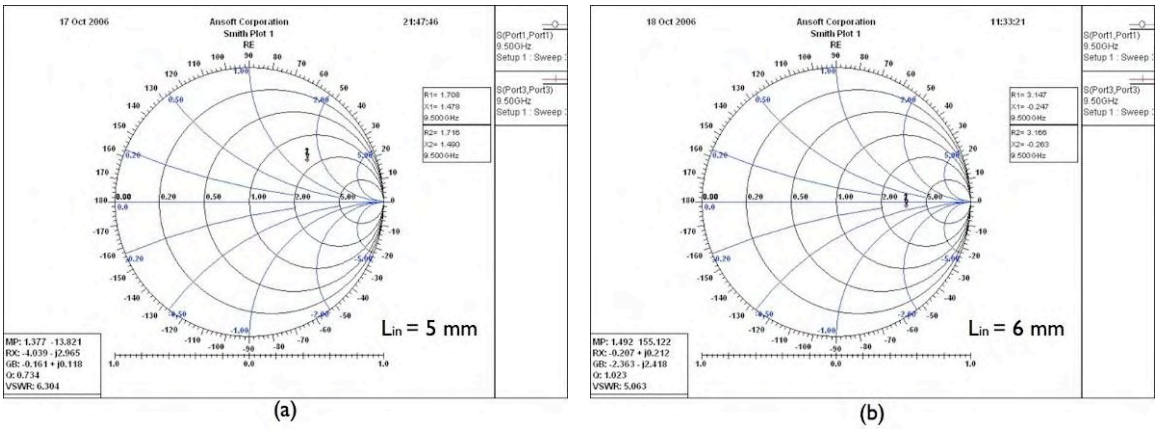

Figure 3.30 Return Loss (a) before and (b) after adjusting Lin.

3.4.2 Load Radiating Element

The load-radiating element is design similarly as the 4-port element. This element has to be designed to have the same progressive phase as the previous element to avoid deformation of the radiation pattern. This element also has more gain that the 4-port element due to the fact that it will radiate all the energy fed to it. Figure 3.31 shows the basic geometry of the patch load.

The high isolation between the two orthogonal resonant modes allows the radiation of linear or circular polarization. The design of the cross-patch can be performed by dimensioning each arm of the cross through standard computer-aided design (CAD) formulas for rectangular patches [17]. Sloping line sections are introduced to make the feed lines cross the slots at right angles to their center for maximum coupling.

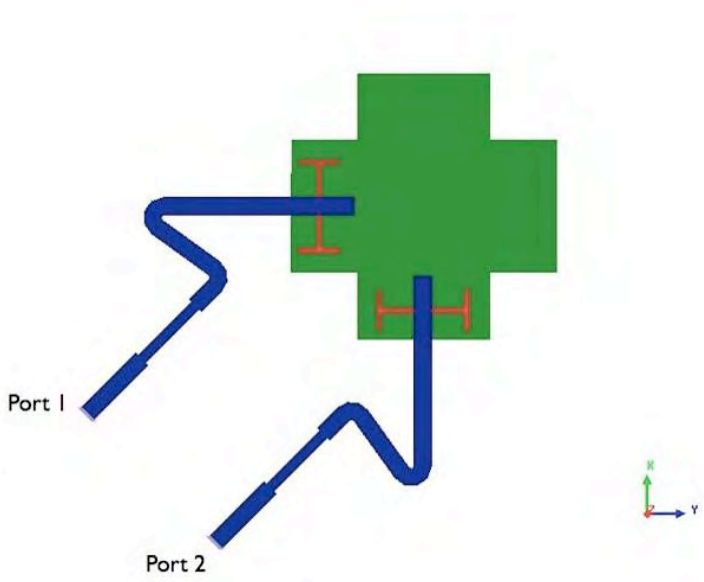

Figure 3.31 Geometry of the basic patch load, H-shaped slot-coupled cross-patch element.

As a result, the various antenna elements can be easily connected to form an equi-spaced array and a useful degree of freedom is introduced to perform the small adjustments that might be required for the final optimization of the excitation phases. Quarter-wave transformers are included in the feed network of the four-port element to impedance match the antenna at its input ports.

3.5 Prototype Fabrication

All the MSAs were simulated with the electromagnetic simulator Designer by Ansoft. To validate the results of the simulations, the MSA arrays were fabricated in a milling machine, the scattering parameters were measured using a network analyzer, and its radiation pattern were measured in the anechoic chamber. The design procedures and measurements were performed at the UPRM Radiation Laboratory.

4 RESULTS AND DISCUSSION

For radar applications it is important to have a very low return loss (< 20 dB) to avoid leakage due to saturation in a circulator between the transmitter and the receiver, for example. This means that a VSWR of 1.1 or lower would be needed, and the design presented meets this specification. For a precise QPE the transmitting/receiving polarization must be as pure as possible and the sidelobe level (SLL) as low as possible to avoid clutter. The SLL achieved was below the -20 dB and cross-polarization was below -30 dB for many of the arrays presented here. The mayor difference was the HPBW, which dictates the range of the antenna for the radar given a desired resolution. For example, a HPBW of 6º, which is the lowest HPBW achieved, gives a range of 9.5 Km. For a HPBW of 9º and 10º, the ranges are 6.4 Km and 5.73 Km respectively. Figure 4.1 shows the range of the antenna array for the desired cross-range resolution for the radar (+/- 500 m) as a function of HPBW.

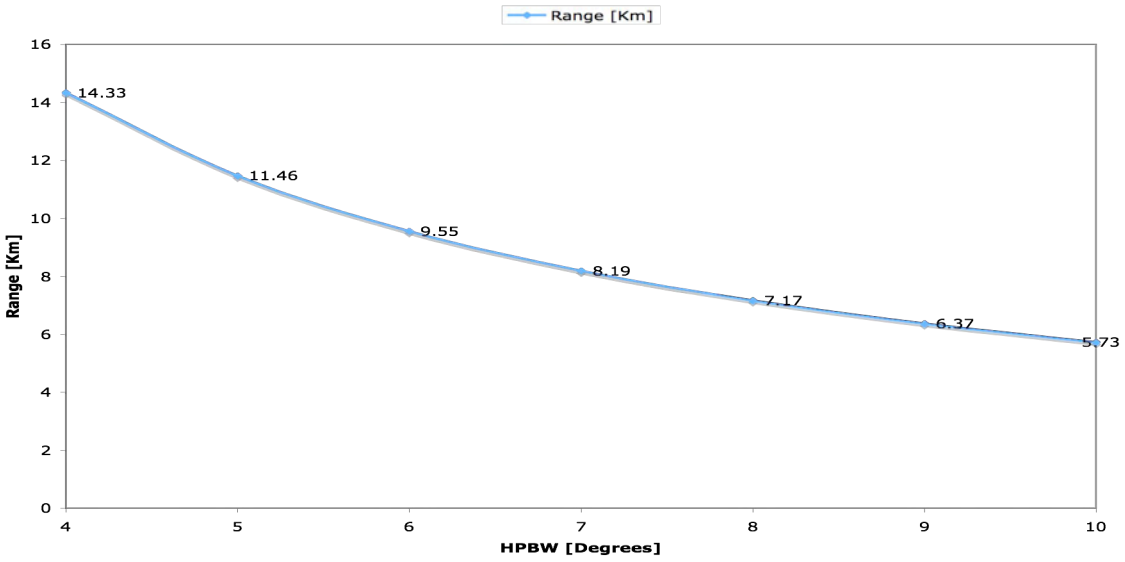

Figure 4.1 Plot of Range in Km as a function of HPBW in degrees for the desired resolution of the OTG radar.

This chapter discusses the results from both the individual elements that conform the linear array, as well the results obtained from the array itself. The specifications for

this antenna are: Half-Power Beamwidth (HPBW) around 6º, Bandwidth (BW) around 250 MHz, Sidelobe level (SLL) below -20 dB, Cross-Polarization below -30 dB and Front-to-back ratio below -13 dB. Results and comparisons based on the design parameters are also presented. The cross-patch elements have been designed and analyzed using Ansoft's Designer. All data is presented at 9.5 GHz except the VSWR plot, which is presented as a frequency sweep.

4.1 Individual radiating elements

In this section, the results for the 4-port radiating element and a patch load radiating element (PL) that will be used for a series feed linear array for CASA's Student Test-Bed radar. The results obtained for the array simulations are presented and discussed.

4.1.1 Simulation results of the 4 port Radiating Element

Based on the procedure explained in the previous chapter, the 4-port single element for the sub-array is presented in this section. Table 4.1 shows the final dimensions and variables values used for this element, and Table 4.2 presents the most relevant S parameters, like return loss and isolation between ports for both polarizations. Figure 4.2 shows a layout of a radiating element with its variable dimensions. Figure 4.3 presents the input impedance for ports 1 and 3 normalized with a characteristic impedance of 50 Ω, and Figure 4.4 shows the radiation pattern for the radiating element discussed in this section. The bandwidth of the element is shown in Figure 4.5, this figure plots the return loss and isolation between input ports in a frequency sweep from 9 to 10 GHz.

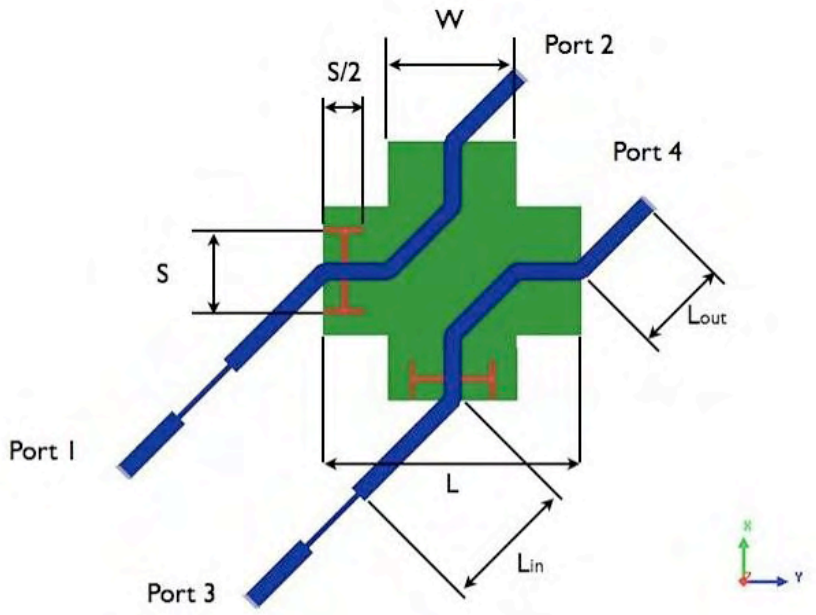

Figure 4.2 Geometry of the basic 4-port H-shaped slot-coupled cross-patch element.

Table 4.1. Final values for the 4-port element antenna.

Variable	λ_o	n	m	L	W	S	Lin	Lout	ds	Ws
Value	31.579 mm	0.25	0.425	$m\lambda_o$	L/2	$n\lambda_o$	6.9 mm	6.65 mm	L/2.5	S/35

Table 4.2. Results for the 4-port element antenna.

Measurement	S_{11}	S_{21}	S_{31}	S_{33}	S_{41}	S_{43}	Zreal	Zimag	VSWR port1	VSWR port2
Result	-30.64 dB	-3.30 dB	-30.67 dB	-28.87 dB	-29 dB	-3.35 dB	48.13 Ω	-2.2 Ω	1.06	1.07

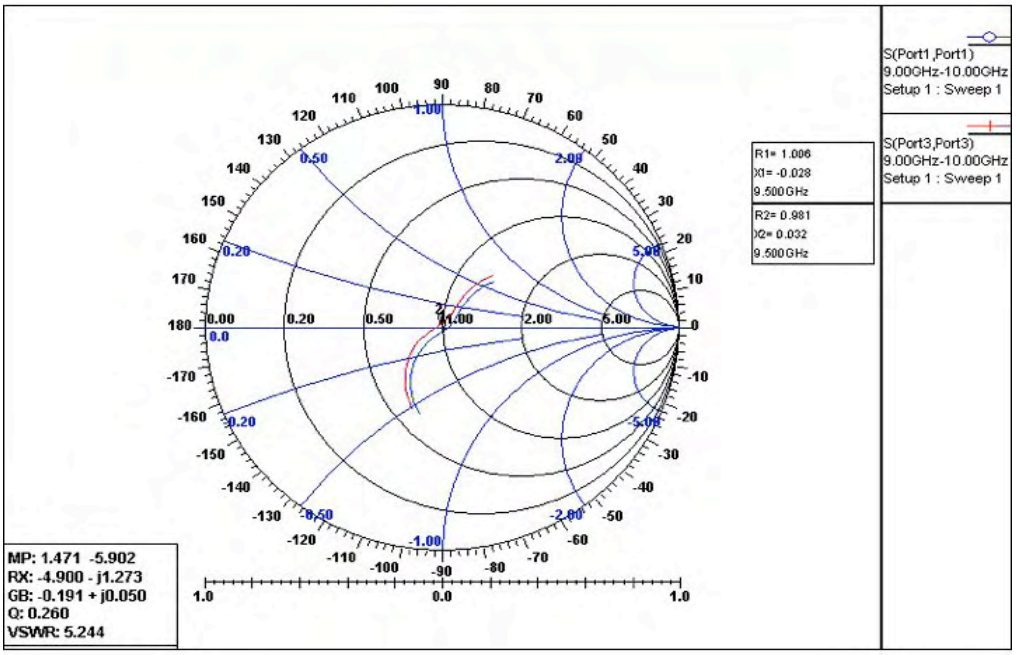

Figure 4.3 Input impedance for both input ports for 4-port radiating element.

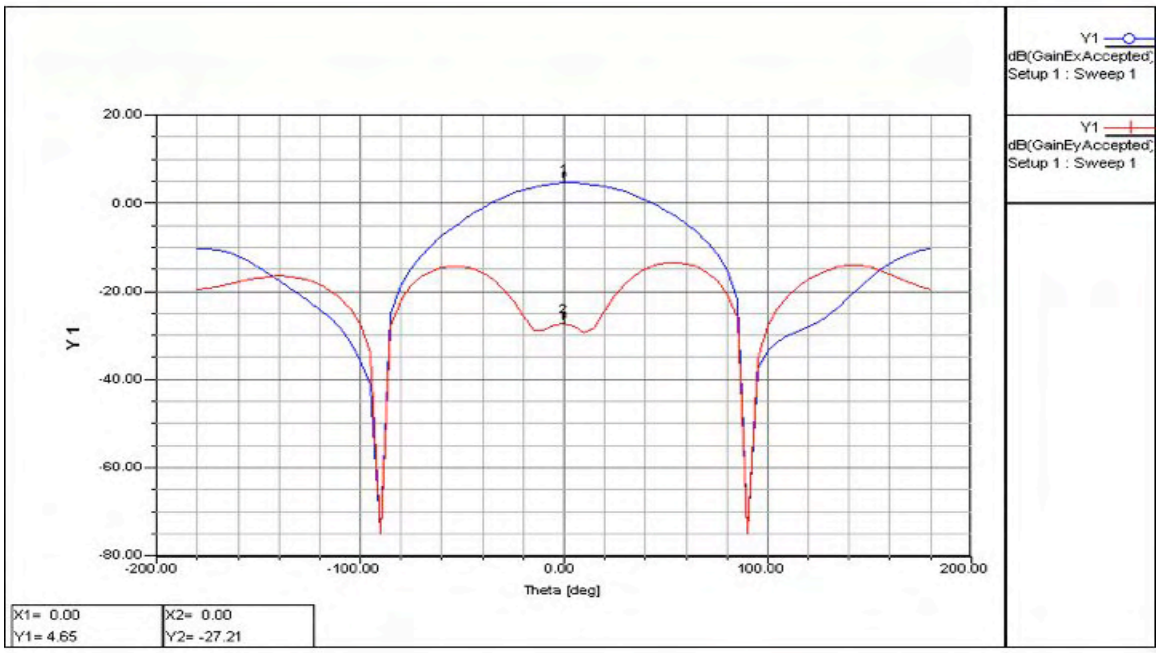

Figure 4.4 Radiation pattern for 4-port radiating element at 9.5 GHz.

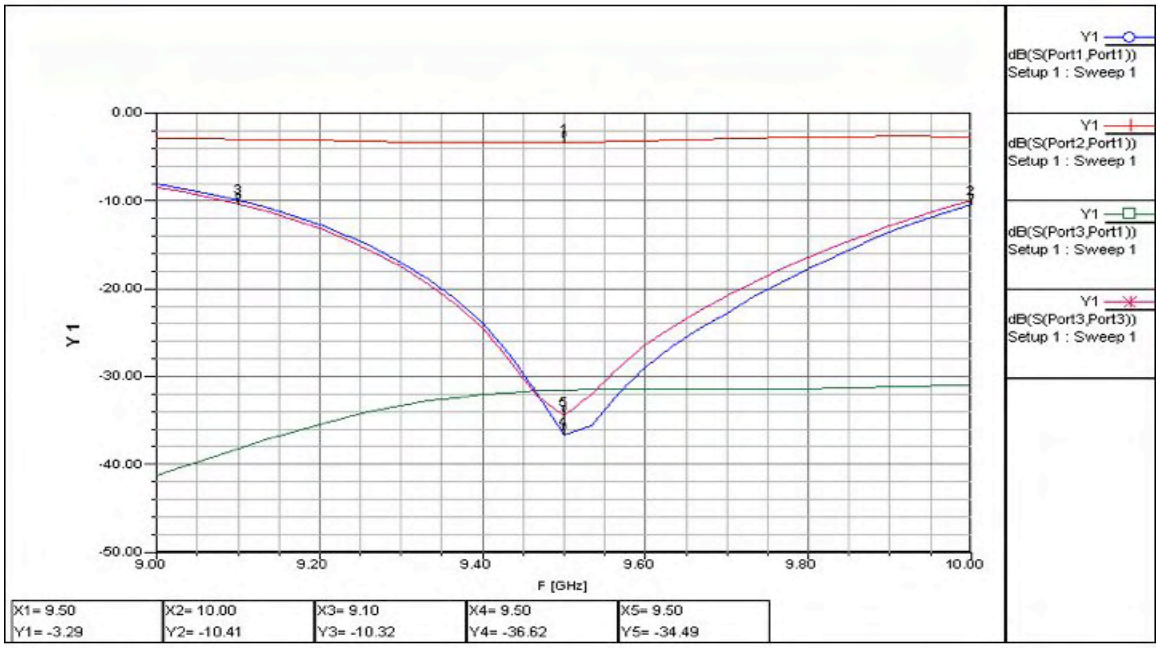

Figure 4.5 S-parameters for the 4-port element. The -10 dB bandwidth is 900 MHz.

Due to the similarity of the results for both polarizations (port 1 and port 3), the results presented are from port 1 active only. The advantage of the antenna symmetric arrangement and the aperture coupling feeding technique is that very low cross-polarization levels are observed. Note that the 4-port element design has a cross-polarization around -32 dB. The isolation between ports (S_{41} and S_{31}) is around -30 dB, and the return loss is around -29 dB, which gives a VSWR close to 1.1. The transmission coefficient is around -3.35 dB and the gain is 4.78 dB. A wide impedance bandwidth of 10.5 % is obtained due to the fact that the aperture is a non-resonating slot.

4.1.2 Simulation results of the Load Radiating Element

For the load-radiating element, since it is desired to radiate all remaining energy, a resonating element must be designed. The design in [17] suggests that the size and position of the aperture-coupling slot and the size of the patch will differ from the 4-port element in order to achieve 50 Ω input impedance. In order to have all the radiating

elements of equal size the dimensions of the patch and the coupling-slot patch of the 4-port element were used for the radiating element as well. Figure 4.6 shows the final layout for this element, and Table 4.3 presents the results obtained for this element.

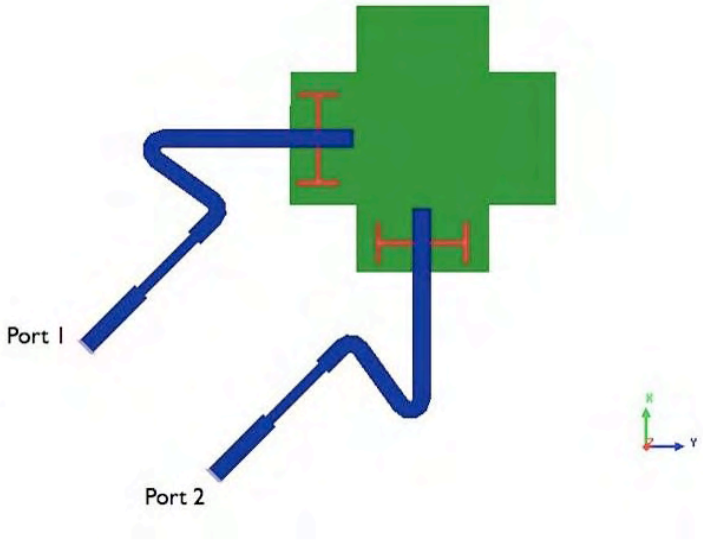

Figure 4.6 Basic layout of patch load radiating element.

Table 4.3. Results for redesign load element at 9.5 GHz.

Measurement	S_{11}	S_{21}	S_{22}	Z_{real}	Z_{imag}	VSWR port1	VSWR port2
Result	-22.13 dB	- 22.29 dB	-20.76 dB	49.25 Ω	7.75 Ω	1.17	1.2

The load element exhibits a cross-polarization around – 26.28 dB, which is 5.79 dB higher than the 4-port element, yet more than 3 dB better than it previous versions. Because this element is designed to radiate all the energy applied, it has almost twice the gain (7.45 dB) that the 4-port element. Figure 4.7 and Figure 4.8 present the radiation pattern of this element and its input impedance in a Smith Chart. Figure 4.9 shows the return loss and insertion loss plots of a frequency sweep from 9 GHz to 10 GHz where it

can be seen that this element has a bandwidth around 5.8 %, which is expected since the resonant type of the excitation is responsible for a narrower impedance bandwidth.

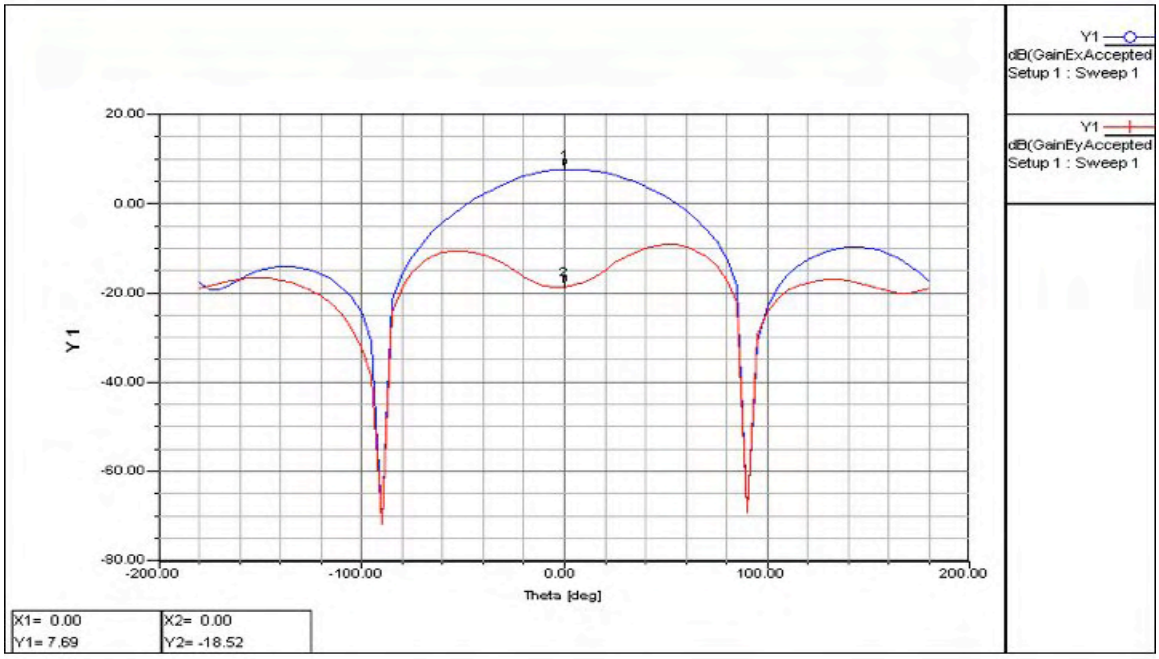

Figure 4.7 Radiation pattern for the patch load radiating element at 9.5 GHz.

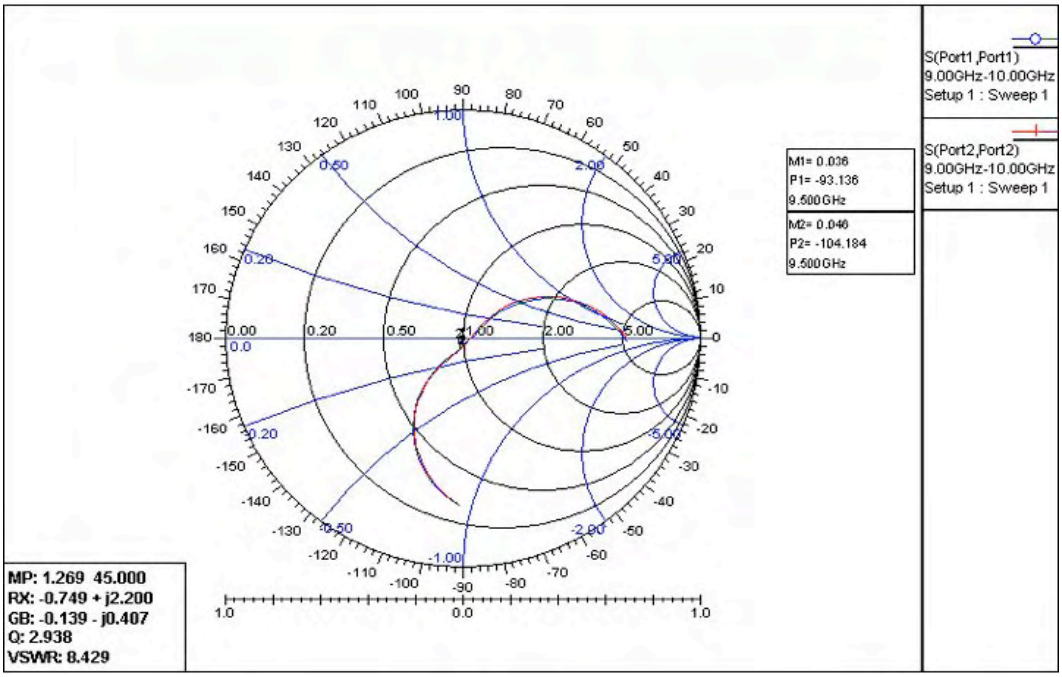

Figure 4.8 Input impedance for both input ports for the load radiating element.

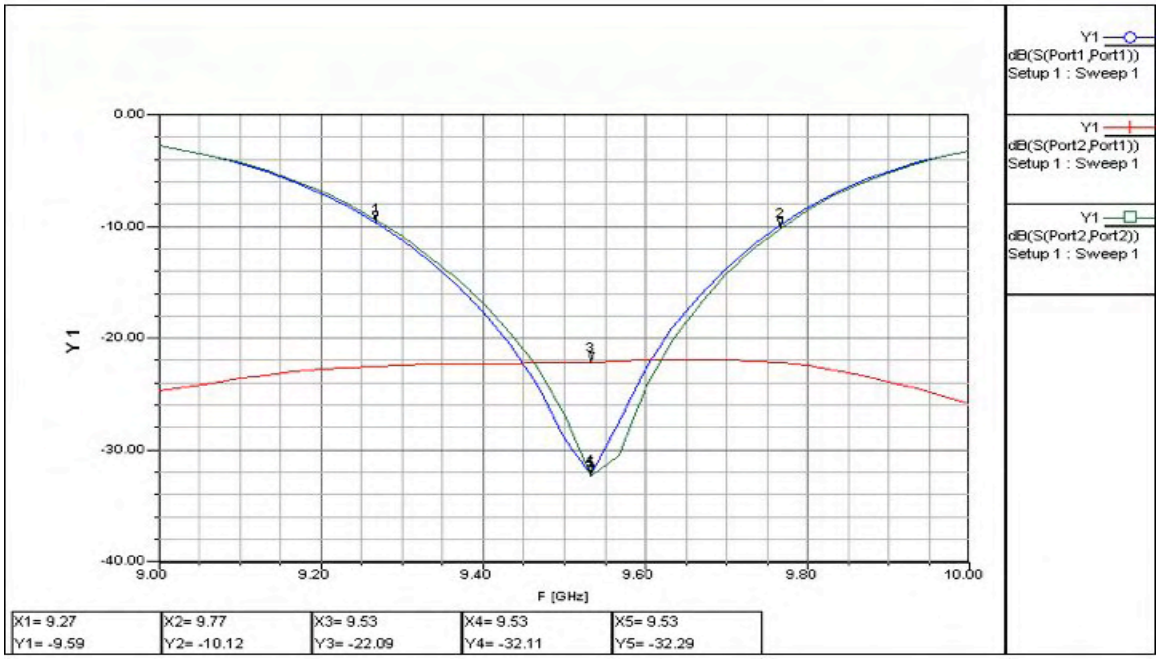

Figure 4.9 S-parameters for the load radiating element. The -10 dB bandwidth around 500 MHz.

4.2 Simulation results of Array using Designer

The linear array consists in connecting the four–port radiating element in series and adjusting L_{out} to compensate for phase offset if necessary. Two linear arrays of 12 elements composed of two sub-arrays of 6 elements each were simulated. The arrays are placed one mirroring the other and have to be fed with a phase offset of 180º as shown in Figure 4.10.

The first one contained only the four-port element with 50 Ω ports at the end to simulate load resistors of the same resistance. The second one consists of five of the 4-port elements loaded with the patch load element. The following presents the results for these linear antenna arrays.

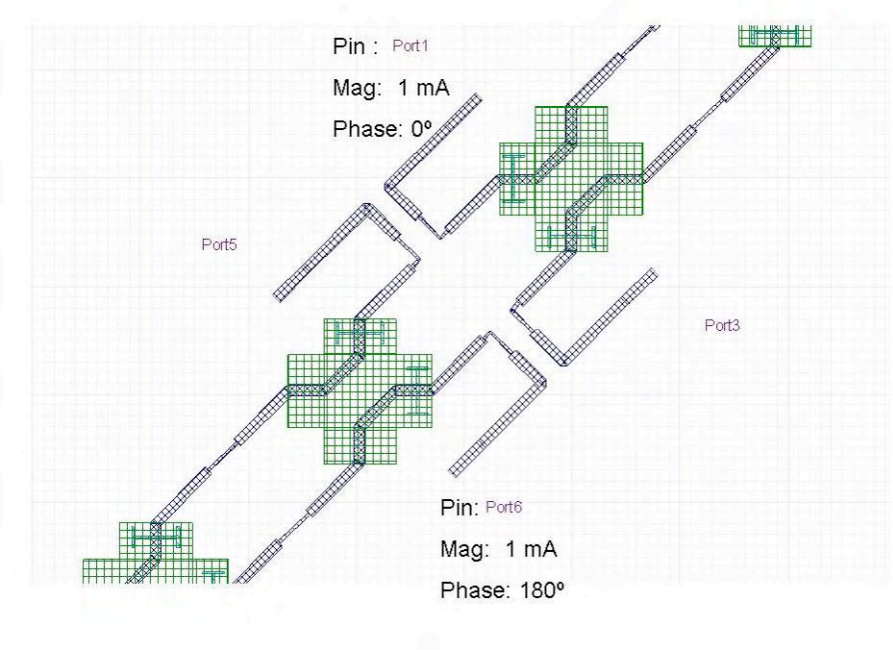

Figure 4.10 Port excitation for horizontal polarization.

4.2.1 Array of 4-port Radiating Elements

It is important to point out that because the array uses the same element connected in series, and the 4-port element is a non-resonating element, a current distribution is achieved similar to a traveling wave antenna. The ability of frequency scanning is disabled because each sub-array will scan in opposite direction to one another. This occurs because each sub-array is positioned in a manner that creates a center-fed linear array.

The first array consists of 2 sub-arrays composed by only 4-port elements loaded at their ends with 50 Ω resistors to dissipate the power remaining at the end of each sub array. This section discusses the results obtained for different sizes of arrays ranging from 2 elements in each sub array (4 elements in total) to 7 elements in each sub array. Table 4.3 shows the results obtained by adding one element to each sub-array up to seven elements each sub-array.

Table 4.4. Results at 9.5 GHz for sub-arrays using only the 4-port element in series.

Quantity of elements in sub-array	2	3	4	5	6	7
Zin_avg	45.86 +j1.46	45.58 +j3.75	45.51 +j5.54	45.66 +j6.20	45.01 +j6.96	45.51 +j6.99
RL_avg [dB]	-27.11	-23.22	-22.41	-21.75	-20.00	-21.95
S21 [dB]	-6.21	-8.9	-11.51	-14.02	-16.58	-18.79
S31 [dB]	-29.59	-28.87	-27.59	-28.31	-28.05	-27.71
S51 [dB]	-23.91	-23.37	-23.19	-23.15	-23.00	-23.28
SLL [dB]	15.14	19.52	22.19	21.19	21.72	20.32
HPBW	~ 16°	~ 11°	~ 8°	~7°	~ 6°	6°
XP [dB]	29.96	38.49	38.78	32	29.61	28.29
FBR [dB]	15.55	16.20	16.53	16.66	16.76	16.85
Gain [dB]	12.46	14.72	16.00	16.98	17.53	17.98

By connecting the 4-port element in series it can be seen in Table 4.4 that the gain and SLL tend to stabilize due to the fact that a constant percentage of the power entering a 4-port element is being radiated broadside and the remaining power spread along the array itself, transmitted from one element to the next. As the amplitude of the **E** field decreases, the **H** field also decreases, making the Coupling between the feed line, the slot and the microstrip patch decrease due to the proportionality between the **H** field and Coupling. As seen in Table 4.4 an element added to the sub-array (from 2 to 6) will radiate in average about 2.59 dB, and pass forward the remaining power. When the element number 7 is added to each sub-array, note that the power radiated drops to 2.2 dB suggesting that adding further elements to the array will increased the effective area of the antenna but increasing only .4 dB in the gain of the array. Figure 4.11 presents a graph that plots gain of the array and HPBW as a function of quantity of elements in the array. Note that sub arrays of 6 and 7 elements have the HPBW requested. The 6-element sub-array results are comparable with the 7 elements sub-array, making the 6 elements sub-array is a better choice for testing.

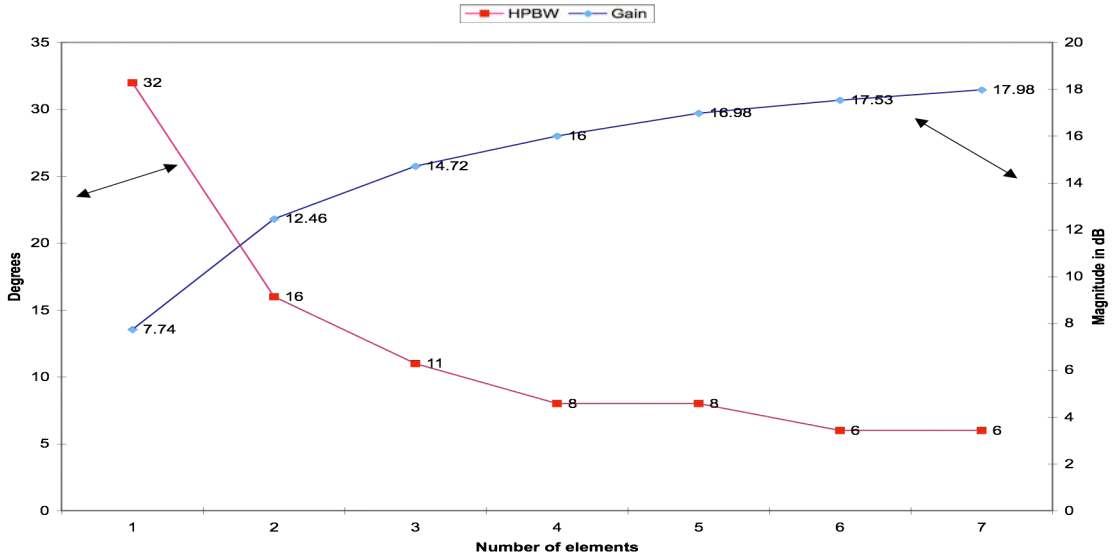

Figure 4.11 Gain and HPBW as a function of number of elements in the array.

For the arrays simulated, the average return loss for the array ports is below -20 dB. This means that the average of the VSWR is around 1.1. With the port configuration of Figure 4.10, the isolation between ports 1 and 3 (S_{31}) and ports 1 and 5 (S_{51}) is around -28 dB and -23 dB, respectively. It was desired to maintain the isolation between ports as close to -30 dB as possible, but in order to optimize and lower S_{51}, the distance between the center elements of the array (the first element of the sub-arrays) must be increased. By doing this, the difference in distance between each element of the array produces high SLL, beam broadening and grating lobes.

The phase offset at the end of each sub array ranges from 2º to 4º, depending in how far the element is from the feed point. As we move farther away from the input ports, less power is radiated by the elements and a larger phase offset is observed. For an array of 12 elements, 6 elements per sub-array, terminated with 50 Ω ports, the Front-to-Back ratio (FBR) is -16.76 dB. Sidelobe level (SLL) and cross-polarization (XP) have values of 21.7 dB and -29.6 dB respectively, just 0.4 dB shy of our 30 dB specification limits for cross polarization. Note that the array composed of sub-arrays of 4 elements

has the lowest cross-polarization level, which is almost -39 dB, and SLL of 22 dB. The rest of the arrays maintained a cross-polarization of about -30 dB.

Figure 4.12 to Figure 4.17 shows the radiation patterns for arrays consisting of sub-arrays of 2 to 7 elements for each sub-array.

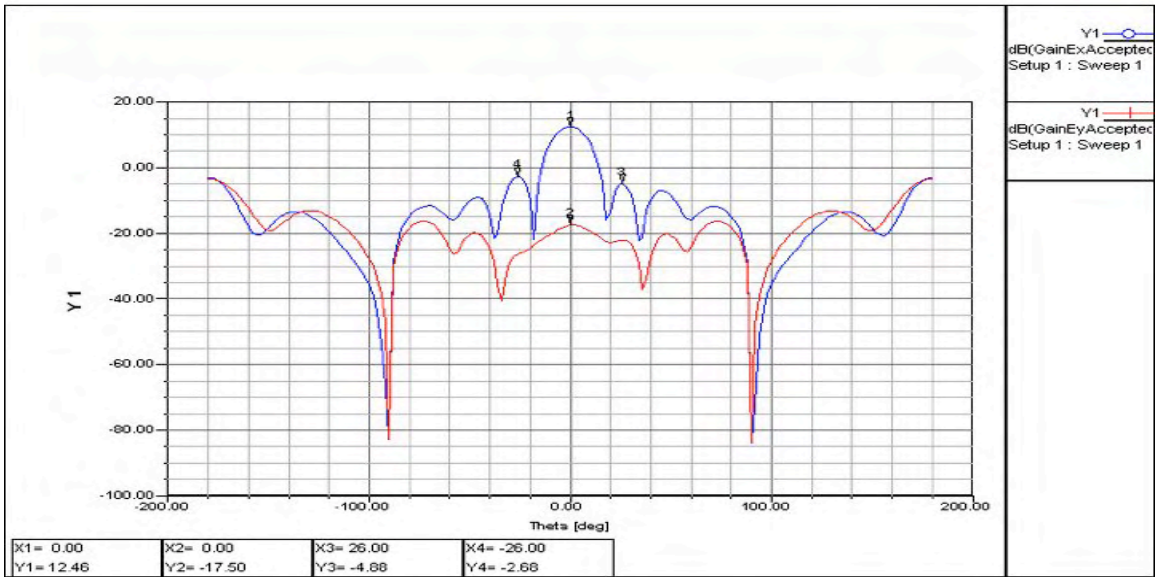

Figure 4.12 Radiation pattern of array composed of two sub-array of 2 elements.

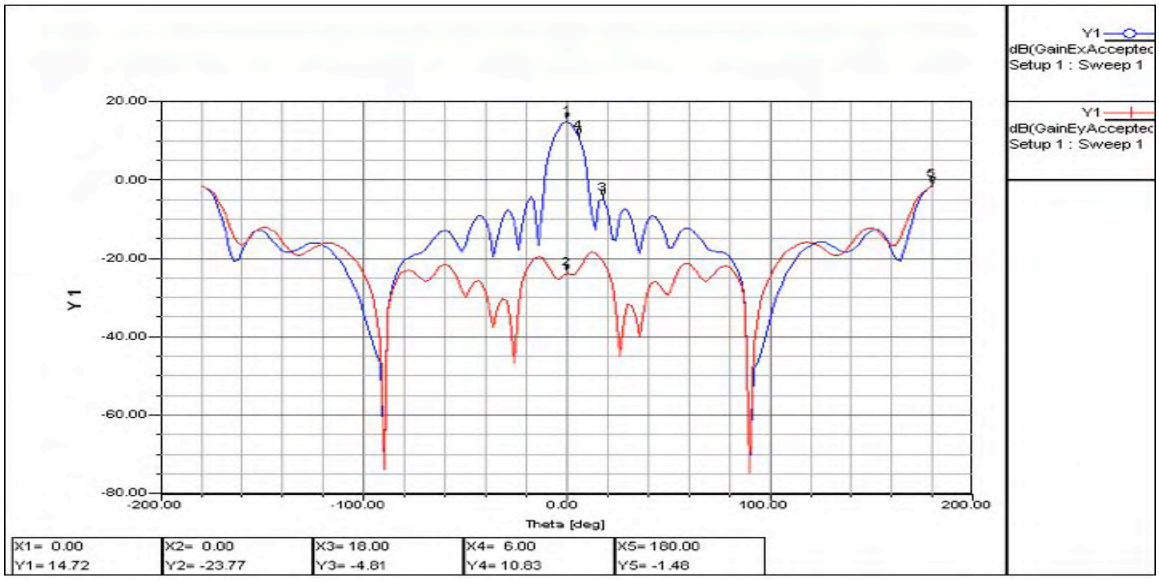

Figure 4.13 Radiation pattern of array composed of two sub-array of 3 elements.

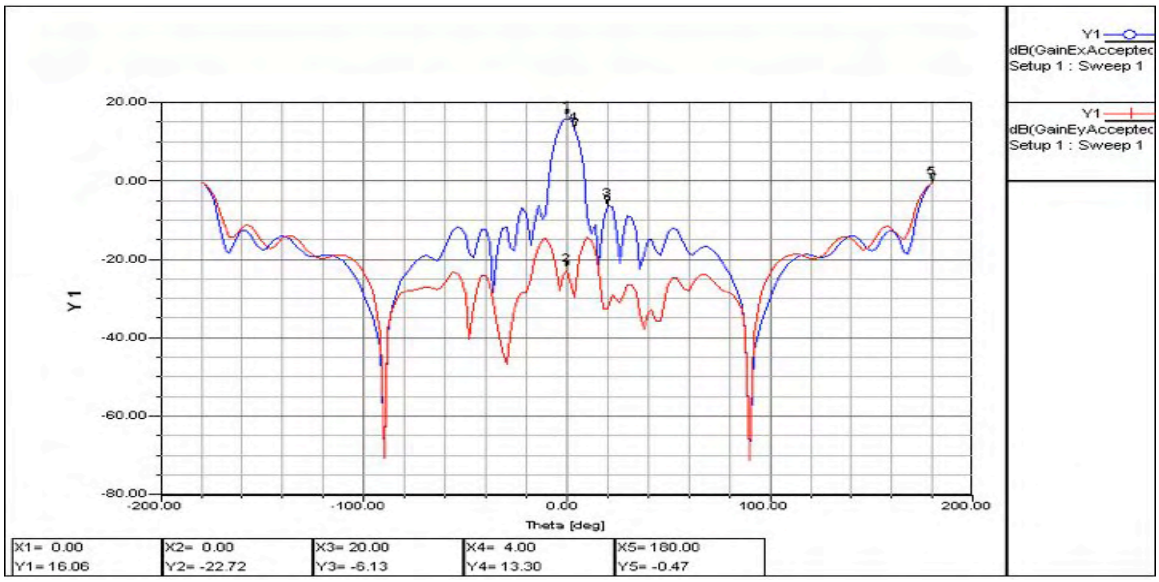

Figure 4.14 Radiation pattern of array composed of two sub-array of 4 elements.

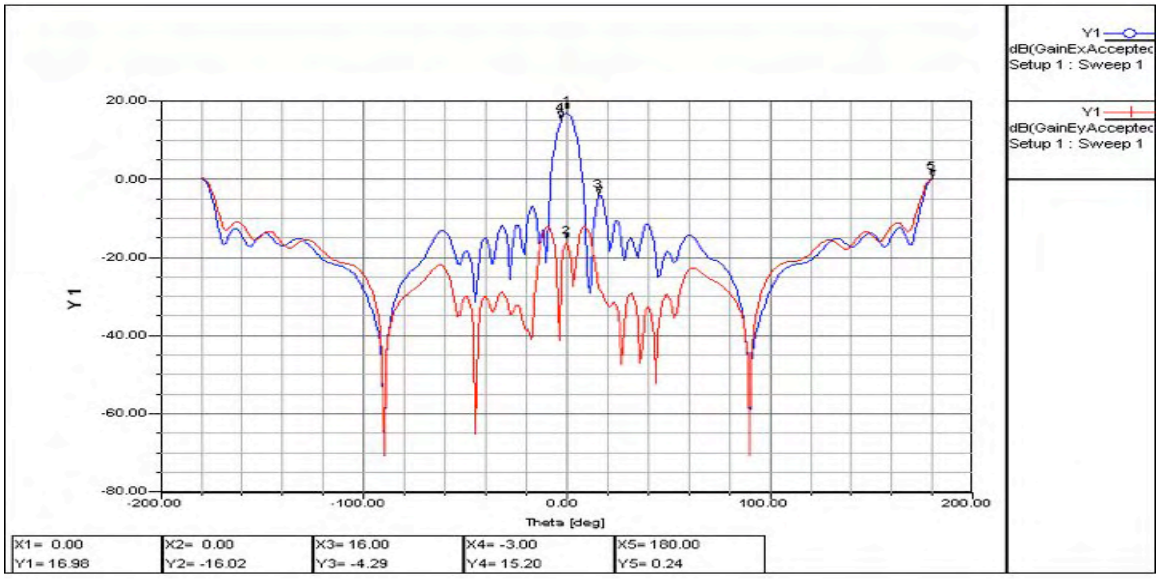

Figure 4.15 Radiation pattern of array composed of two sub-array of 5 elements.

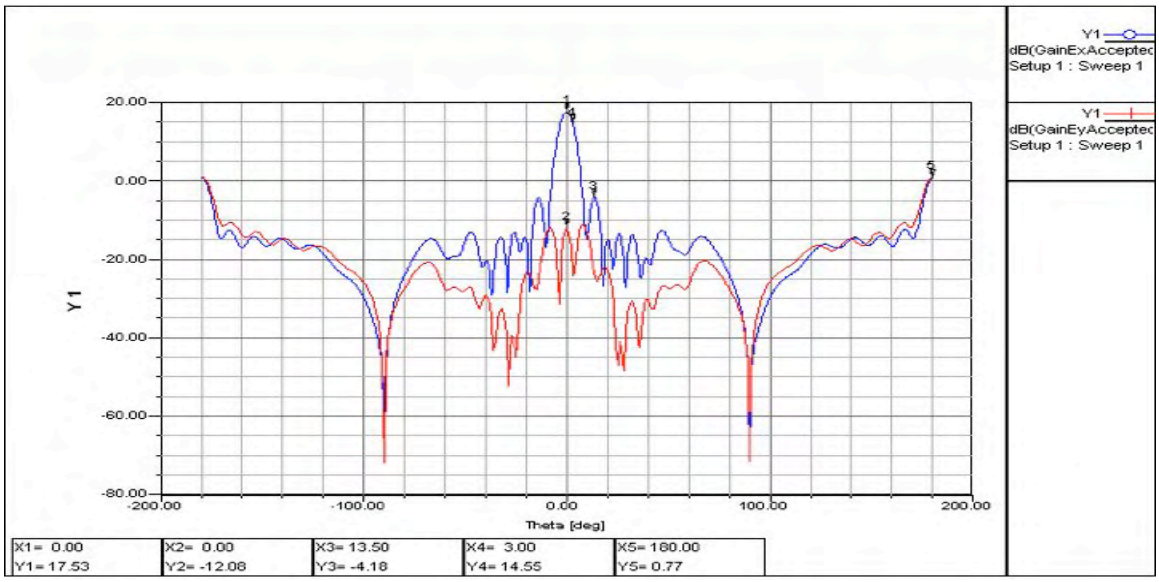

Figure 4.16 Radiation pattern of array composed of two sub-array of 6 elements.

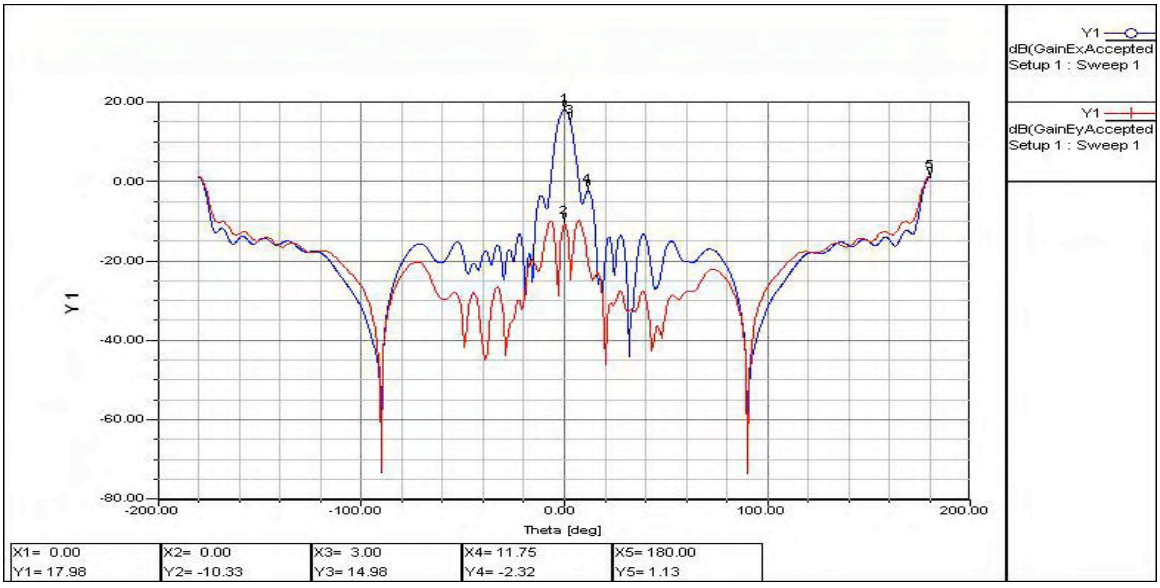

Figure 4.17 Radiation pattern of array composed of two sub-array of 7 elements.

4.2.2 Array with Radiating Element Load

The second array consists of 2 sub-arrays of six elements, five 4-port elements and a load element at the outer ends of the array. Figure 4.18 shows a layout of the array

discussed, and Figure 4.19 presents its input impedance normalized in a Smith Chart. From the Smith Chart in Figure 4.19 it can be seen that the average input impedance of the array is about 45.96 + j5.29 Ω, giving a return loss of approximately -23.16 dB. Figure 4.20 shows the radiation pattern for the array. It can be seen that the gain of the array drops 1.29 dB, from 17.53 dB to 16.24 dB, and that the front to back ratio is about -16.24 dB, as expected. Significant changes are seen in the cross-polarization, SLL and HPBW. The cross-polarization achieved is -37 dB, which is around 7.5 dB better than the array with out the PL. The SLL and HPBW change significantly due to the fact that adding the radiating load changes the current distribution of the array. The SLL is 5.55 dB lower for the array with the radiating element; 16.17 dB for the array with PL and 21.72 dB for the array without it. Changing the last element with the PL not only raised the SLL but also broaden the main beam of the array causing an increment in the HPBW of 3º. The HPBW is incremented using the PL from 6º to 9º.

The decrease in SLL is due to the fact that the last two elements of each sub-array (PL) radiate the remaining power. The load element has twice the gain that the 4-port element, the far edges of the array radiating more power than the elements before them.

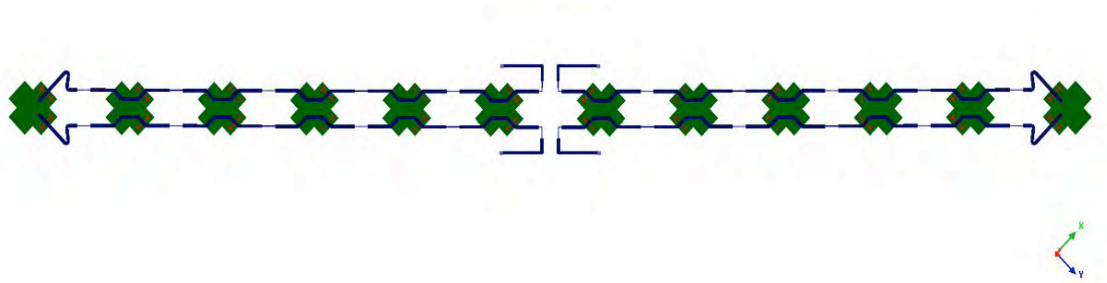

Figure 4.18 Layout of array loaded with radiating elements, 6 elements per sub-arrays.

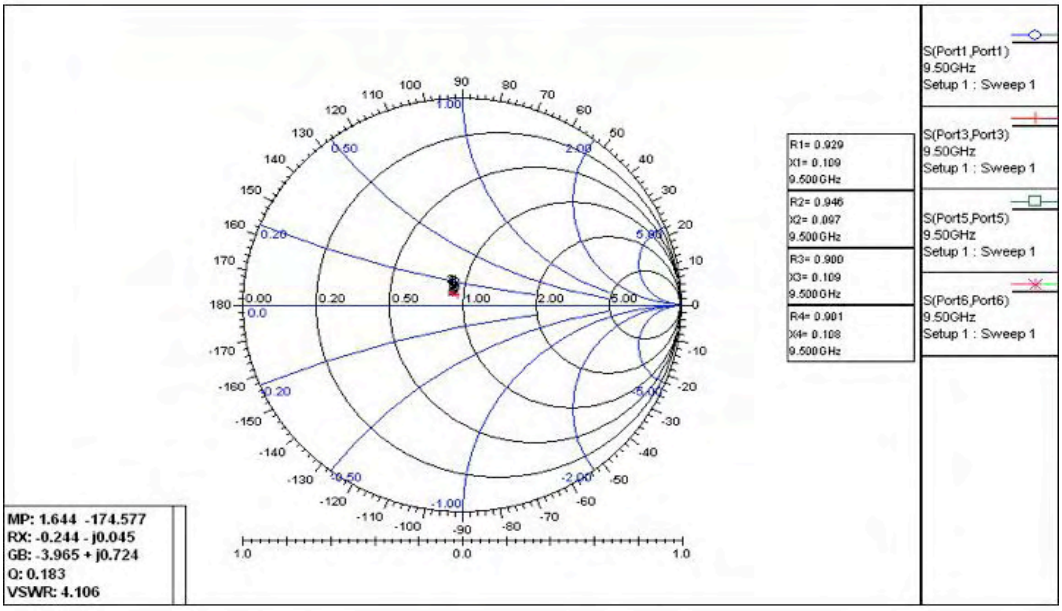

Figure 4.19 Input impedance for 12 element linear array using load radiating elements in Smith Chart normalized to 50 Ω at 9.5 GHz.

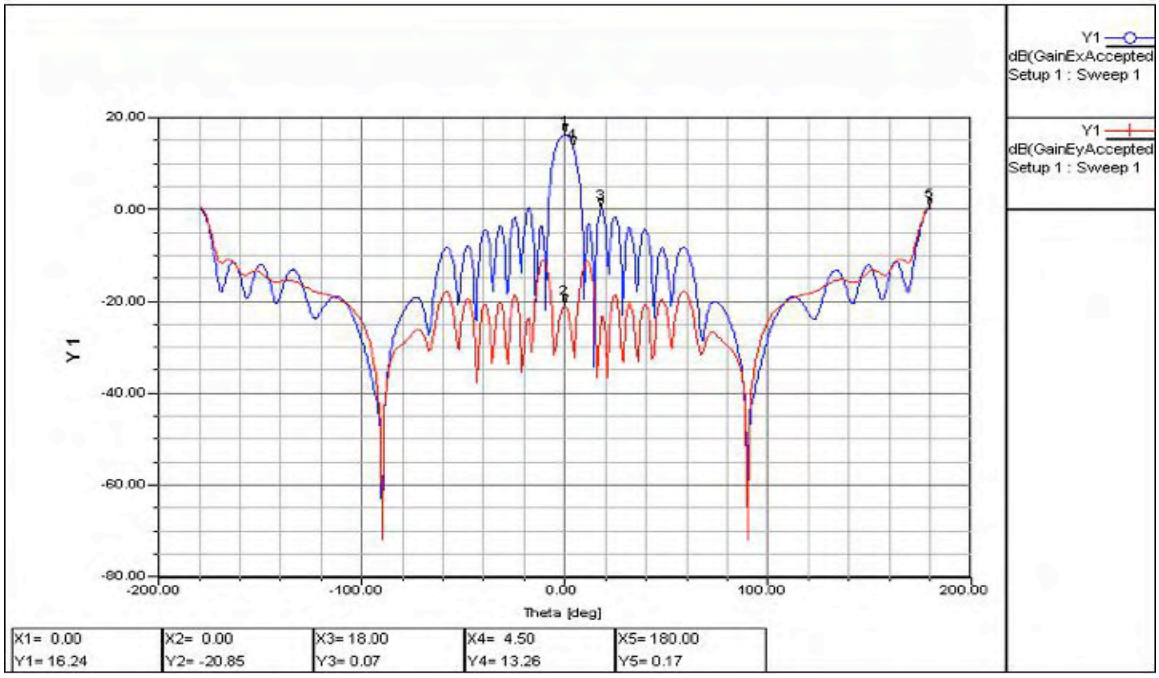

Figure 4.20 Radiation pattern for a 12 element linear array with load radiating element at 9.5 GHz.

A 14 element linear array (7 element for each sub-array), again using a PL for the last element of the array was simulated. Figure 4.21 shows a Smith Chart with the input impedance of each of the four ports of the array. In average the input impedance of the array is 46.2 + j5.65 Ω, which gives a return loss of -23.02 dB. The radiation pattern of this array is presented in Figure 4.22. Comparing this array with its counter part in the previous section, again a drop in gain occurs for this array, this time less than 1 dB. The gain for the array discuss in this section is 17.1 dB, which is .88 dB lower than the array without the PL. As for the front-to-back ratio, it is still around -16 dB, dropping from -16.85 dB to -16.43 dB. Just as the array discussed earlier in this section the current distribution in the array is altered by the use of the PL, but the changes is less significant in the SLL. The difference in SLL is of .77 dB, having 19.55 dB for the array with PLs and 20.32 for the array without it. Still the use of the PL broadens the main beam causing a raise in HPBW from 6º to 9º. The cross-polarization, again shows improvement with -33.35 dB, which is 5.06 dB better than the array without the PL.

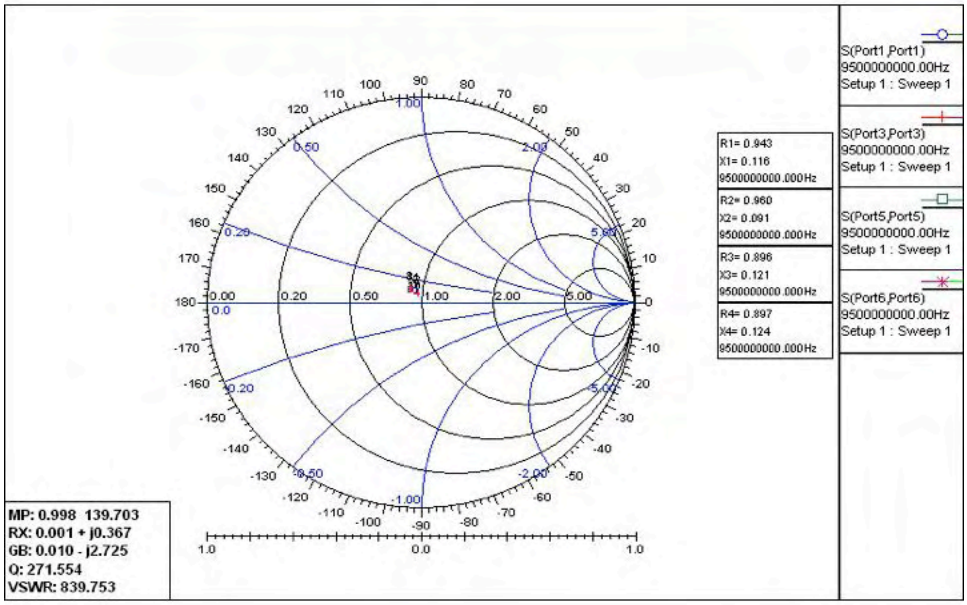

Figure 4.21 Input impedance for 14 element linear array using load radiating elements in Smith Chart normalized to 50 Ω at 9.5 GHz.

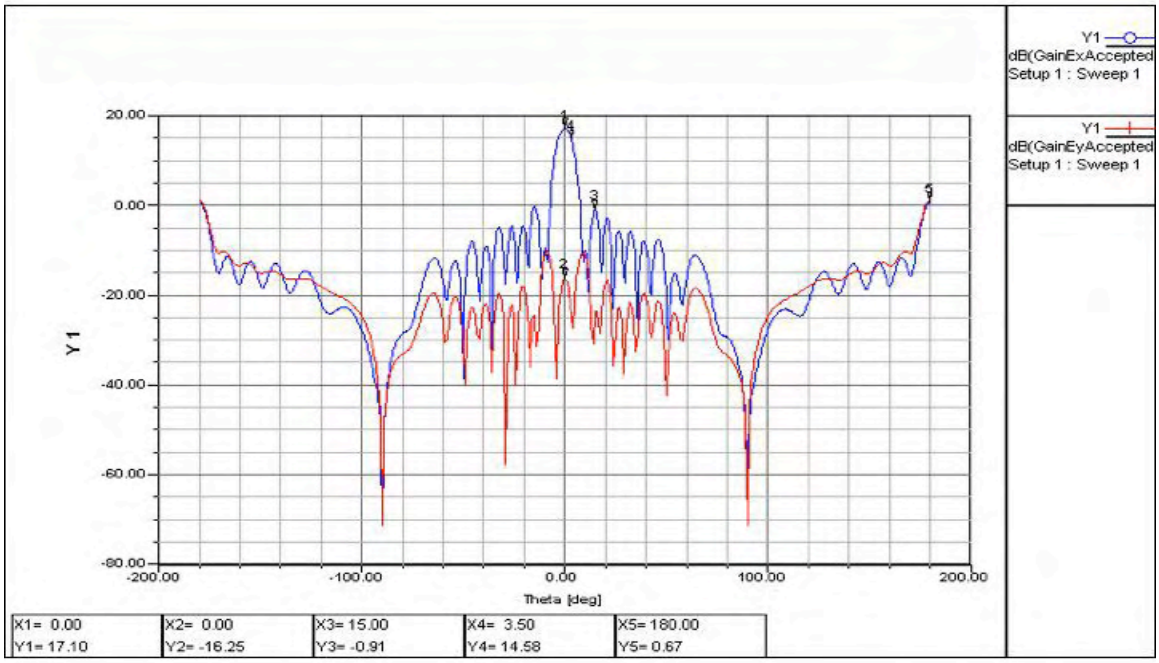

Figure 4.22 Radiation pattern for a 14 element linear array with load radiating element at 9.5 GHz.

Table 4.5 summarizes the results obtained for the arrays discussed in this section.

Table 4.5. Results at 9.5 GHz sub-arrays composed of 4-port element in series and PL at the end.

Quantity of elements in sub-array	Zin_avg	RL_avg [dB]	S31 [dB]	S51 [dB]	SLL [dB]	HPBW	XP [dB]	FBR [dB]	Gain [dB]
6	45.96 +j5.29	-23.16	-26.85	-23.67	16.17	~ 9°	37.09	16.07	16.24
7	46.2 +j5.65	-23.02	-28.04	-23.26	18.01	~7°	33.35	16.43	17.1

By using the load radiating element or patch load (PL), the cross-polarization is improved significantly, but the SLL and specially the HPBW are degraded to undesired levels. The following sections discuss alterations of the array. The first alteration is in the feed lines and the second alteration is in the position of the slots. For the sake of

comparison all the arrays discussed from this point forward are composed of 12 and 14 elements.

4.2.3 Array of 4-port Radiating Elements with curved feed lines

The array presented in this section is basically the same discussed earlier, but the feed lines under the coupling slots are slightly modified. Figure 4.23 shows the modification made to the feed line, which is making the feed line curves, thus smoother on the line bends than the original array.

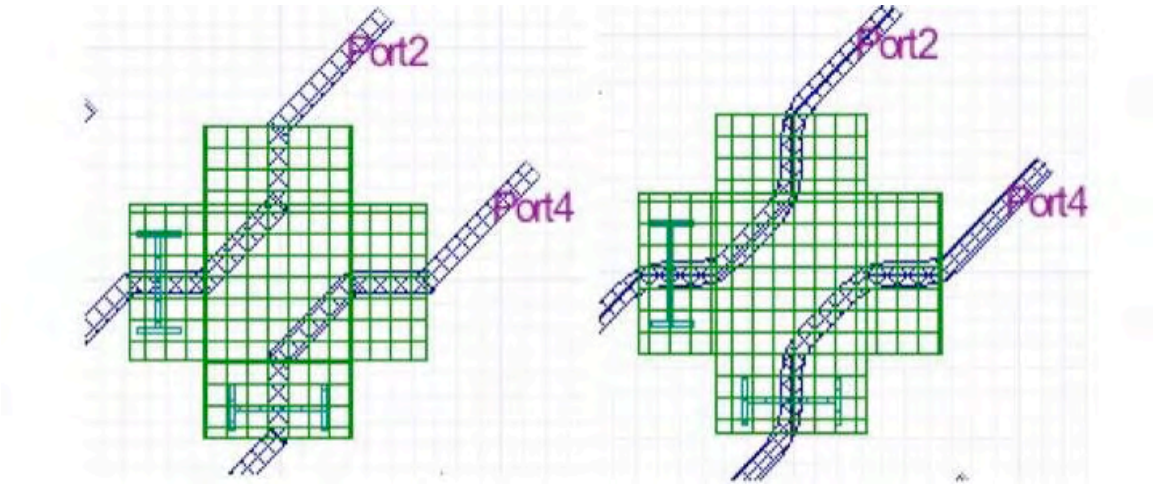

Figure 4.23 Original feed lines of the array (left), and modified feed line discussed in this section (right).

Again the array presented consists of 2 sub-arrays of composed by only 4-port elements loaded at their ends with 50 Ω resistors to dissipate the power at the end of the sub arrays. This section discusses the results obtained for sizes of arrays of 6 elements each sub array (12 elements in total) to 7 elements each sub array. Table 4.6 presents the results obtained for these two arrays.

Table 4.6. Results at 9.5 GHz for sub-arrays using the 4-port element in series with curved feed lines.

Quantity of elements in sub-array	Zin	S11 [dB]	S31 [dB]	S51 [dB]	S66 [dB]	SLL [dB]	HPBW	XP [dB]	FBR [dB]	Gain [dB]
6	44.7 +j0.13	-24.81	-26.77	-23.67	-24.63	28.30	~ 7°	31.56	16.78	17.17
7	45.24 -j0.78	-26.83	-25.91	-23.82	-24.45	31.82	~7°	31.82	16.85	17.48

As seen in Table 4.6, the average input impedance for the array of 12 elements is 45.28 + j0.56 Ω giving a return loss of -26 dB. The isolation between ports 1 and 3 (S_{31}) and port 1 and 5 (S_{51}) for this array is around -26.77 dB and -23.67 dB respectively. The Front-to-Back ratio (FBR) is -16.78 dB, almost the same as the original array with the same amount of elements. Cross-polarization (XP) for the array is -31.56 dB, about 1.5 dB above specification limits for cross-polarization. Sidelobe levels (SLL), on the other hand, are lowered in these arrays significantly with values of 28.3 dB for the 12 elements array. Though the results of arrays with less elements than 6 are not presented, it is important to mention that the array composed of sub-arrays of 3 and 4 elements has the lowest cross-polarization level, with -37.8 dB and -37.5 dB respectively, and SLL below 20 dB.

For the array of 14 elements the average input impedance is 45.5 – j0.1 Ω, which gives a return loss of -26.53 dB. Isolation between ports 1 and 3 (S_{31}) and port 1 and 5 (S_{51}) for this array is around -25.91 dB and -23.82 dB respectively. This array has an impressive SLL of -31.82 dB and a cross-polarization of -31.82 dB. Front-to-back ratio is exactly the same as its original version (-16.85 dB).

Even though the isolation between ports 1 and 5 remains almost the same, the isolation between ports 1 and 3 in both arrays degrades by almost 2 dB. Also the HPBW drops from 6º to 7º, and the total gain of the array drops around .5 dB in both the 12 elements and the 14 elements array. Figure 4.24 and Figure 4.25 shows the radiation

patterns for arrays consisting of sub-arrays of 6 and 7 elements for each sub-array with curved feed lines.

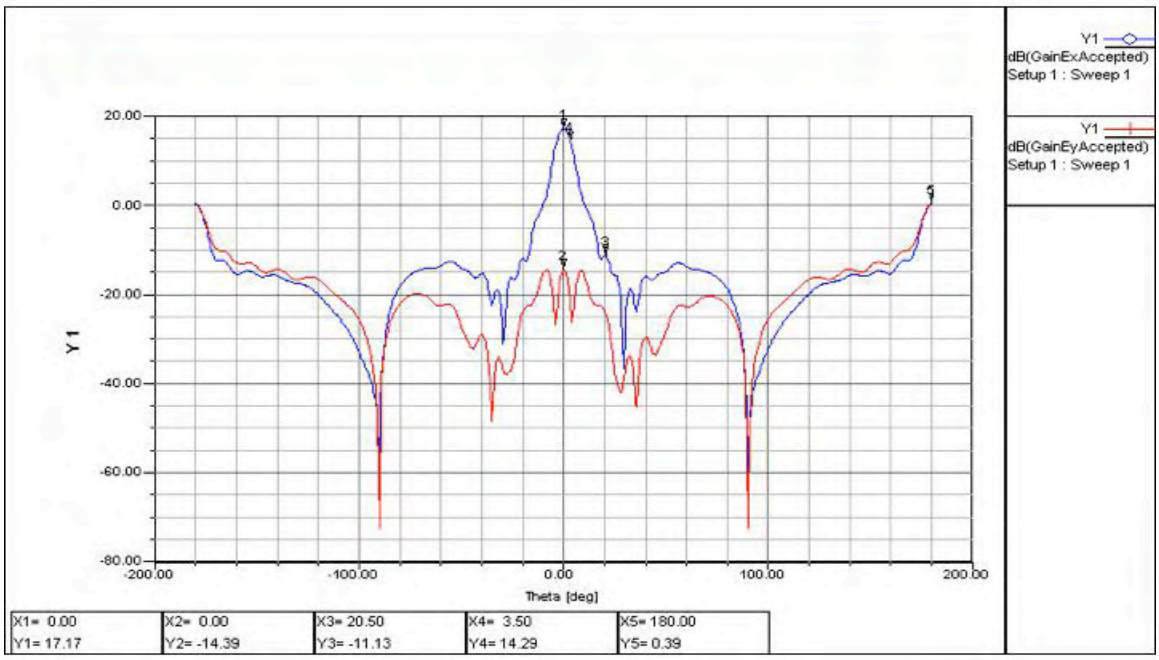

Figure 4.24 Radiation pattern of array composed of two sub-array of 6 elements with curved feed lines.

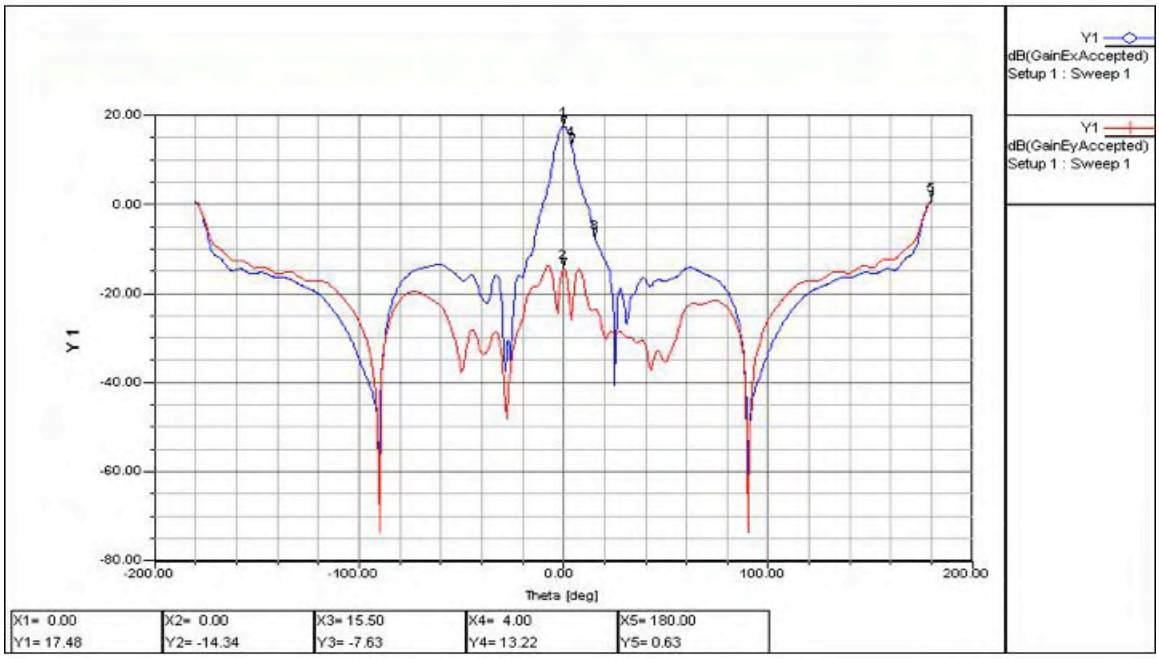

Figure 4.25 Radiation pattern of array composed of two sub-array of 7 elements with curved feed lines.

4.2.4 Array with curved feed lines and Load Radiating Element

Just as the original array configuration a load element at the outer ends of the array with curved feed lines is added. Figure 4.26 presents the input impedance normalized in a Smith Chart for an array of 12 elements. From the Smith Chart in Figure 4.26 it can be seen that the average input impedance of the array is about 45.28 + j0.56 Ω, giving a return loss of approximately -26 dB. Figure 4.27 shows the radiation pattern for the array. It can be seen that the gain of the array drops 1.19 dB, from 17.17 dB to 15.98 dB, and the front to back ratio is about 15.93 dB. Just as before, with the original array configuration, the addition of the PL makes significant changes in the cross-polarization, SLL and HPBW. The cross-polarization achieved is -37.63 dB, which is around 6 dB better than the array with out the PL. The HPBW is incremented using the PL from 7º to 10º, and the SLL exhibits a radical difference of almost 12 dB lower for the array with the radiating element, 16.53 dB for the array with PL and 28.3 dB for the array without it.

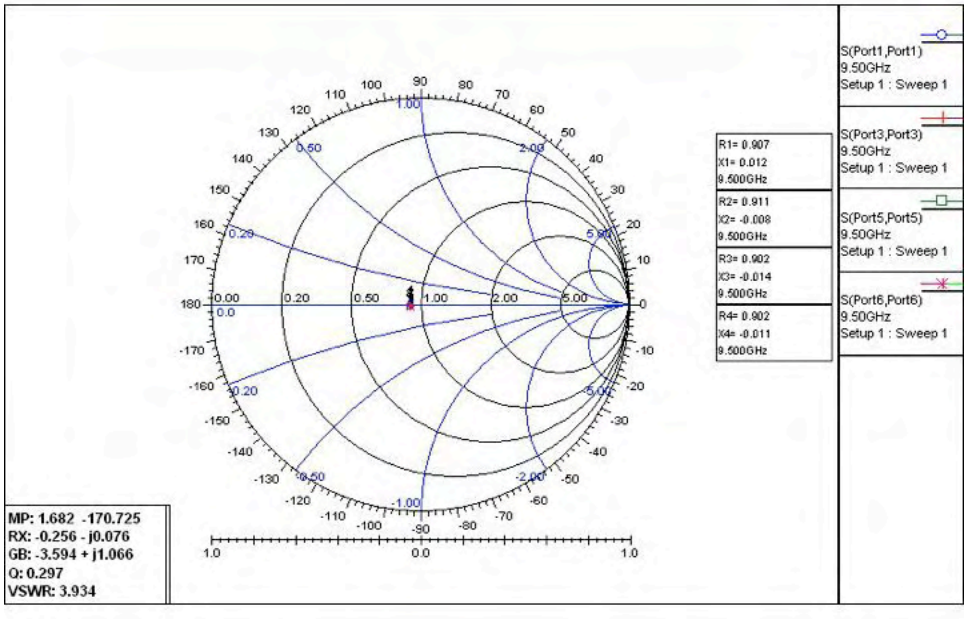

Figure 4.26 Input impedance for 12 element linear array with curved feed lines and load radiating elements in Smith Chart normalized to 50 Ω at 9.5 GHz.

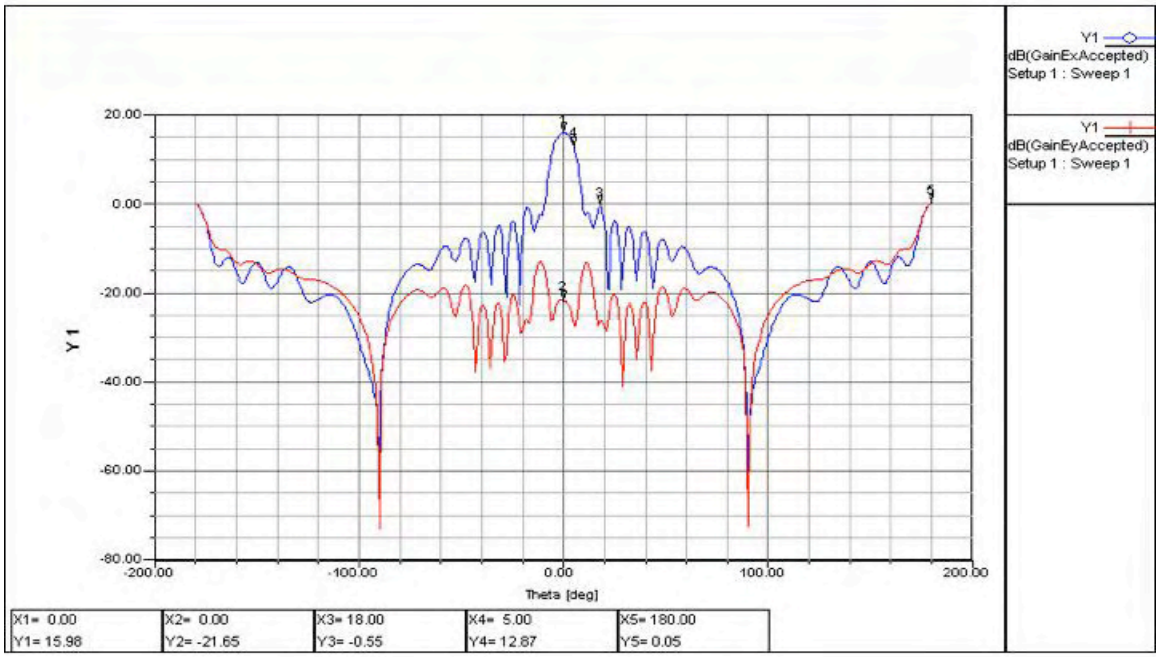

Figure 4.27 Radiation pattern for a 12 element linear array with curved feed lines and load radiating element at 9.5 GHz.

A 14 element linear array (7 element for each sub-array), again using a PL for the last element of the array was simulated with curved feed lines. Figure 4.28 shows a Smith Chart with the input impedance of each of the four ports of the array. At 9.5 GHz the input impedance of the array is 45.5 – j0.1 Ω, which gives a return loss of -26.5 dB. Figure 4.29 shows the radiation pattern of this array. The gain for the array under discussion is 16.76 dB, which is .72 dB lower than the array without the PL. The front-to-back ratio is -16.36 dB, just dropping 0.31 dB. The difference in SLL is a staggering 14.2 dB dB, having 17.35 dB for the array with PLs and 31.82 for the array without it. Still the use of the PL broadens the main beam causing a raise in HPBW from 7º to 8º. Again the cross-polarization shows improvement with -35.56 dB, which is 3.74 dB better than the array without the PL.

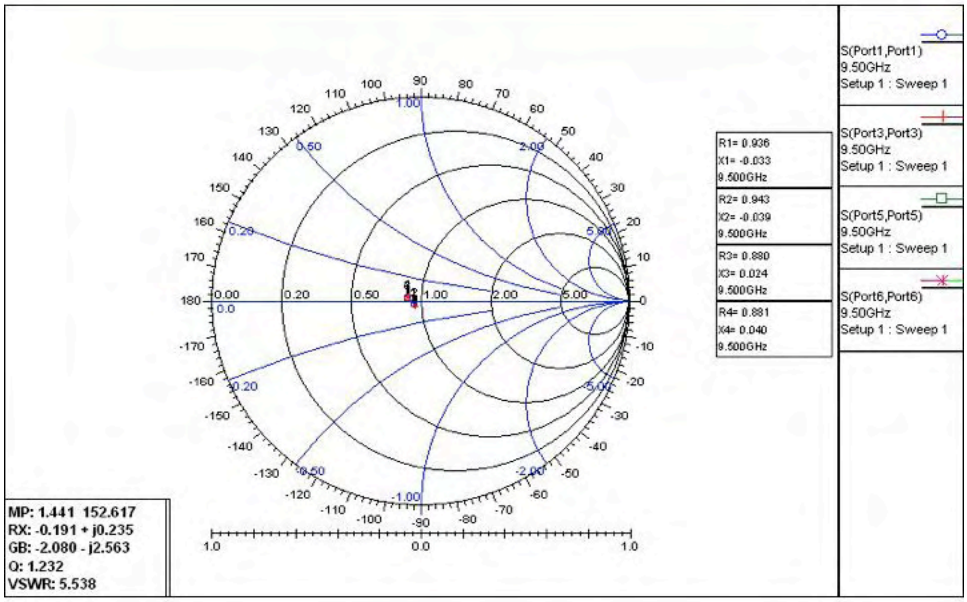

Figure 4.28 Input impedance for 14 element linear array using curved feed lines and load radiating elements in Smith Chart normalized to 50 Ω at 9.5 GHz.

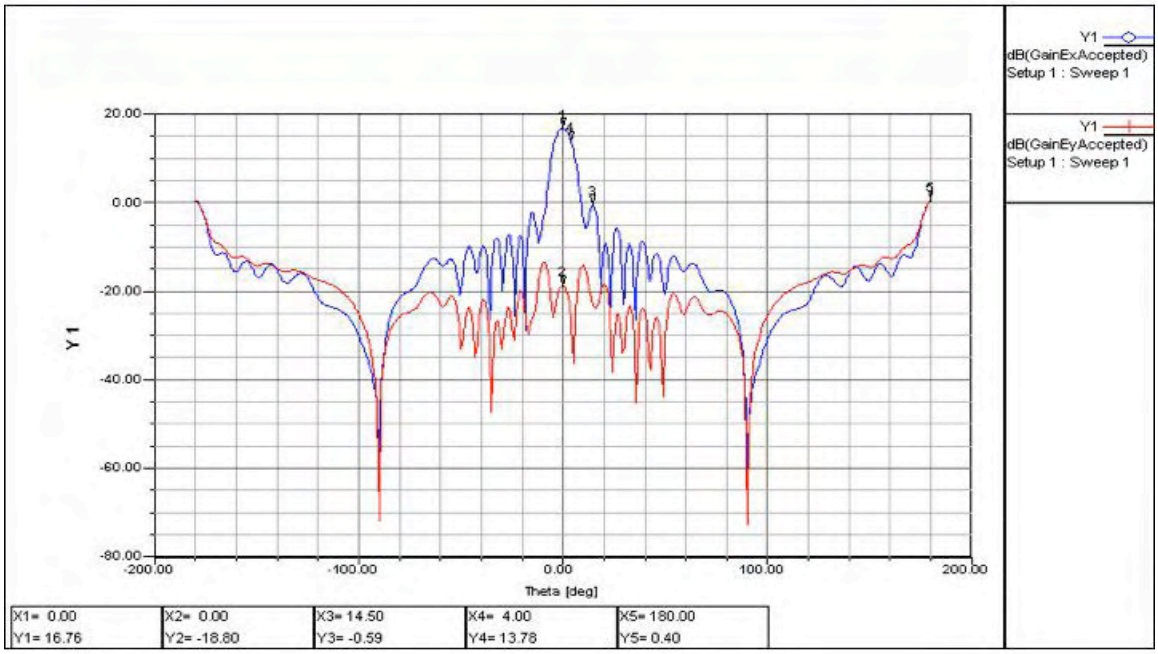

Figure 4.29 Radiation pattern for a 14 element linear array with curved feed lines and load radiating element at 9.5 GHz.

Table 4.7 summarizes the results presented in this section.

Table 4.7. Results at 9.5 GHz for sub-arrays using the 4-port element in series with curved feed lines and PL at the end.

Quantity of elements in sub-array	Zin_avg	RL_avg [dB]	S31 [dB]	S51 [dB]	SLL [dB]	HPBW	XP [dB]	FBR [dB]	Gain [dB]
6	45.28 +j0.56	-26.00	-26.85	-23.67	16.53	~ 10°	37.63	15.93	15.98
7	45.5 -j0.1	-26.50	-26.45	-23.91	17.35	~8°	35.56	16.36	16.76

So far the data presented indicates that for better cross-polarization a radiating element must be used, thus sacrificing the sidelobe level of the array. If good SLL are desired, resistive loads instead of the PL must be used. The fact that the addition of the PL changes the current distribution of the array, a middle point must be found in order to achieved desirables SLL and cross-polarization with degrading the input impedance of the array. Next section presents the original array manually tapered trying to have better SLL using PLs in the array with sacrificing return loss and cross-polarization to an undesired level.

4.2.5 Array of 4-port Radiating Elements with manual tapering

The array presented in this section is the same discussed in section 4.2.2, but the position of the coupling slot under the cross-patch is not the same throughout the array. The current distribution of this array can be controlled with the position of the aperture-coupling slot as suggested in [17]. There was a time when a Taylor distribution was considered for this array, but first it was desired to try and develop an array with the same element along the array. This will ease time and the design of the array, provided that in [17] the same array configuration had excellent cross-polarization and SLL around 20 dB. In this section, what it is tried to do is to "fix" the progressive phase between elements. In the previous sections it is mention that depending on the position of the element in the array the phase offset and the S_{21} varies. The previous array configurations have a steady phase offset up to the third element, from that point forward it increases. Figure 4.30

shows the modification made in the coupling slot, which is making a different current distribution than original array in order to compensate the relation that with less power, less coupling, therefore different phase offset than the previous element. The arrows in Figure 4.30 points to the direction where the slots where moved.

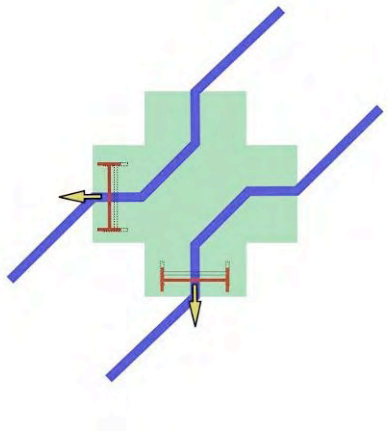

Figure 4.30 Modifications made in the position of the coupling slots to compensate the phase offset in the array.

The procedure followed here was simple, the coupling slots where moved inward and outward to see how the array behaved. Better results where obtained in the phase offset by moving the slots outward. This is expected since when moved outward, less coupling occurs, allowing more power to pass to the next element. The coupling slots where moved in steps, each steps where half the width of the slot (Ws/2 = .113 mm). Because the phase offset starts to increase from the third element, the slots moved at the beginning where the ones from elements 4 and 5, leaving intact the patch load's coupling slots. Better results where obtained when altering the position of the slots of the array beginning from the third element.

Table 4.8 presents the results obtained for the best 8 arrays configurations. The first four arrays have 6 elements in each sub-array including the PL, and the other 4 have 7 elements in each sub-array.

Table 4.8. Results at 9.5 GHz for sub-arrays of 12 and 14 elements displacing the coupling slots of some of the patch antennas.

Quantity of elements in sub-array	Zin_avg	RL_avg [dB]	S31 [dB]	S51 [dB]	SLL [dB]	HPBW	XP [dB]	FBR [dB]	Gain [dB]	Element number of coupling-slot shift		
										0.113 mm	0.226 mm	0.339 mm
6a	43.15 +j1.14	-22.55	-26.61	-23.08	19.3	~ 9°	39.11	15.84	16.11	3	4, 5	-
6b	43.52 +j1.94	-22.80	-26.86	-23.10	18.15	~ 9°	38.83	15.91	16.17	3, 4	5	-
6c	43.74 +j2.25	-22.97	-27.07	-23.08	17.62	~ 9°	38.39	15.91	16.16	3, 4, 5	-	-
6d	44.86 +j4.11	-23.18	-27.63	-23.21	17.74	~ 9°	37.3	16.03	16.24	4, 5	-	-
7a	43.01 +j0.86	-22.42	-25.90	-23.01	21.57	~ 9°	38.42	16.14	16.79	3	4, 5	6
7b	43.08 +j0.98	-22.50	-25.96	-23.04	21.14	~ 8.5°	38.6	16.14	16.79	3	4, 5, 6	-
7c	43.39 +j1.81	-22.74	-26.20	-23.03	20.52	~ 8°	37.23	16.2	16.88	3, 4	5, 6	-
7d	43.59 +j2.94	-22.86	-26.35	-23.05	19.48	~ 8°	36.77	16.24	16.93	3, 4, 5	6	-

The arrays presented in table 4.8 with numbers *6a* to *6d* are arrays composed of 12 elements. The letters are used to differentiate the arrays, depending on the position of the coupling-slots. For the 12 elements arrays the cross-polarization (XP) achieved is better that any other 12 elements array using PL. Array *6a* has a cross-polarization of 39.11 dB, which is about 1.5 dB better that the best XP achieved for an array with PLs. All 4 arrays exhibits good return loss, ranging from -23.08 to -23.21 dB. The HPBW for is around 9º, and the FBR ranges from -15.84 to 16.03 dB for these arrays. Isolation between port S_{31} and S_{51} ranges from -26.61 to -27.63 dB and -23.08 to -23.21 dB respectively. Figure 4.31 shows the radiation pattern for the linear array *6a*.

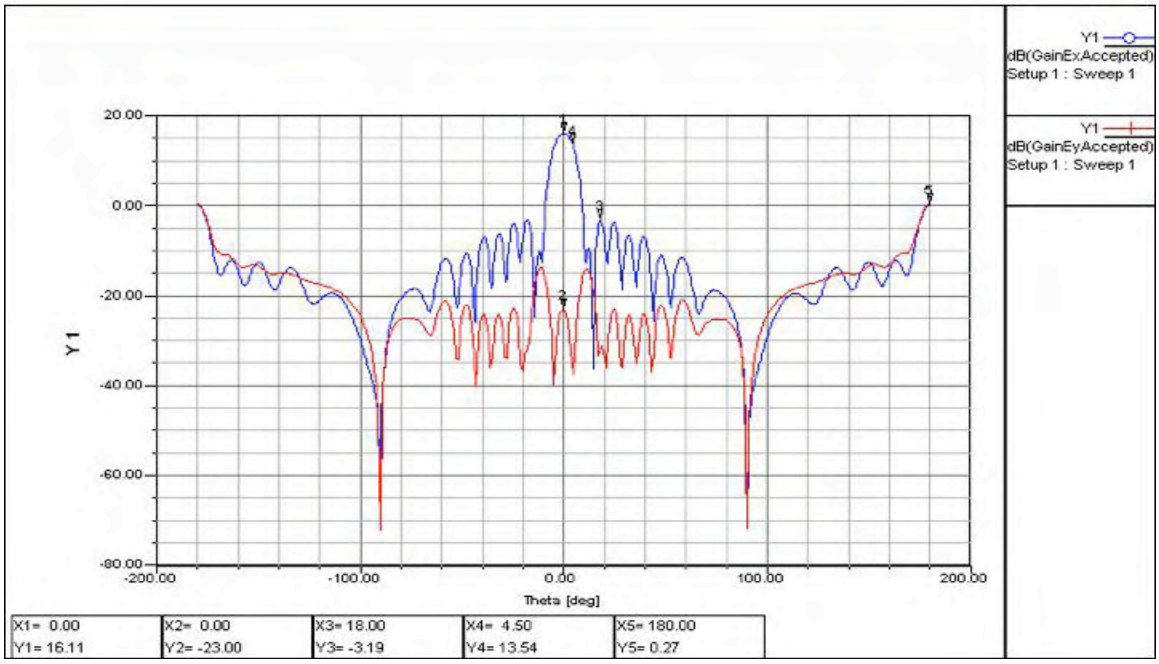

Figure 4.31 Radiation pattern for linear array 6a.

The mayor concern was that when using PL elements low SLL were achieved. These arrays demonstrate that moving the coupling slots of the array outward would force the array to radiate less power in some elements in order to ensure that more power reaches the outer elements of the array. SLL for these arrays show improvement ranging from 17.62 to 19.3 dB. Of these four arrays even though they show improvements in the array characteristics, only array *6a* is the only one that meet the specifications desired, having a return loss of -22.55 dB, FBR of -15.84 dB, and XP of -39.11 dB. In the other hand the HPBW could not be made lower than 9º.

The arrays *7a* to *7d* have better results than their previous versions in almost all their measurements. RL ranges from -22.4 to -22.86 dB and FBR ranges from -16.7 to -16.93 dB, which is an improvement of at least .3 dB, and XP ranges from -36.77 to -38.6 dB, which is an improvement from 1.2 dB up to 3dB, depending on the array. Mayor improvement is seen in the SLL of these arrays, given the fact that the best SLL of their previous versions is 18 dB. Only one of the arrays presented here has SLL above 20 dB, which is 19.48 dB (*7d*) and the other three have SLL 21.57 dB, 21.14 dB and 20.52 dB.

HPBW ranges from 9º to 8º, which is at least 1º below what is achieved earlier in section 4.2.2. Figure 4.32 presents the radiation pattern for the linear array *7b* and Figure 4.33 presents the radiation pattern for the array *7c*.

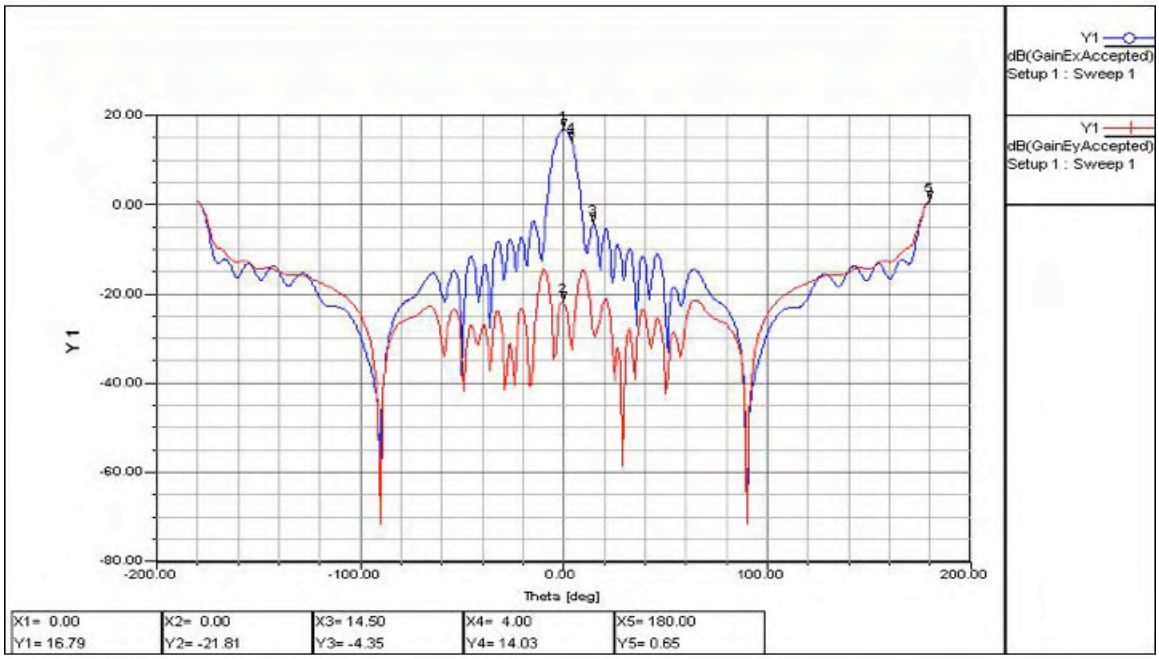

Figure 4.32 Radiation pattern for linear array 7b.

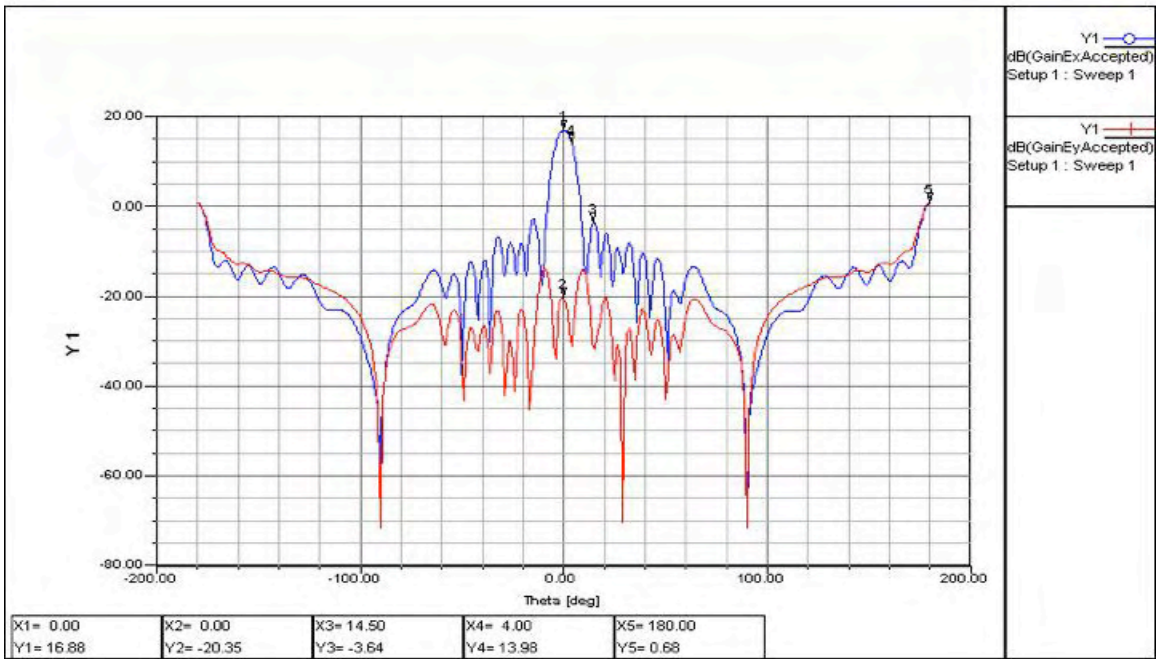

Figure 4.33 Radiation pattern for linear array 7c.

4.3 Measured Results

In order to obtain the best results possible, half of the antenna system was built in the Radiation Laboratory's milling machine (patches on FoamClad) and the other half was sent to Modular Components National to be etched (coupling apertures and feed lines). This was done in order to minimize errors due to non-uniformity in the feed lines and specially the coupling apertures. After all the layers were done separately the antennas were assembled using a mask system with register rods to ensure that the layers were assembled accordingly. The results of the antennas measured in the Radiation Laboratory anechoic chamber are presented in the following sections.

4.3.1 Single radiating element

Two 4-port elements and a patch load were constructed for testing. For the testing of the 4-port single radiating elements, two different terminating methods were used. One of the elements was terminated with the 50Ω chip resistor using vias to connect the resistors to the ground. The other used radial stubs to create an RF short circuit. The return loss for both ports (H and V) for the 4-port element using vias is presented in Figure 4.34 and for the 4-port element using radial stubs in Figure 4.35. The isolation between each port is presented in Figure 4.36 for the element with vias and Figure 4.37 for the element with radial stubs. Figure 4.38 shows the radiation pattern of one of the 4-port radiating elements. Note in Figure 4.34 and 4.35 that even though the resonant frequency for the element is not 9.5 GHz, the return loss is still around -20 dB at this frequency. The isolation between the input ports is around 2 dB better than the simulated results at the design frequency. Note in the radiation pattern presented in Figure 4.38 that the XP is around 34 dB, which is 2 dB better that the simulation, and the FBR is 26 dB, which is around 11 dB better than the simulated results.

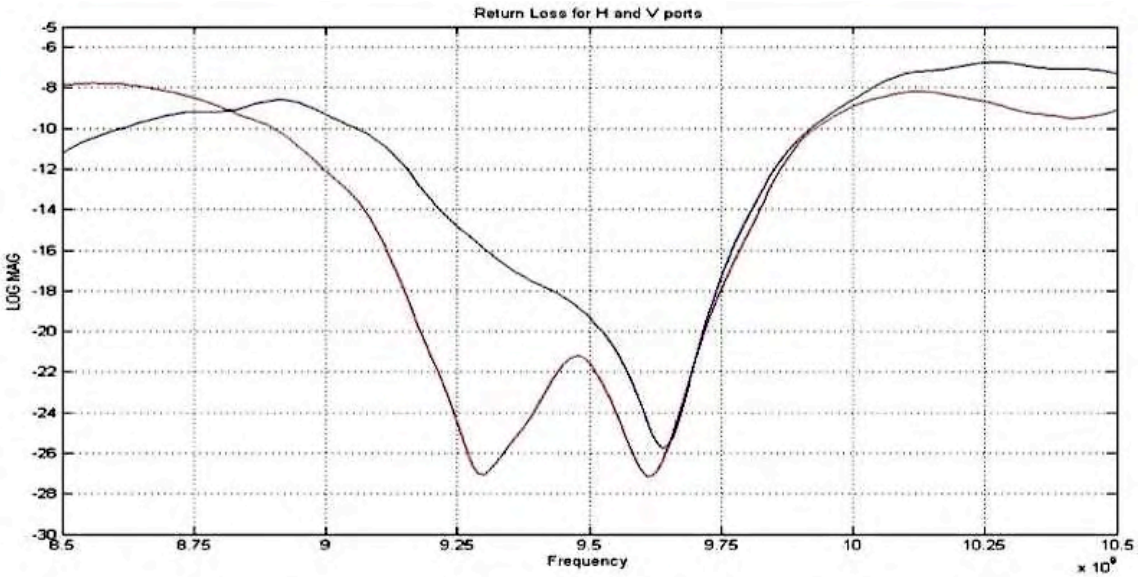

Figure 4.34 Return loss from 8.5 GHz to 10.5 GHz for the 4-port antenna with radial vias.

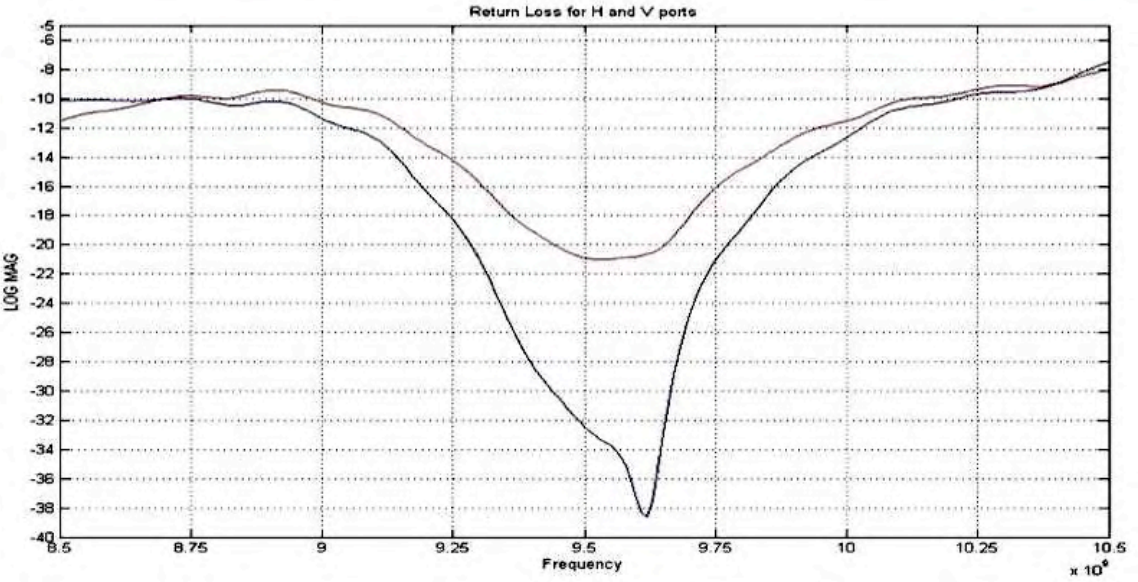

Figure 4.35 Return loss from 8.5 GHz to 10.5 GHz for the 4-port antenna with radial stubs.

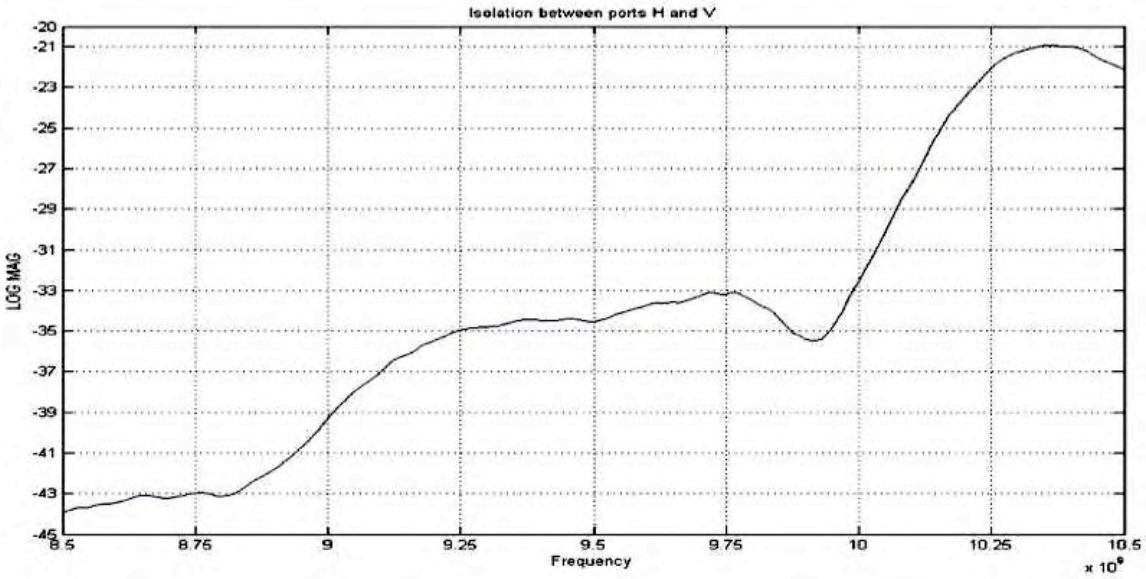

Figure 4.36 Isolation between ports H and V from 8.5 GHz to 10.5 GHz for the 4-port antenna with vias.

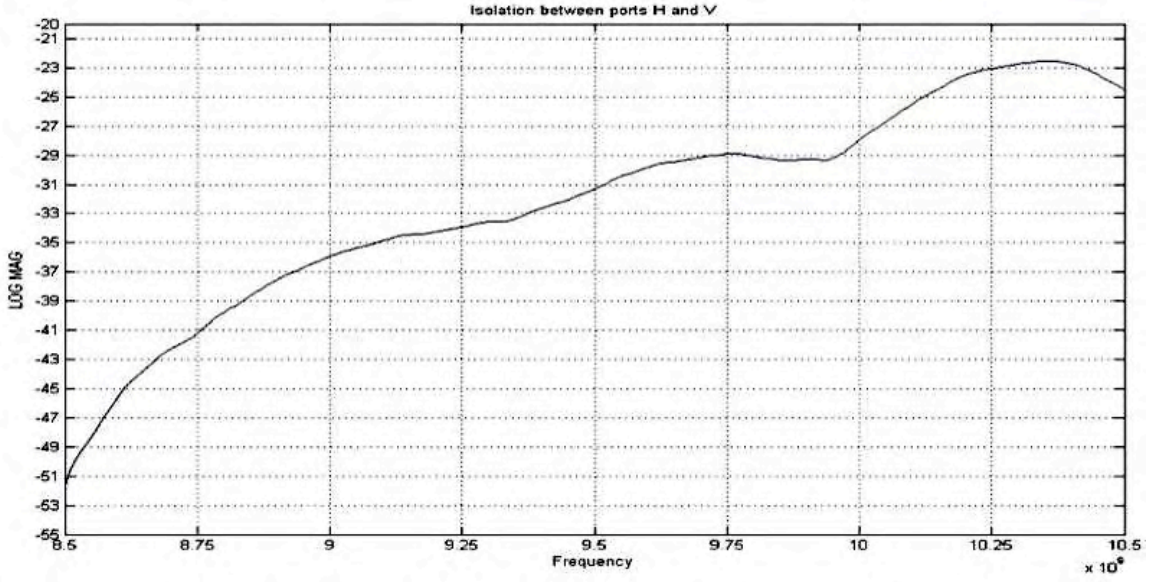

Figure 4.37 Isolation between ports H and V from 8.5 GHz to 10.5 GHz for the 4-port antenna with stubs.

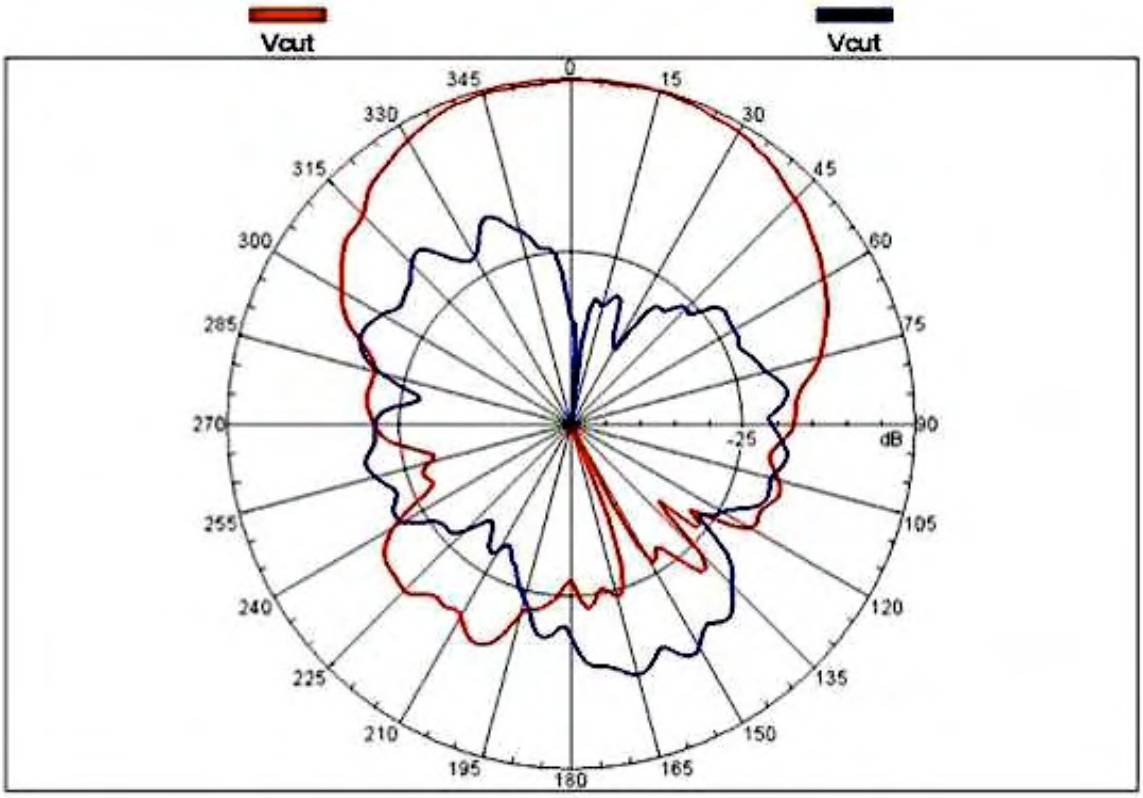

Figure 4.38 Radiation pattern for the 4-port antenna at 9.5 GHz.

For the patch load antenna, the results the resonant frequency shifted to 9.2 GHz. Figure 4.39 shows the return loss for each of its input ports. Even though the best response in impedance is at 9.2 GHz the lowest return loss measured is around -14 dB. At 9.5 GHz the isolation is around 22.5 dB, which is similar to the simulated results. Figure 4.40 presents the isolation between input ports for this element. The radiation pattern for this antenna is presented in Figure 4.41, where it can be seen that the XP is around 25 dB, which is around 1.7 dB lower that the simulated results. The FBR measured is around 15 dB, which coincides with the simulated results. Because the antenna was designed and simulated at 9.5 GHz, the radiation pattern was measured at this frequency.

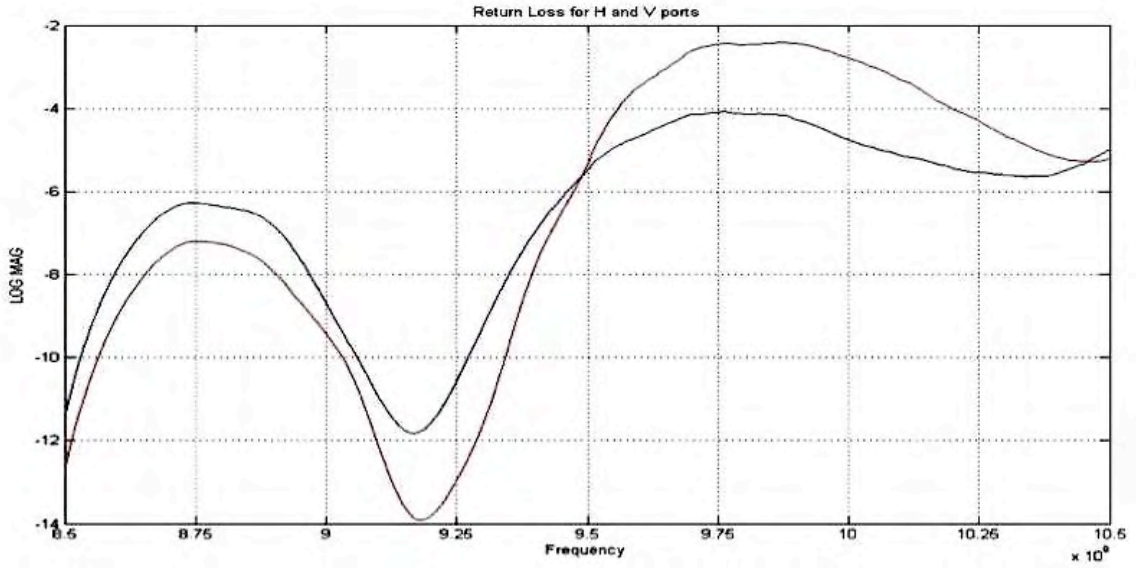

Figure 4.39 Return loss from 8.5 GHz to 10.5 GHz for the Patch Load antenna.

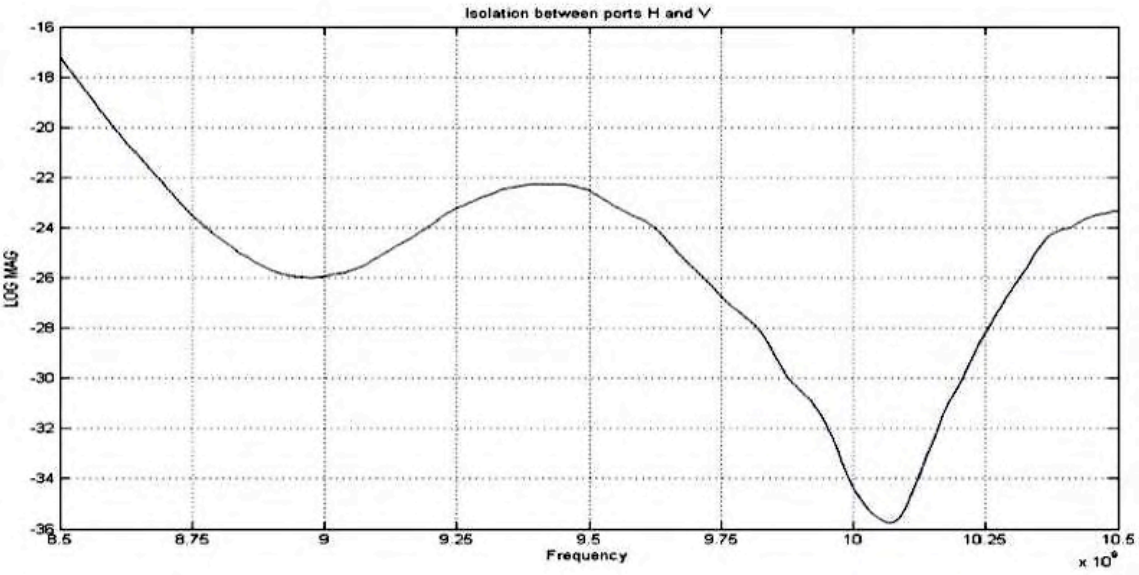

Figure 4.40 Isolation between input ports from 8.5 GHz to 10.5 GHz for the Patch Load antenna.

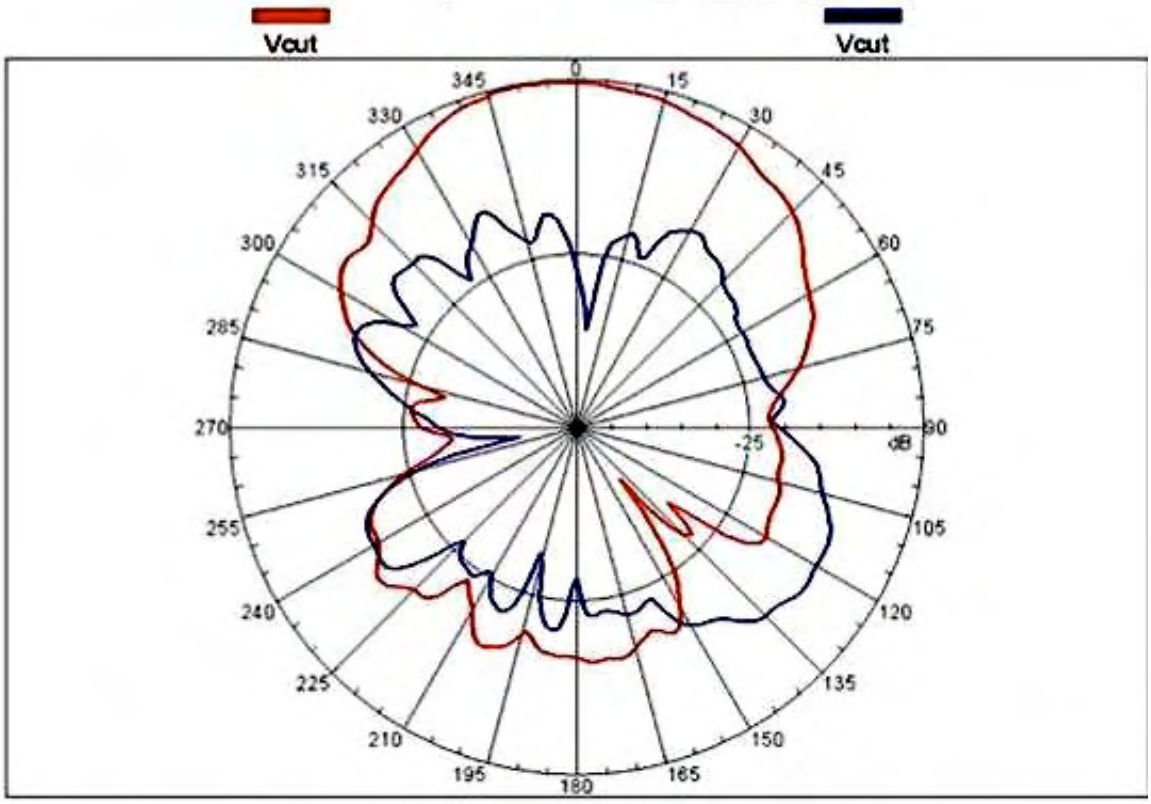

Figure 4.41 Radiation pattern for the patch load antenna at 9.5 GHz.

4.3.2 Linear Array

For the case of the linear array, because of its size, the assembling method was redesigned in order to minimize any errors in misalignment between the two boards (antennas and feed lines). Five arrays were built for the testing of the design. The following sections present the measured results for these arrays.

4.3.2.1 Array of 4-port element with loading resistors

This array, which consists of only the 4-port element connected in cascade, was terminated using 50 Ω chip resistors and radial stubs. Figure 4.42 and 4.43 presents the return loss of the ports H and V respectively. Note that the resonant frequency again is around 9.1 GHz. The radiation pattern at 9.1 GHz is presented in Figure 4.44. Unlike the

measured results for the single elements, which were measured at 9.5 GHz, the arrays main beam was deformed at the design frequency. Because of this, the results presented for the arrays are at their measured resonant frequency.

Despise the shift in frequency, the HPBW for the array was 7.28º, 1.28º larger that the simulated result. SLL measured were around 20 dB, about 2 dB lower that the simulated results. XP measured is around 24 dB, almost 8 dB lower than the results simulated, and the FBR is 26 dB, about 10 dB better that the simulated results.

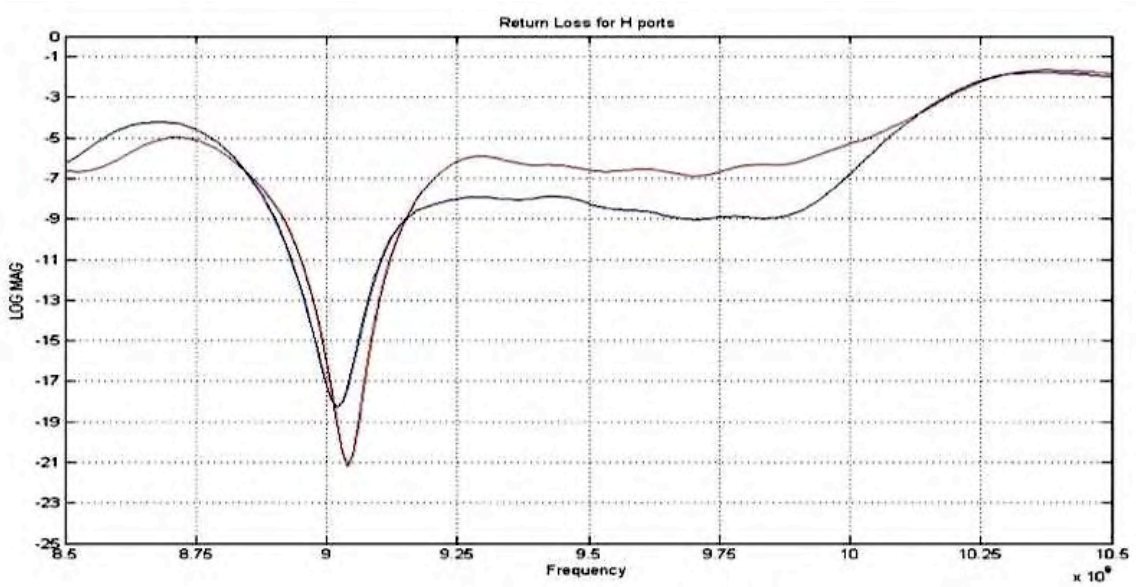

Figure 4.42 Return loss for the H ports from 8.5 GHz to 10.5 GHz for the array with 50Ω loading resistors.

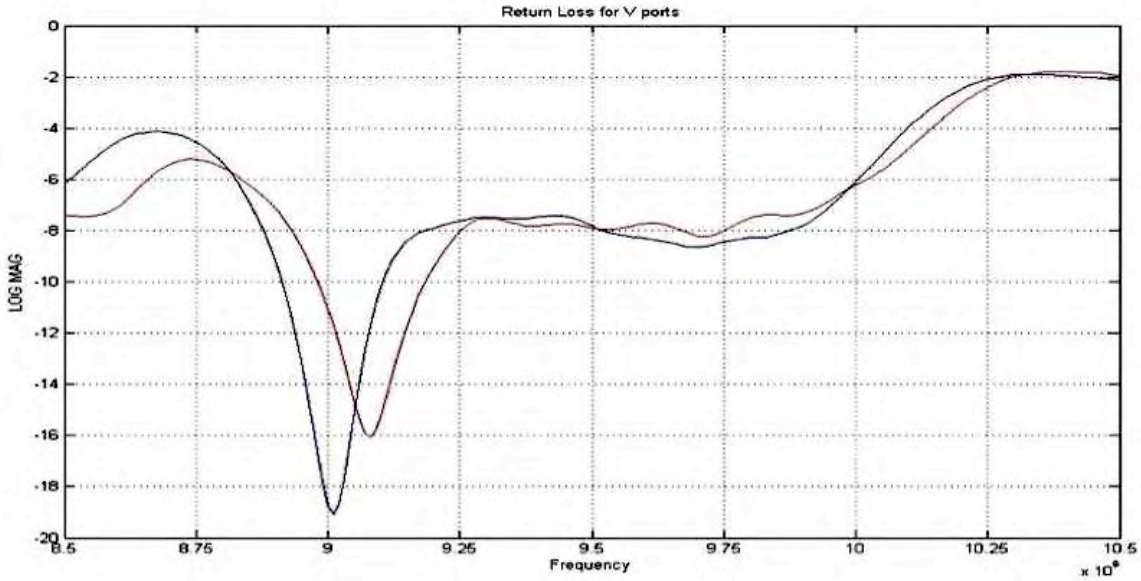

Figure 4.43 Return loss for the V ports from 8.5 GHz to 10.5 GHz for the array with 50Ω loading resistors.

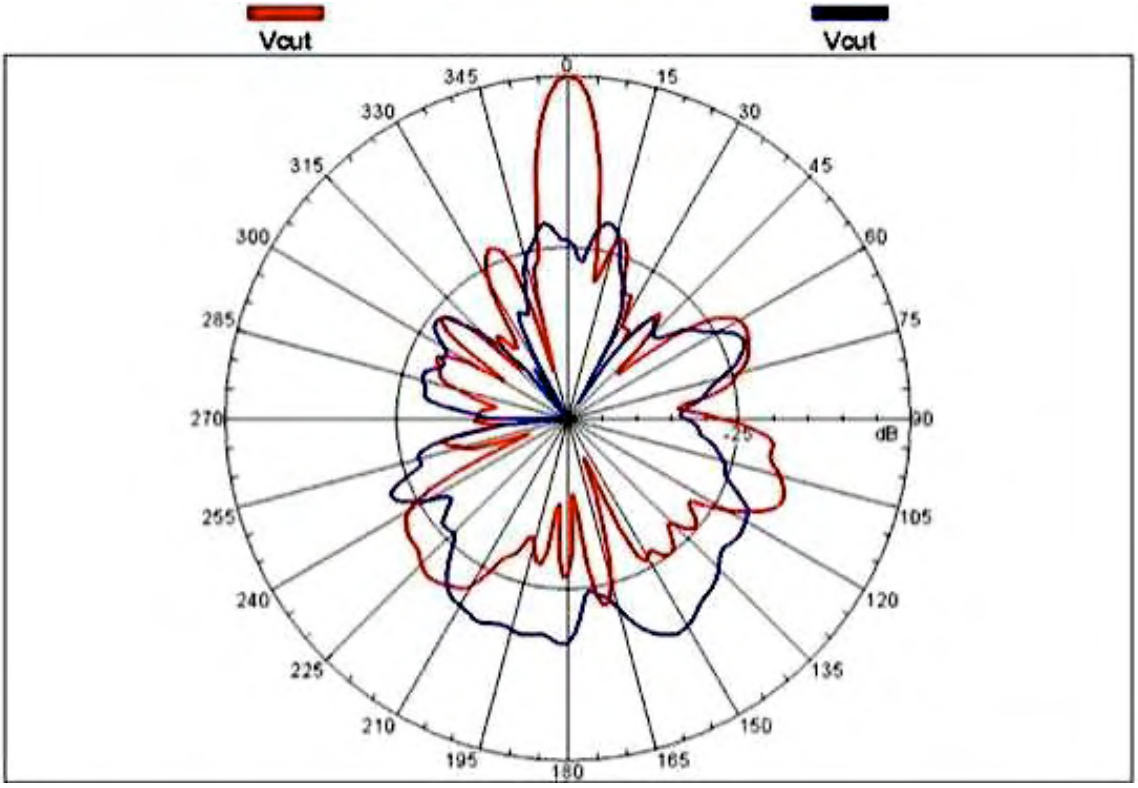

Figure 4.44 Radiation pattern for linear array with 50Ω loading resistors at 9.1 GHz.

4.3.2.2 Array of 4-port element with Patch load

For the array with patch loads the shift in frequency also occurred. Figure 4.45 and 4.46 presents the return loss measured for the V and H ports respectively. Note once more that the resonant frequency for this array is around 9.15 GHz. Figure 4.47 shows the radiation pattern of the array measured at 9.1 GHz. For this array the HPBW is 9.27º, 0.27º larger than the simulated result. SLL are around 17 dB, which is about 1.2 dB better than the simulated results, and the XP is around 20 dB, about 17 dB lower than expected. The FBR is almost 26 dB, around 8.2 dB better than its simulated results.

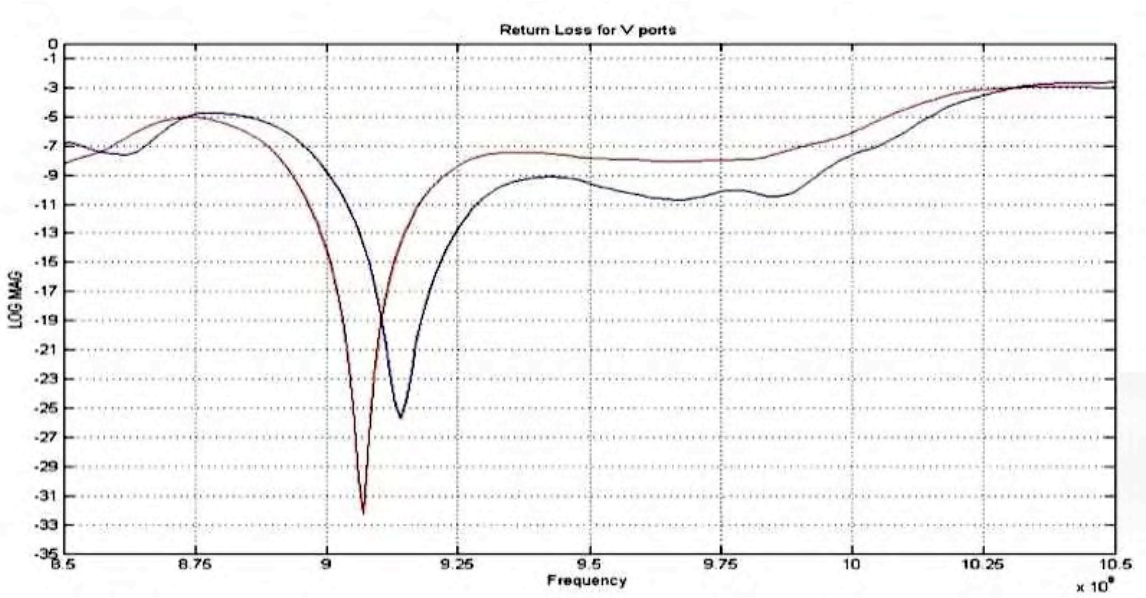

Figure 4.45 Return loss for the V ports from 8.5 GHz to 10.5 GHz for the array with patch loads.

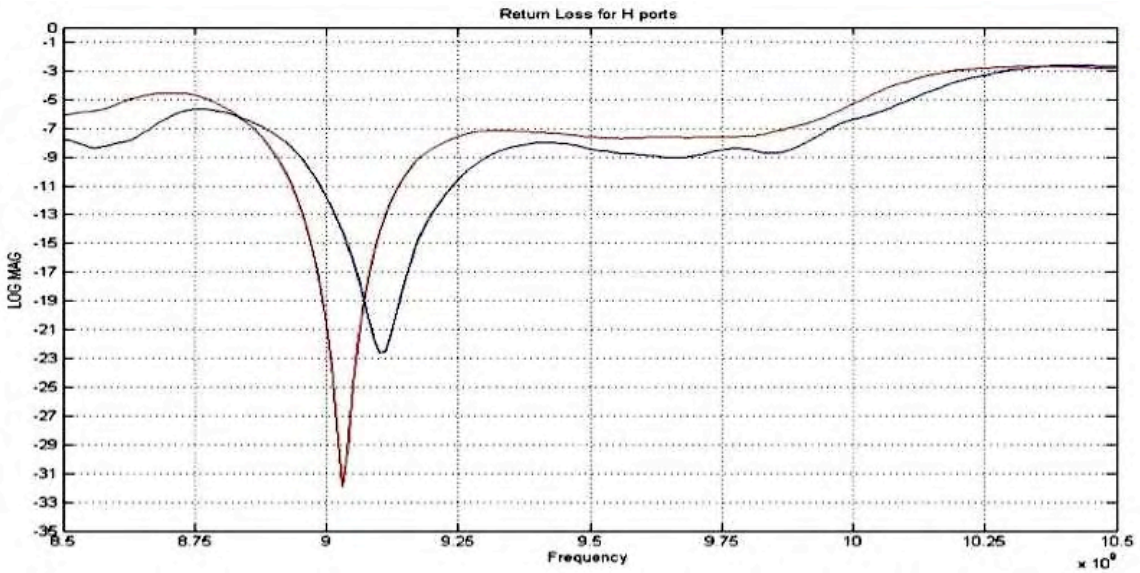

Figure 4.46 Return loss for the H ports from 8.5 GHz to 10.5 GHz for the array with patch loads.

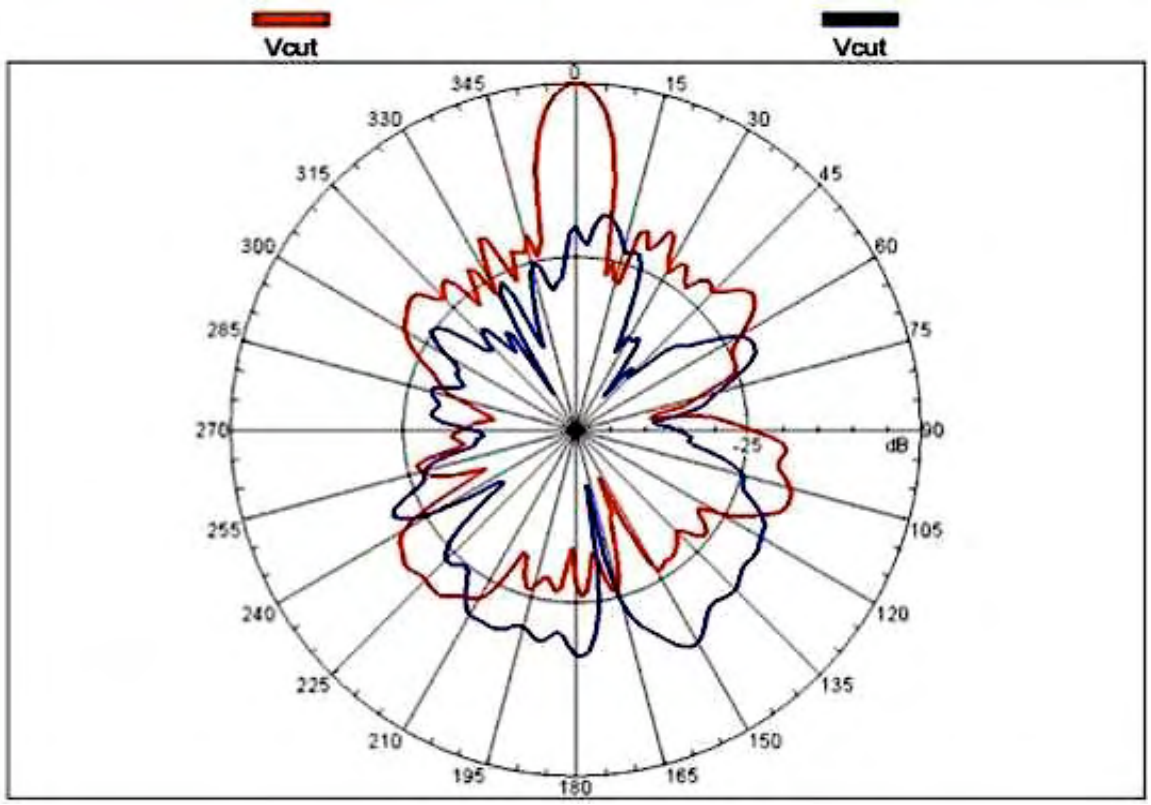

Figure 4.47 Radiation pattern for linear array with patch load at 9.1 GHz.

4.3.2.3 Array with curved feed lines and loading resistors

For the array with curved feed lines and patch loads the return loss for each of its input ports indicates that its resonant frequency is around 9.1 GHz. The frequency response for each of its ports V and H are shown in Figure 4.48 and 4.49 respectively. The SLL measured for this array is 19 dB, about 9 lower than expected and the XP was 25 dB, almost 6.6 dB lower than expected. The HPBW measured was 8.18º, about 1.18º larger than expected. The FBR was about almost 8.2 dB better than the simulated results with 25 dB. The radiation pattern for this array is presented in Figure 4.50.

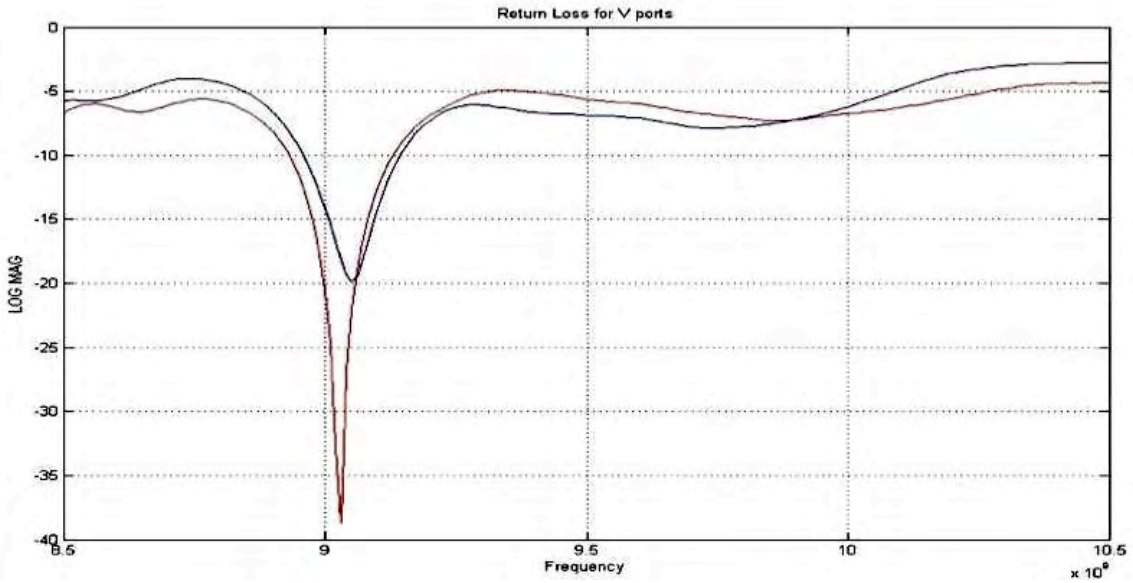

Figure 4.48 Return loss for the V ports from 8.5 GHz to 10.5 GHz for the array with curved feed lines and 50Ω loading resistors.

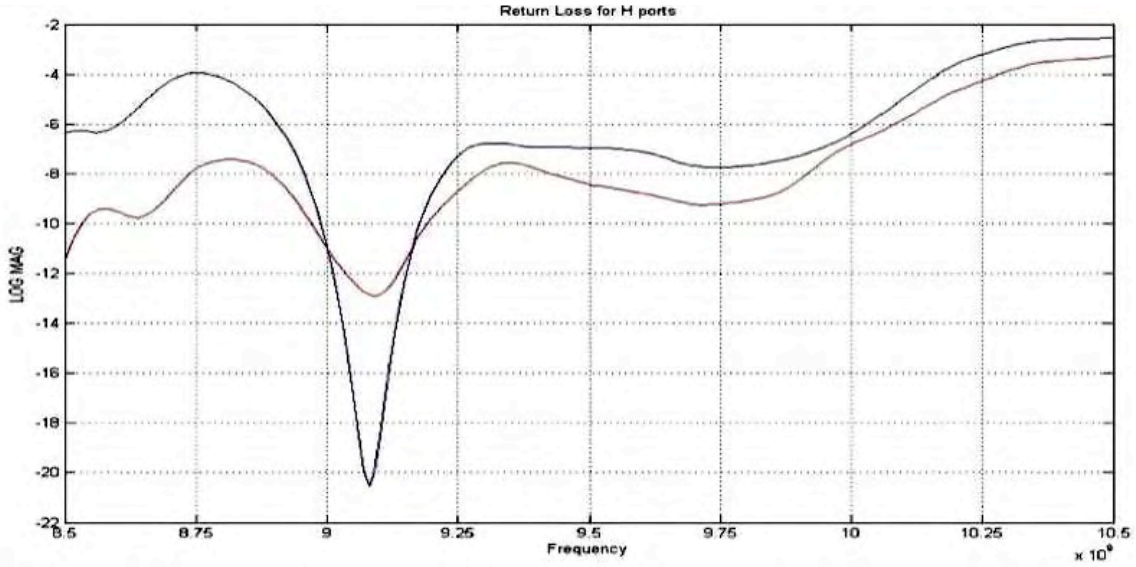

Figure 4.49 Return loss for the H ports from 8.5 GHz to 10.5 GHz for the array with curved feed lines and 50Ω loading resistors.

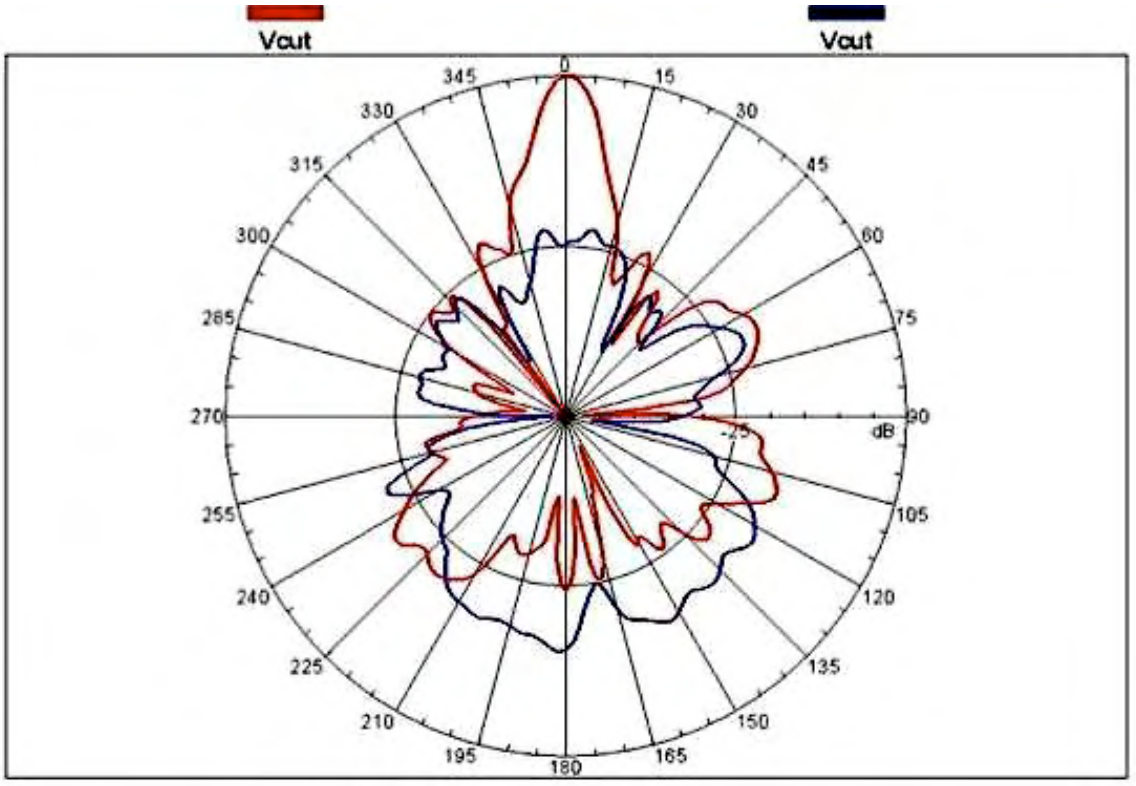

Figure 4.50 Radiation pattern for linear array with curved feed lines and 50Ω loading resistors at 9.1 GHz.

4.3.2.4 Array with curved feed lines and patch load

The array with curved feed lines and patch loads also showed a shift it in operating frequency. Figures 4.51 and 4.52 presents the return loss for its V and H ports respectively. The XP measured was 20 dB, which was about 17.6 dB lower that expected. The SLL was around 1.5 dB lower that the simulated results with 15 dB, and the FBR measured was 25 dB, about 9 dB better than expected. The HPBW measured was 10.5º, just 0.5º larger than expected. Figure 4.53 presents the radiation pattern for this array at 9.1 GHz.

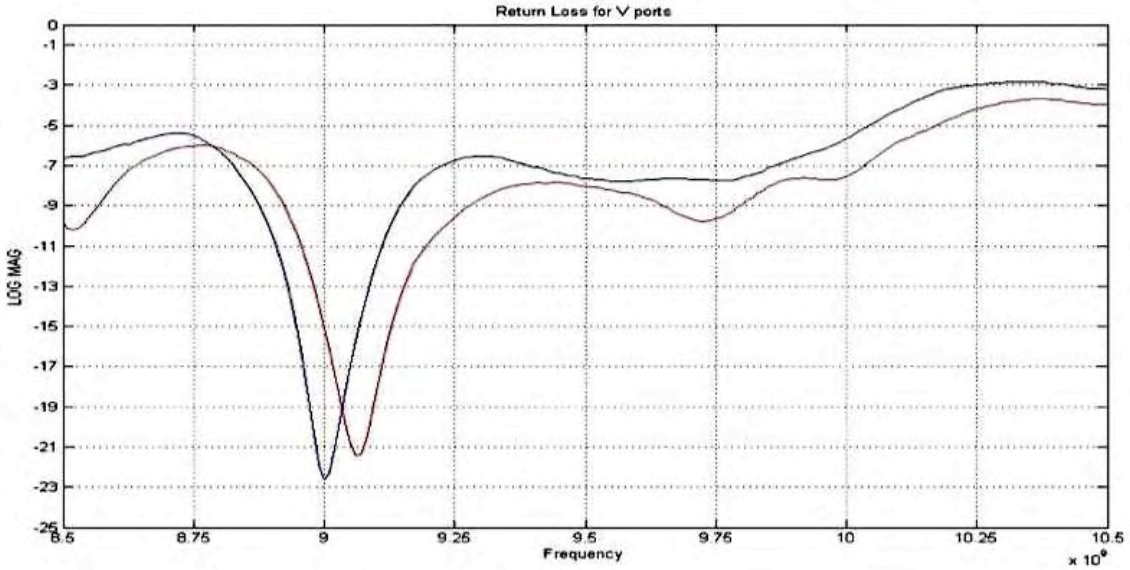

Figure 4.51 Return loss for the V ports from 8.5 GHz to 10.5 GHz for the array with curved feed lines and patch loads.

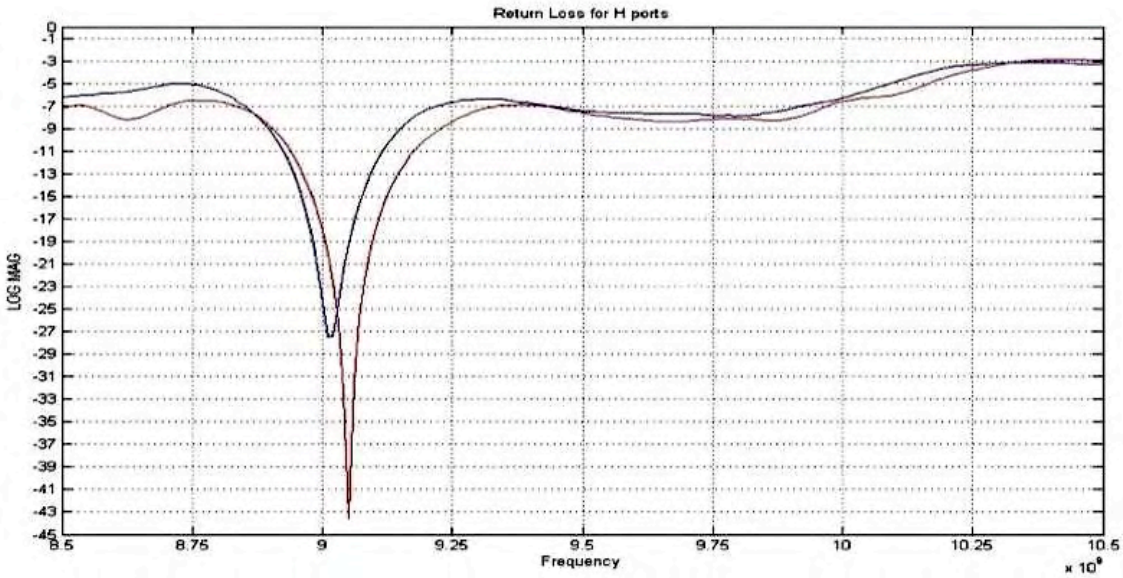

Figure 4.52 Return loss for the H ports from 8.5 GHz to 10.5 GHz for the array with curved feed lines and patch loads.

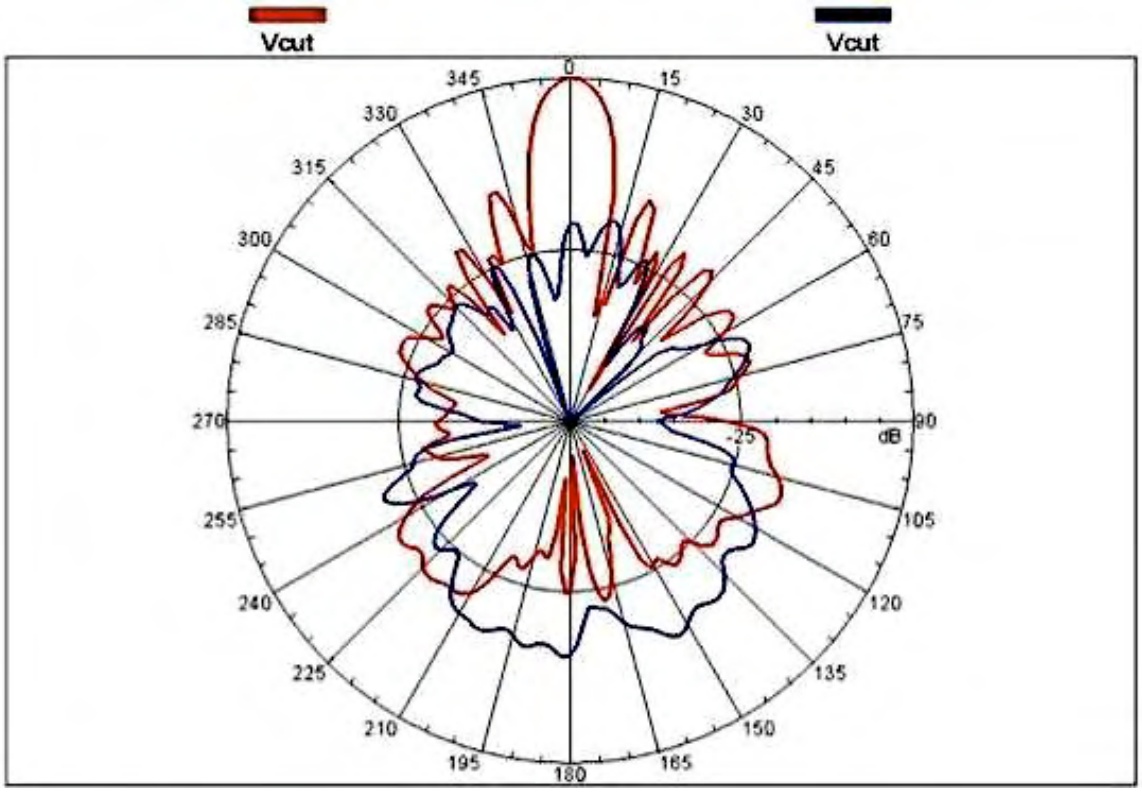

Figure 4.53 Radiation pattern for linear array with curved feed lines and patch loads at 9.1 GHz.

4.3.2.5 Array with manual tapering

The array with the positions of the coupling apertures modified suffered from the same frequency shift like the previous arrays discussed. Figure 4.54 and 4.55 presents the return loss for its V and H ports respectably. The HPBW measured was 8.45º, which was around 0.55º better than the simulated result, and the SLL was 15 dB, 4 dB lower than expected. The XP and the FBR measured were 20 dB and 30 dB respectively. The XP measured was 19 lower than the simulated result and the FBR was around 14 better than the simulated results. The radiation pattern measured for this array is presented in Figure 4.56.

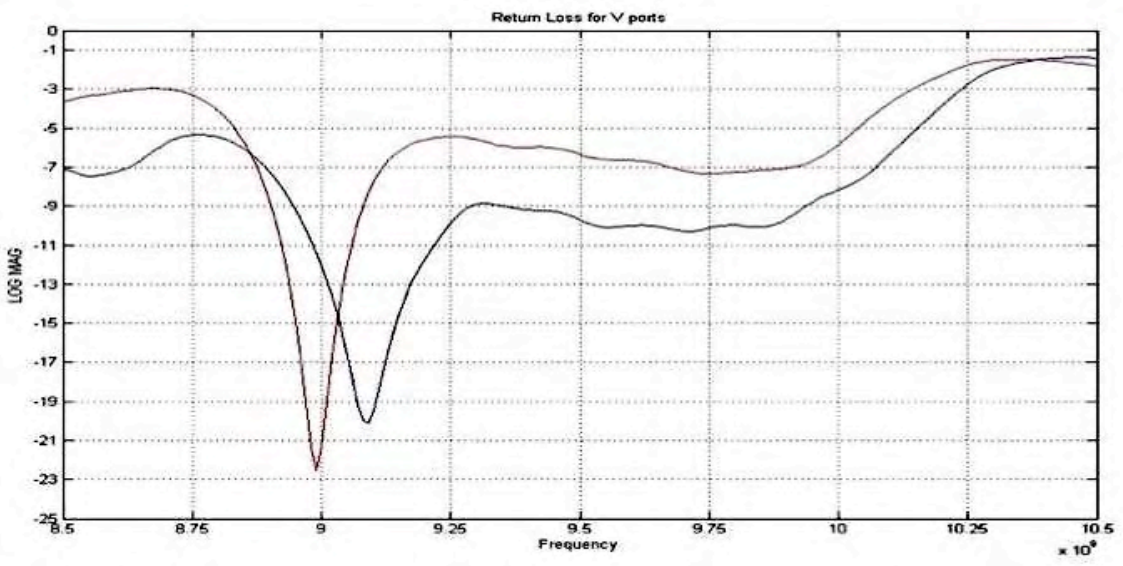

Figure 4.54 Return loss for the V ports from 8.5 GHz to 10.5 GHz for the array with manual tapering.

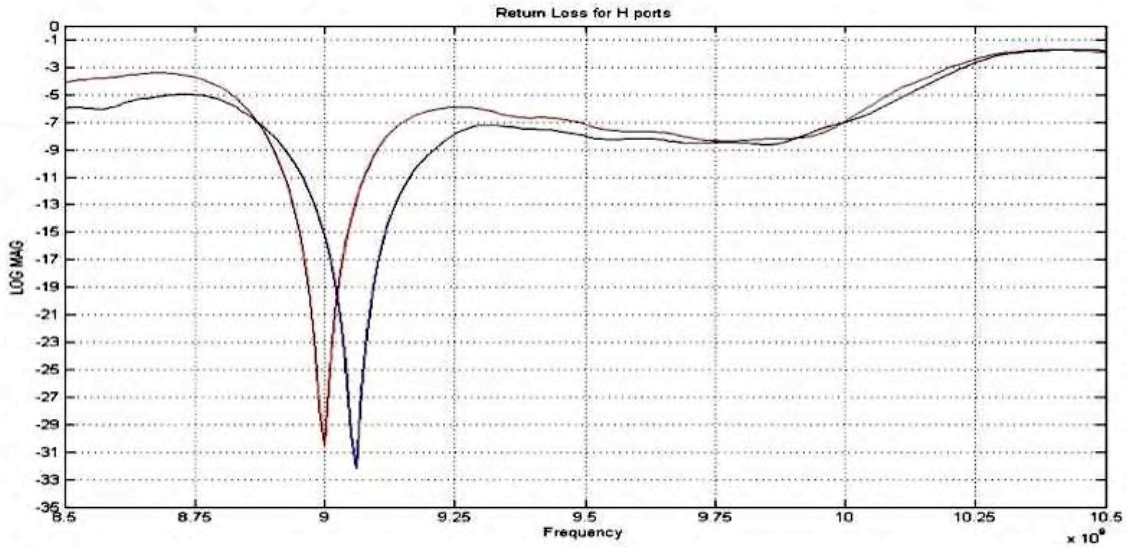

Figure 4.55 Return loss for the H ports from 8.5 GHz to 10.5 GHz for the array with manual tapering

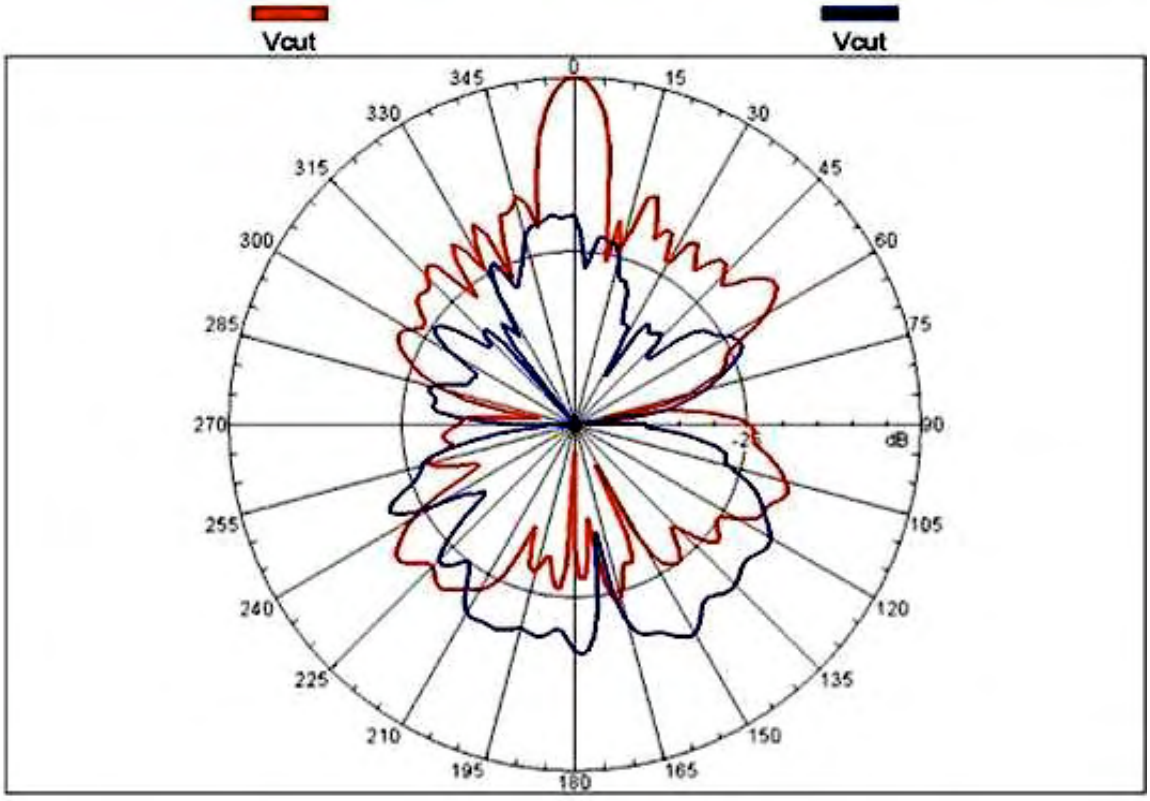

Figure 4.56 Radiation pattern for linear array with manual tapering at 9.1 GHz.

4.4 Possible Errors

There are several stages along the fabrication of the prototypes antennas that could have influenced the measured results. The following sections explain how these steps could have caused the measured results to differ from the simulations and how they could be fixed.

4.4.1 Fabrication

The fabrication process is very important. In this case it was desired to build the whole prototype in the Radiation Laboratory's milling machine. Because the milling machine leaves non-uniform edges for the lines and the coupling apertures, the circuit board was etch by Modular Components National (MCN). This minimizes the errors that could arise due to line and slots edge resolution. On the other hand this could create a new source of error in the assembling. This possible source of error will be address in the next section. Figure 4.57 and 4.58 shows a microstrip line and a coupling aperture made in the milling machine and one etched by MNC respectively.

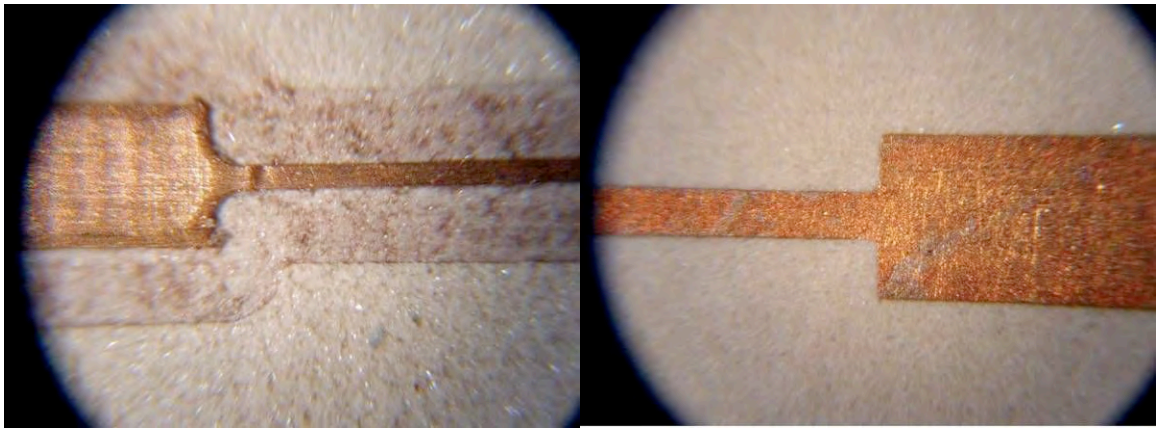

Figure 4.57 Microstrip line made with milling machine (left) and etched (right).

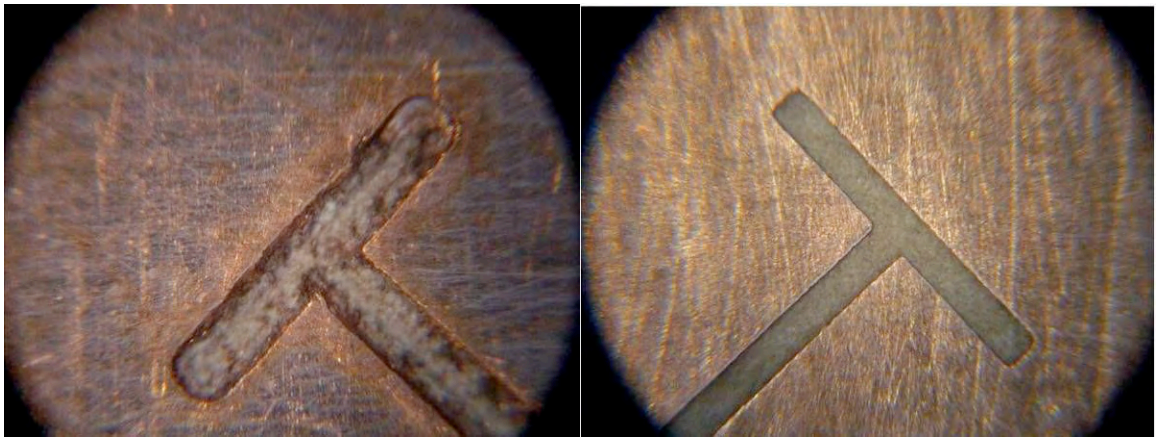

Figure 4.58 Coupling aperture made with milling machine (left) and etched (right).

4.4.2 Assembly

Several precautions were considered at the time of assembling. The mask developed at the Physics' department machine shop, were developed with a resolution of 1 mil. Still this wasn't enough. The fact that both boards were made separately using the same CAD drawing implied that reference made (registers) would be at the same positions. This was not the case. MCN claimed a resolution in the board of +0.005 mils. The lines and slots met this specification but the registers did not, complicating the assembly process. Figure 4.59 shows the positions of the registers in the CAD drawing in red and the position measured in the board in black. It is important to note that these measurements were made with a micrometer device with a resolution of 0.0001 inch.

The errors measured in the positions for the arrays implied that if the antenna boards have the correct positions a misalignment between the two boards would occur. This problem can be seen in Figure 4.60.

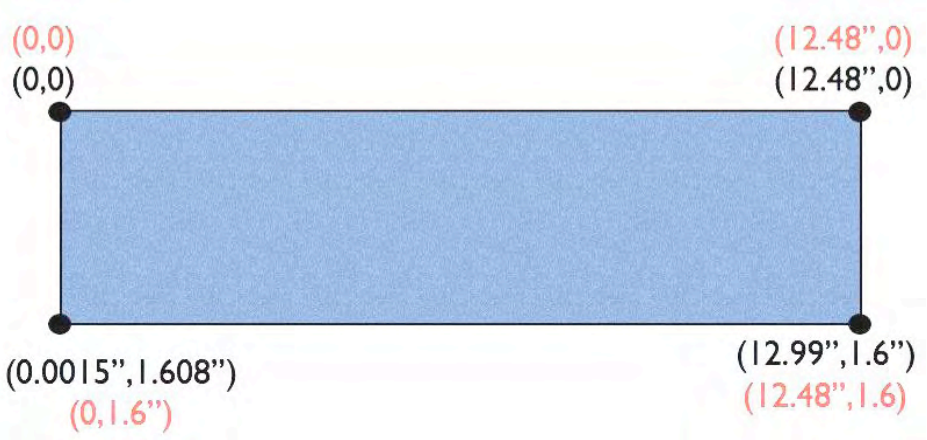

Figure 4.59 Positions for the registers for a linear array. The red coordinates are the CAD coordinates and the black coordinates are the measured positions.

Figure 4.60 Error in registers positions in linear array circuit boards

Another problem was that the milling machine removes more or less copper than expected; a problem that came to our attention at the final stages of this project. For example, a microstrip line with width of 1 mm could end up with a width of 0.8 mm. At X-Band this difference can cause a large impact on the impedance of the line, and as a result an unpredictable effect on the design. Especially in this case where the antenna prototypes boards were made separately. Figure 4.61 shows the measured width of the antennas on the array. The calculated width for the 4-port elements was 13.21 mm. The difference between the measured and the calculated is 0.14 mm, in this case the patch antennas were larger. This may be main cause for the shift to a lower frequency.

Figure 4.61 Patch width measured for one of the 4-port.

4.5 Matlab Simulation for current estimation of the array and radiation pattern

It is very important to know what is the current distribution of an array for the designer. Most of the time the designer knows this before even simulating an array, but in our case the only thing that is known is the results of a single radiating element and the radiation pattern of this elements used as a linear array. One of the options that the electromagnetic simulator provides is a display of current intensity and phase, but the user cannot have access to the exact data. This makes the estimation of the current distribution extremely difficult and very subjective. Subjective because the only thing the software provides is a gradient colored scale as a legend with interpolated values along the scale. In order to be able to estimate the current distribution of the array the ABCD matrix of a single element was used.

The 2 x 2 transmission, or better known as the ABCD matrix can be used to characterize a microwave network that consists of two ports networks connected in cascade. The advantage of this matrix is that the ABCD matrix, of the cascade

connection of two or more 2-port networks can be easily found by multiplying the ABCD matrices of the individuals' 2-ports. The ABCD matrix is defined for a 2-port network in terms of voltages and currents is presented in figure 4.62 (a).

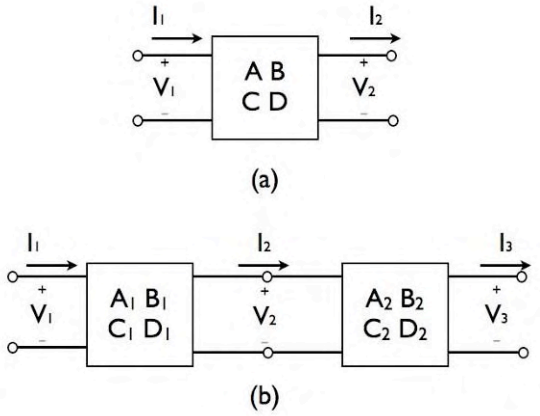

Figure 4.62 (a) A 2-port network and (b) a cascade connection of 2-port networks.

$$V_1 = AV_2 + BI_2 \qquad (4.1)$$

$$I_1 = CV_2 + DI_2 \qquad (4.2)$$

Or in matrix form,

$$\begin{bmatrix} V_1 \\ I_1 \end{bmatrix} = \begin{bmatrix} A & B \\ C & D \end{bmatrix} \begin{bmatrix} V_2 \\ I_2 \end{bmatrix}$$

The convention that I_2 flows out of port 2 will be used when dealing with ABCD matrices so that in a cascade network, I_2 will be the same current that flows into the adjacent network as shown in figure 4.62 (b).

In this case it is desired to calculate the currents in the network knowing the initial current and the S parameter matrix that can be transformed in an ABDC matrix. It can be said that

$$I_2 = I_1\left(\frac{A - CZ_{in1}}{AD - BC}\right) \tag{4.3}$$

$$Z_{in} = Z_o\left(\frac{1 + S_{11}}{1 - S_{11}}\right) \tag{4.4}$$

The process for the current estimation is the following: simulate a single radiating element and extract the S parameter matrix from the simulator, then in a program created in Matlab, the current distribution of *N* elements in cascade is calculated using the ABCD matrix and equations 3 and 4.

In this case, because the linear array is composed of 2 sub-arrays where the input power fed to them flows away from each other, and their separation between elements are not the same; the equation of array factor was used in its original form. By placing the array elements along the *x*-axis it can be said that the array factor of an even number *N* of radiating elements is:

$$AF_1 = \sum_{n=N}^{N/2} I_n e^{j\left(k_o D \sin(\theta)\cos(\phi) + \beta\right)} \tag{4.5a}$$

$$AF_2 = \sum_{n=N/2+1}^{N} I_n e^{-j\left(k_o D \sin(\theta)\cos(\phi) - \beta\right)} \tag{4.5b}$$

$$AF_{Total} = AF_1 + AF_2 \tag{4.6}$$

where,

$$D = \frac{d\left(\frac{N}{2}\right)}{2} + \sum_{n=1}^{N/2-1} d(n) \tag{4.7}$$

$$\beta = \frac{B\left(\frac{N}{2}\right)}{2} + \sum_{n=1}^{N/2-1} B(n) \tag{4.8}$$

D and β are the sum of distances and progressive phase from the center of the array corresponding to element *n*. Note that the array factor is calculated knowing that the two

sub-arrays are mirrors to one another. Because of their beam will scan in opposite direction from each other, the sign of β in AF_2 is the negative of AF_1. Using this approach the Matlab program seen in Appendix A roughly estimates the currents along the sub-arrays and calculates the radiation pattern of the linear array. Figure 4.63 presents the currents distribution estimated for the array using the same radiating element throughout the array. Figure 4.64 presents the radiation pattern for such array. It is important to note that in this Matlab program it is assumed that all the energy is radiated in one direction, which in reality that's not the case for the antennas presented in this thesis. The effect of this assumption is perceived in the SLL and the positions of the sidelobes. The difference in SLL for the linear array using the same element in the linear array with load resistors at the ends of each sub-array and the SLL of the radiation pattern presented in figure 4.64 is about 0.08 dB if it is assumed that $Z_{in} = Z_o$, and the progressive phase of the array is 0^o.

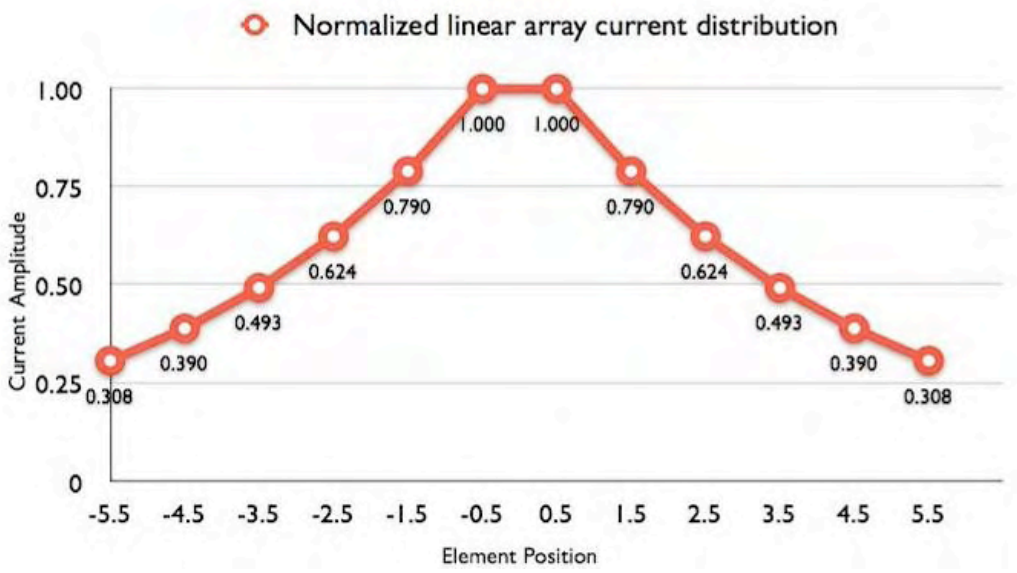

Figure 4.63 Normalized current distribution of linear array estimated.

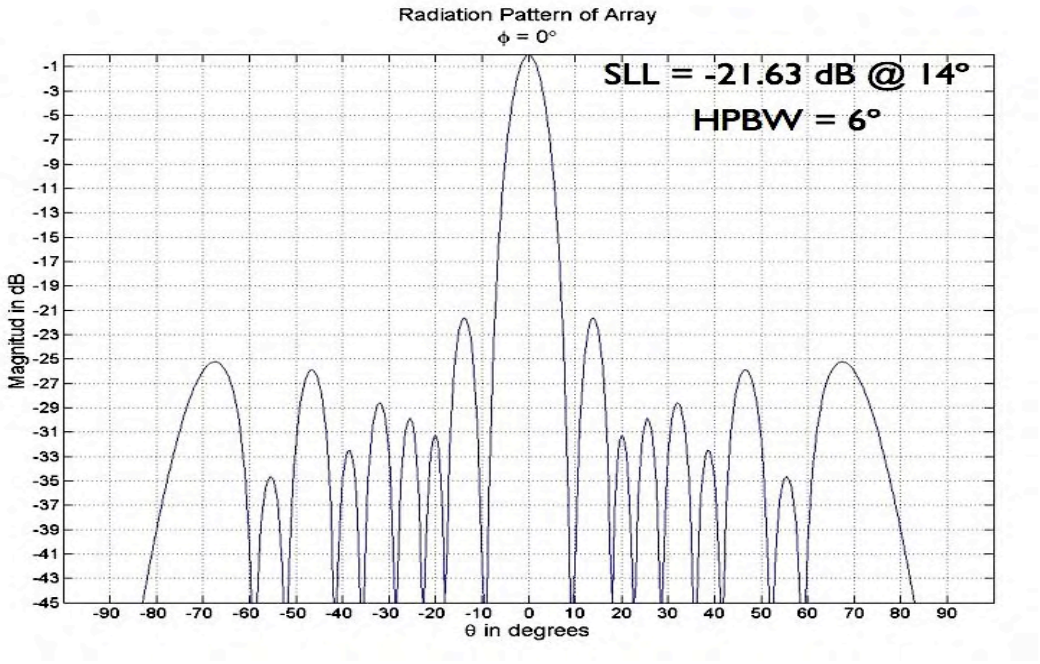

Figure 4.64 Radiation pattern estimated for linear array.

A planar array behavior can be estimated using the data for a single linear array. In this case the planar array is a group of linear array joint together by a corporate feed. Figure 4.65 presents the screen output of the Matlab program. For a corporate feed with Taylor distribution with a progressive phase of 0º the radiation pattern estimated is presented in figure 4.66. Figure 4.66 is a view along the *y*-axis ($\phi = 90^o$) showing the radiation pattern due to the corporate feed distribution. The radiation pattern due to the linear array ($\phi = 0^o$) is the same as the one shown in figure 4.64. Figure 4.67 presents the normalized Taylor current distribution for the corporate feed. This was calculated for SLL of 30 dB for the first 3 sidelobes (ñ = 3). The HPBW calculated is of 6º in both the *E* plane and the *H* plane. Figure 4.68 shows a normalized radiation pattern for the planar array in the visible region, where $U = sin(\theta)\, cos(\phi)$ and $V = sin(\theta)\, sin(\phi)$.

INPUT PARAMETERS
==========

RESONANT FREQUENCY (in GHz) = 9.5000
DIELECTRIC CONSTANT OF THE SUBSTRATE = 1.2000
HEIGHT OF THE SUBSTRATE (in mm) = 1.7500
OUTPUT PARAMETERS
==========

PHYSICAL WIDTH OF PATCH (in mm) = 15.0547
EFFECTIVE LENGH OF PATCH (in mm) = 14.6311
PHYSICAL LENGH OF PATCH (in mm) = 12.4374
DIRECTIVITY OF RECTANGULAR PATCH (dimensionless) = 7.6342
DIRECTIVITY OF RECTANGULAR PATCH (in dB) = 8.8277

RESONANT INPUT RESISTANCE AT LEADING RADIATING EDGE (y=0) Rin0= 208.6896 ohms
Distance vector must be of length N/2.
Enter distance vector [mm]: [28.7 26.5 26.5 26.5 26.5 27.7]
S parameter matrix will be needed for current estimation.
Enter Progressive Phase between elements in degrees: 0

Enter separation between output ports of corporate feed in terms of lambda: .846
Specify nbar
3
Specify desired side lobe level for the first 3 lobes (in dB)
30
Enter Progressive Phase between corporate feed output ports in degrees: 0

HPBW E-PLANE 6.0000 DEGREES
HPBW H-PLANE 6.0000 DEGREES

Figure 4.65 Screen output of Matlab program for planar array pattern estimation.

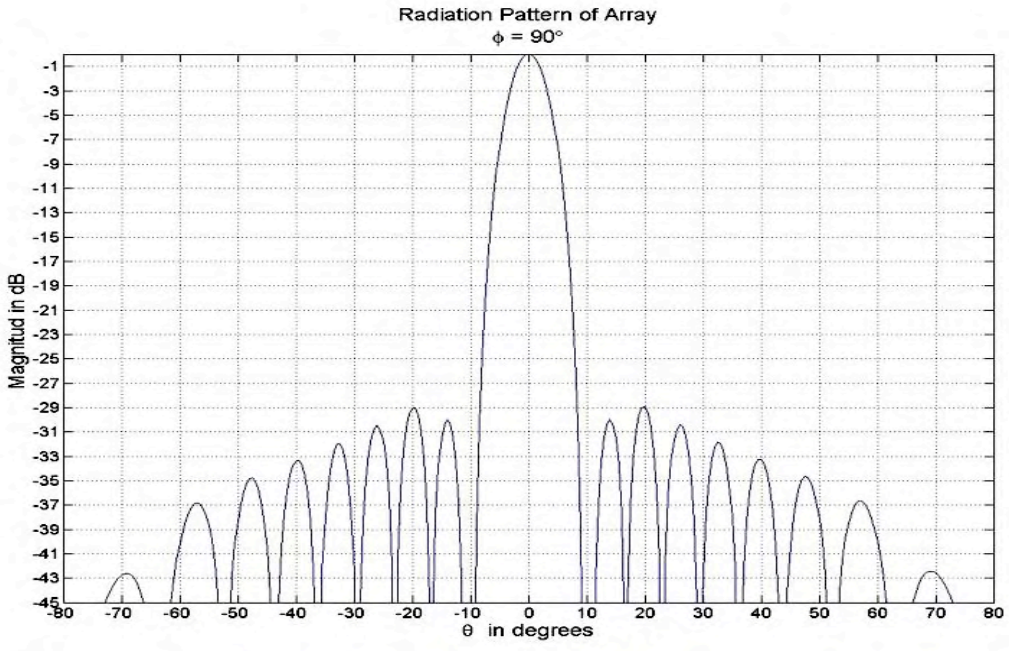

Figure 4.66 Radiation pattern of planar array ($\phi = 90^{o}$).

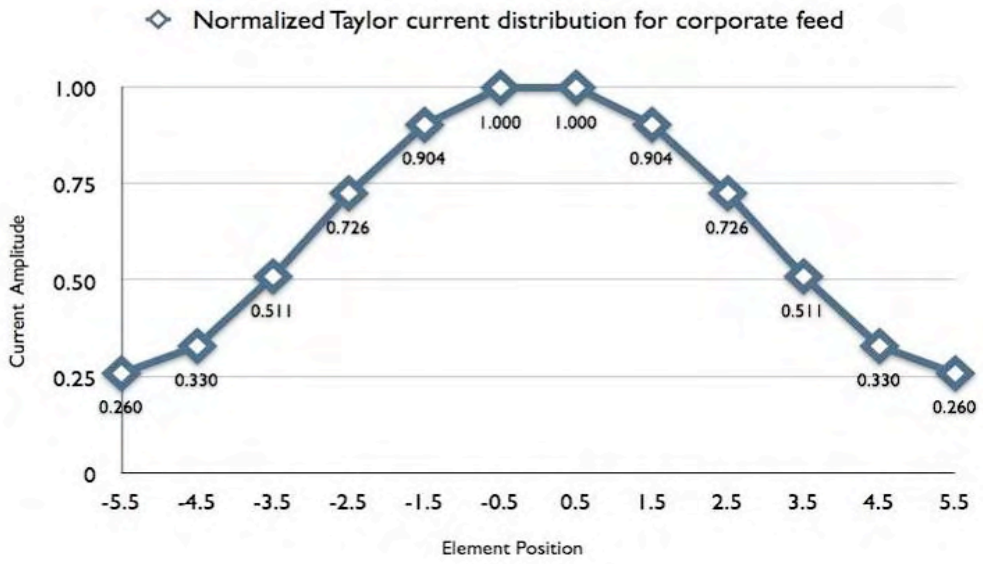

Figure 4.67 Normalized Taylor current distribution estimated for corporate feed.

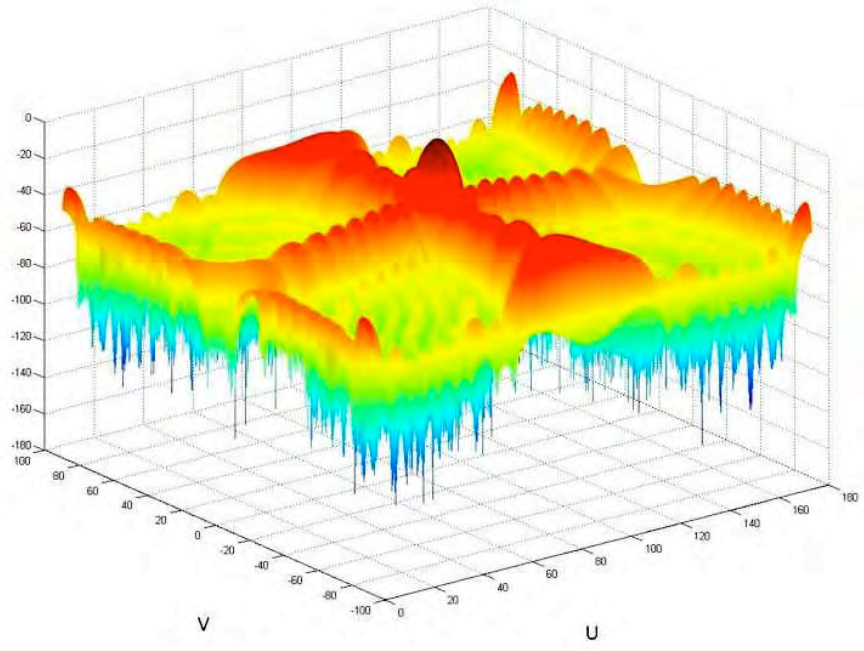

Figure 4.68 Normalized radiation pattern for the planar array in the visible region.

The configuration proposed allows the planar array to move the beam of the array by changing the progressive phase between the output ports of the corporate feed. In

order to scan 15º, which is what it is desired for CASA's radar technology III [31], the output phase of the corporate feed must sweep from 40º to -40º. By doing this the beam of the array at $\phi = 90º$, scans from $\theta = -7.5º$ to $\theta = 7.5º$. In figure 4.69 it can be seen the radiation pattern for the planar array in the plane $\phi = 90º$, for a progressive phase of -40º in the corporate feed, the main beam is position in $\theta = 7.5º$. Also note that at this point the SLL is around 20 dB due to the grating lobe at $\theta = -90º$. Figure 4.70 presents a normalized radiation pattern for the planar array in the visible region.

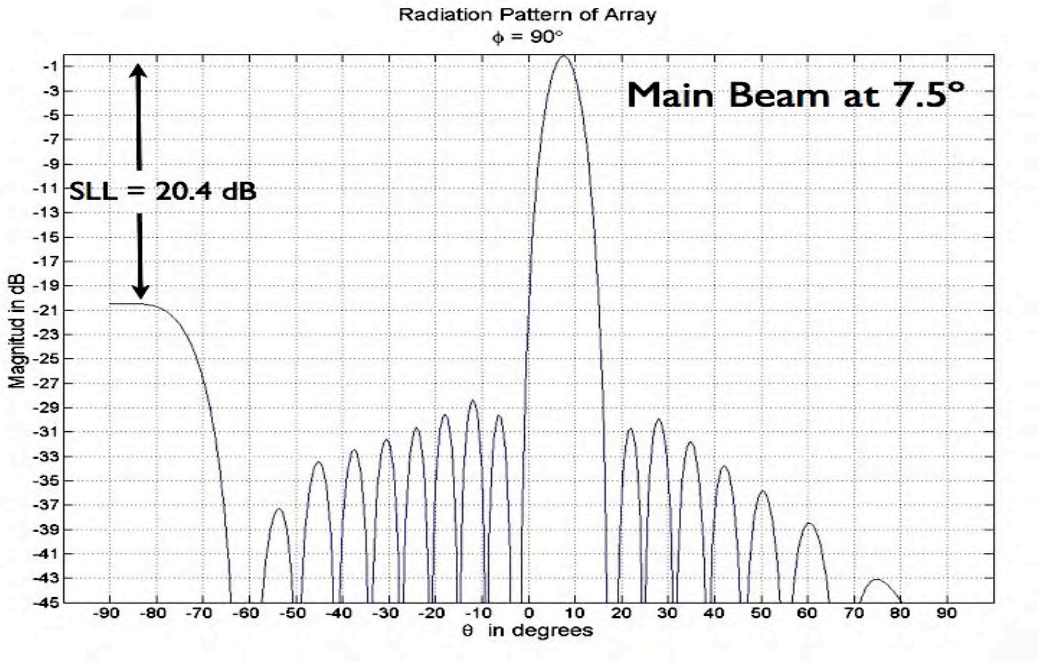

Figure 4.69 Radiation pattern of planar array ($\phi = 90º$) with progressive phase of -40º.

In order to maintain the grating lobe at $\theta = -90º$ 25 dB down relative to the peak of the main beam, the progressive phase between the output ports of the corporate feed should be -30º. Figure 4.71 presents the radiation pattern for the planar array in the plane $\phi = 90º$ for a progressive phase of -30º in the corporate feed. The main beam for this configuration is position in $\theta = 5.5º$.

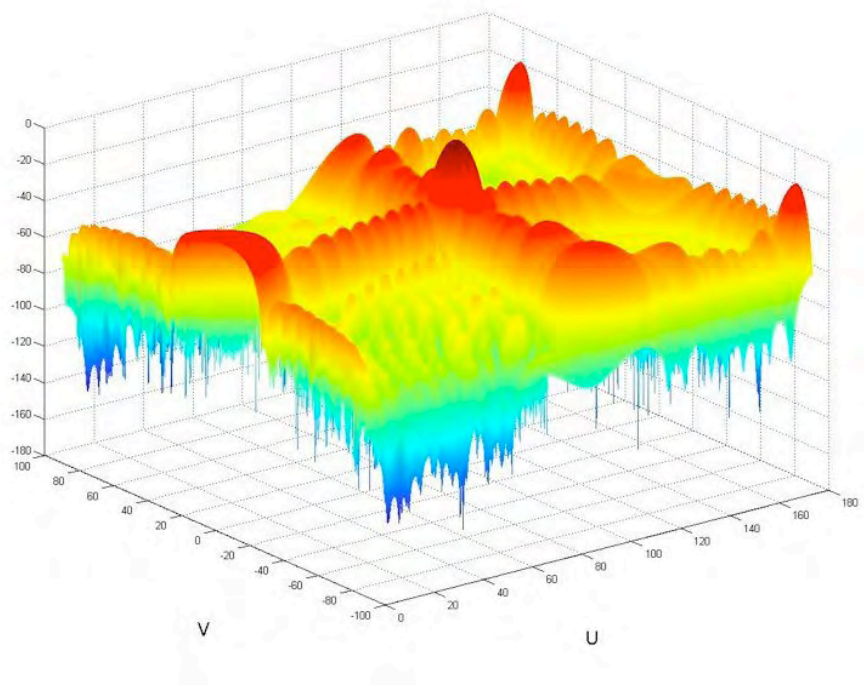

Figure 4.70 Normalized radiation pattern for the planar array in the visible region with main beam at θ = 7.5º.

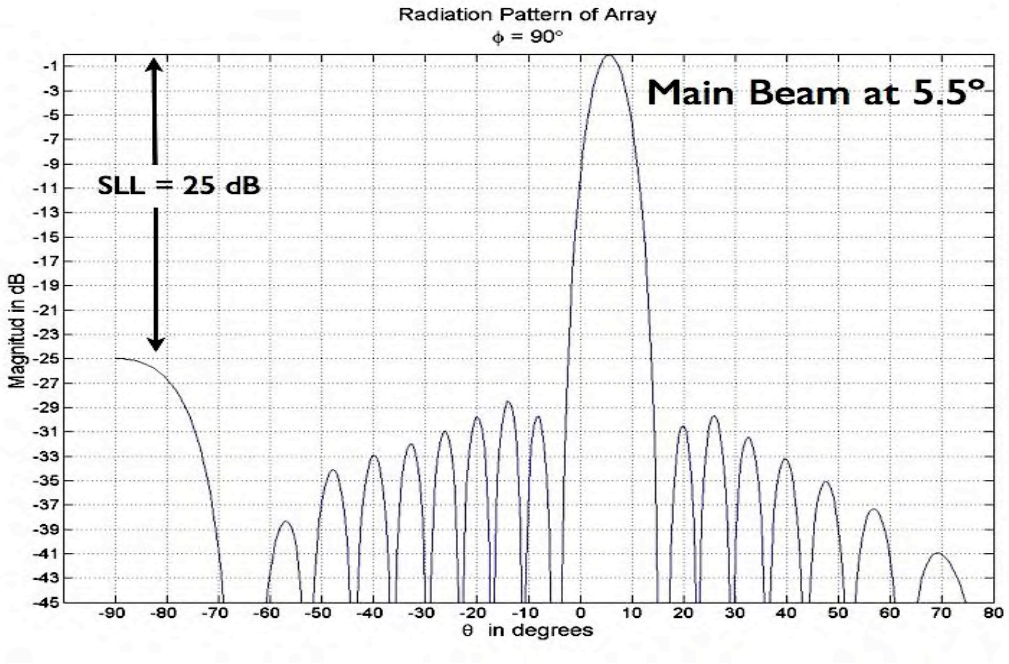

Figure 4.71 Radiation pattern of planar array (ϕ = 90º) with progressive phase of -30º.

5 CONCLUSIONS

A single polarized antenna was designed and simulated to study the effect of coupling and cross-polarization of a planar array. Poor SLL was achieved due to coupling between the corporate feed and the patch antennas. Different structures for dual polarization antennas were considered, but the results of the single polarized array indicated that for good cross-polarization (less than -20 dB) the corporate feed must be in a plane different than the radiating patches. In order to achieve good polarization purity, different techniques were considered, and aperture coupling stood up as a possible solution due to the impressive results presented in [17] and [18].

A series fed-array based in the design in [17], having a center frequency of 9.5 GHz, was proposed. This kind of array could comprise identical elements if mirroring sub-arrays are employed. Selecting an appropriate position of the coupling slot of the radiating element controls the amount of power radiated the element, thus controlling the amount of power delivered to the next one. By using the same element, the ratio between the amount of power at the input and power transmitted to next element must be chosen accordingly in order to achieve the array properties desired (HPBW, SLL, XP, BW, etc), due to the fact that a natural tapering occurs in the array.

A different set of materials than the ones used in [17] were used for the design presented for various reasons, specifically the fact that we could not obtain good results for any of the standard thicknesses available for Honeycomb distributors. The smaller thickness found was 2.75 mm, and in order to achieved coupling between the slots and the patch a thickness of 1.7 mm was needed, which means that different materials with thickness around 1.7 mm and a low dielectric constant, ideally as close to one as possible were considered.

FoamClad, which has a permittivity of 1.2 and a thickness of 1.75 mm was selected for the layer where the cross patch were placed, and RO 3006, with permittivity

of 6.15 and thickness of 0.625mm was selected for the feed line layer. One of the advantages of FoamClad is that it could be bought with copper cladding on one side and adhesive on the other. This feature facilitates the assembly of the antenna and its cost, because only hand pressure is needed to ensure that the foam is glued to the other laminate. On the other hand, FoamClad is not as rigid as Honeycomb, this may cause a problem at the moment of assembling the antenna. Misalignment of the board in the order of microns (um), could have a drastic effect in the results of the antenna. A simple guideline for the design of the radiating elements of the array was presented and the results of its final design configuration for various arrays.

Multiple arrays were presented and discussed, some using resistive loads to dissipate the remaining power at the end of the array, others using a radiating element or patch load. The results presented here indicate that:

- For good SLL = resistive loads
- Good XP = Patch Loads
- Good HPBW = resistive loads

The arrays using PLs behaved differently than the arrays with resistive load because current distribution differs from one another. The fact that the PL had twice the gain that the 4-port radiating element indicates that the last element of the array will have a weight higher than the its previous element.

An array using curved feed lines was also discussed. The behavior of this array was practically the same as the original array when PLs were added at their ends. By making the feed lines curved at their bends improved the return loss, XP and SLL. XP improvements are around 2 dB, but the SLL improved around 7.5 dB for the 12 elements array and around 10.5 dB for the 14 elements array. These arrays with curved feed lines seems like the main beam consumes their adjacent sidelobes, having a triangular shape beam.

For the sake of simplicity it was desired to implement the array using the PLs and avoid the use of chip resistors to dissipate the remaining power at the end of the sub-arrays. The positions of the coupling slots were slightly moved outward from the third element forward. The whole idea was to redistribute the energy in the array. Excellent results were obtained for SLL and XP. The overall effect also included the broadening of the main beam, giving a HPBW of 9º and 8º for the arrays consisting of 12 elements and 14 elements respectively.

In order to test the linear array a simple power divider with 180º phase-offset was used to connect the ports needed for one polarization and 50 Ω loads were used in the remaining ports. This only allows testing one polarization at a time and it is not how the antenna should be used if dual-polarization is desired. For the built arrays, the arrays that had the largest SLL (28 dB) and the largest XP (37 db and 39 dB), did not achieved levels near the simulated results. The HPBW measured was almost the same as the simulated result with variations no larger than 1.2º. The FBR measured was better for all the arrays by almost 9 dB.

The errors in fabrication had a mayor impact on the arrays, opposed to the single elements measured results. The measured results were similar to the simulated results at the design frequency for the single elements. The errors for one element in cascade could have made the XP and SLL to differ from the simulations, and the frequency shift could be caused by the larger size of the patches. In other words, the errors that all this variables represent, the size of the of the circuit board (feed lines and the coupling apertures) that was design and built for 9.5 GHz, and the patch antennas board, that had the size error discussed earlier, could be the cause of the frequency shift and the reason that the XP and SLL was not meet. A way to eliminate these sources of errors could be to fabricate the whole system in one place, or ensuring that all the persons working separately use the same reference points.

In order to use the antenna's full capacity, another circuit must be added to the antenna system. Figure 5.1 presents a simple schematic for the circuit needed.

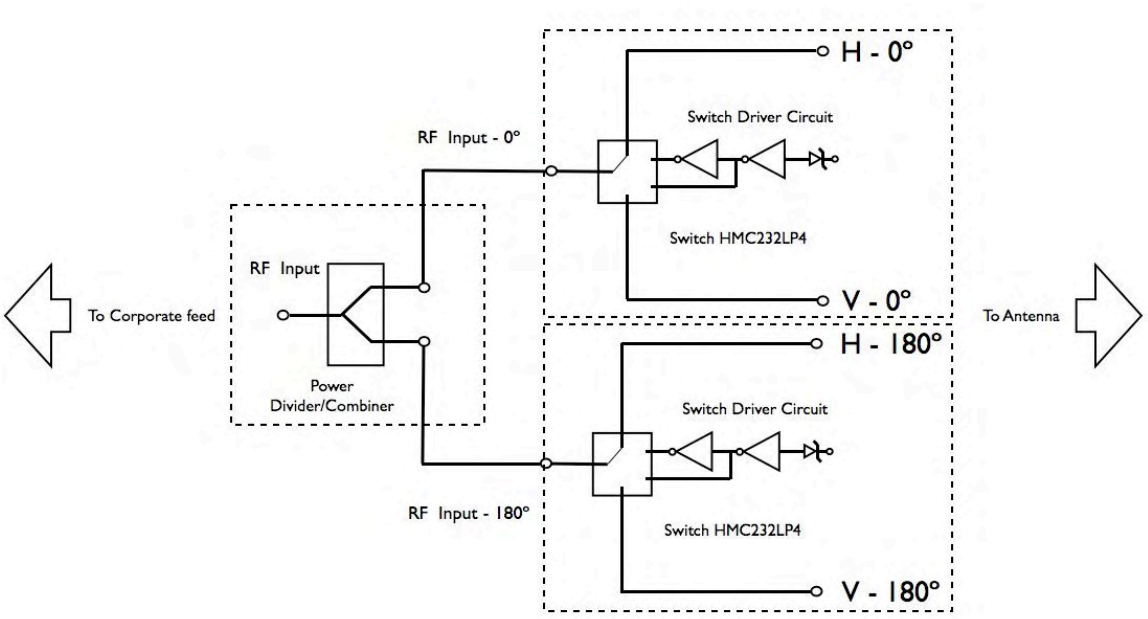

Figure 5.1 Schematic for distributing the RF signal to the array.

This circuit consists of a high isolation non-reflective switch, two inverters and a zener diode for voltage regulation for the switch driver circuit. This circuit, the "switch circuit" controls the polarization that will be fed to the antenna. Figure 5.2 presents a suggested driver circuit for the provided by Hittite for the switch HMC232LP4 used in figure 5.1. Because the antenna has two input ports for each polarization, two switch circuits are needed. A power divider circuit must be used to feed the two switch circuits simultaneously. Figure 5.3 presents a basic layout of how a linear array system should look.

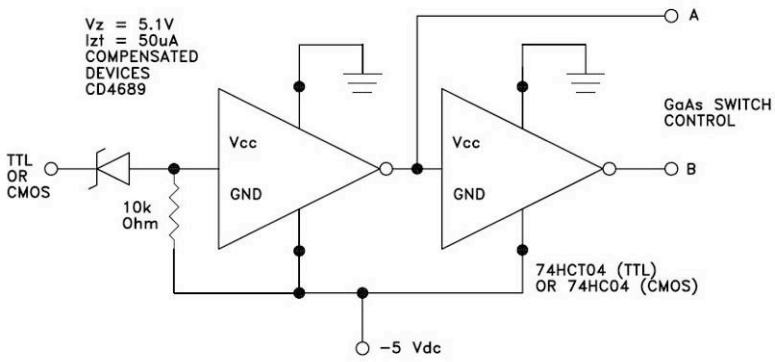

Figure 5.2 Suggested driver circuit provided by Hittite.

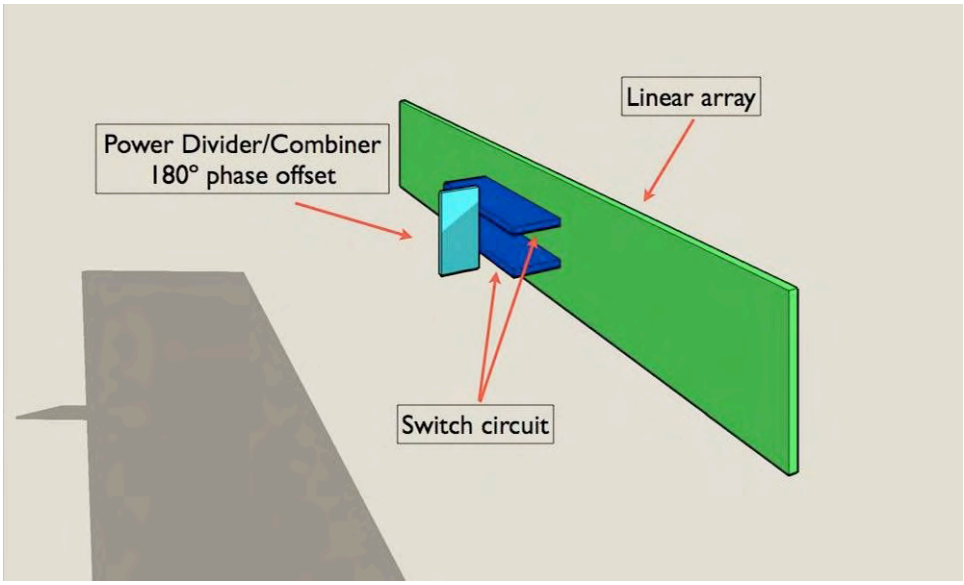

Figure 5.3 3D view of a single linear array system.

The power divider/combiner circuit can be done in one of three ways, a Wilkinson Power divider, a simple power divider or using a chip power splitter. The power divider circuit must provide a phase offset of 180º so that the radiation pattern of the antenna behaves as desired. If is desired to make the antenna system a planar array, a corporate feed must be used. The advantage this provides is that the designer can apply a current distribution to the planar array by using each linear array as a single radiating element. Figure 5.4 presents a 3D view of how a planar array system should look.

This system, which consists of three circuits, the antenna, switch circuit and corporate feed, Should be carefully done in order to avoid increasing losses through out the system and degrade isolation. The switch circuit in this case, if the component suggested is used, should be a coplanar circuit. Because of the assembly suggested there using a coplanar circuit does not present a problem since each circuit are independent from one another. Another feature that this system has is, because the modular approached suggested, this system could be changed to an active or a scanning system as demonstrated in section 4.3. Amplification stages and phase shifters could be added right before entering the antenna system.

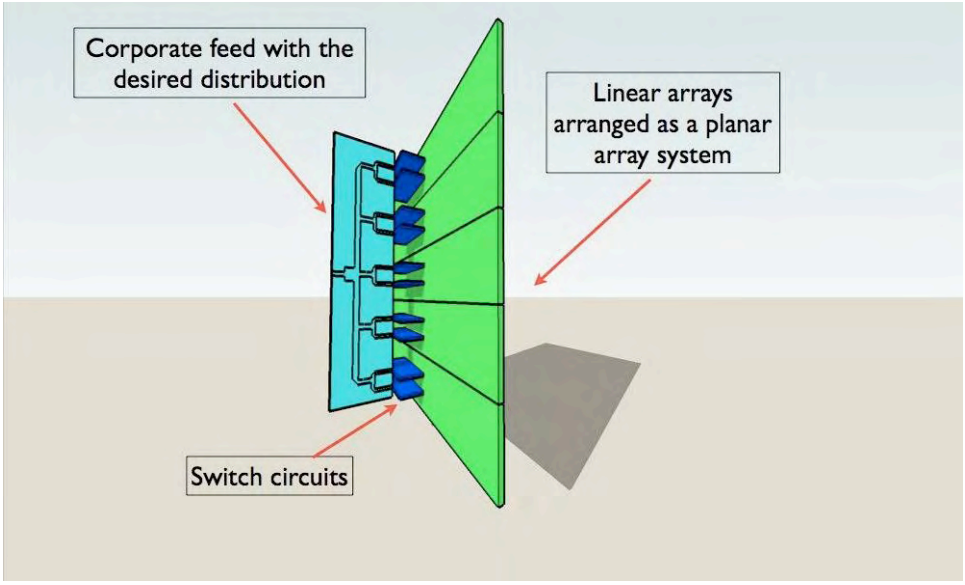

Figure 5.4 3D view of a planar array system.

References

[1] David M. Pozar, “Microstrip Antennas”, IEEE Proceeding, Vol. 80, No. 1, Jan 1992

[2] R.J. Mailloux, J.F. McIlvenna and N.P. Kernweis, “Microstrip Array Technology”, IEEE Trans. Antenna Propg., Vol. AP-29, No. 1, Jan 1981

[3] K.R. Carver and J.W. Mink, “Microstrip Antenna Technology”, IEEE Trans. Antenna Propag., Vol. AP-29, Jan 1981

[4] P.L. Sullivan and D.H. Schaubert, “Analysis of an Aperture Coupled Microstrip Antenna”, IEEE Trans. Antenna Propag., Vol. 8, Jan 1986

[5] D.M. Pozar, “Microstrip antenna aperture-coupled to a microstrip line”, Electron. Lett., vol. 21, no. 2, pp. 49-50, Jan 1985

[6] D.M. Pozar and S.D. Targonski, “Improved coupling for Aperture coupled Microstrip Antennas” Electronics Letters, Vol. 27, No. 113, 20th june 1991

[7] D.M. Pozar, “A Review of Aperture Coupled Microstrip Antennas: History, Operation, Development, and Applications”, UMass, May 1996

[8] T. Metzler, “Microstrip Series Arrays”, IEEE Trans. Antennas Propg., Vol. AP-29, Jan. 1981

[9] Ely Levien , David Treves, Gabi Malamund and Shmuel Shtrikman; “A Study of Microstrip Array Antennas with the Feed Network”, IEEE Trans. Antennas and Propagation, Vol. 37, No. 4, pp 426-434, April 1989

[10] D.M. Pozar and B. Kaufman, “ Design Considerations for Low Sidelobe Microstrip Arrays”, IEEE Trans. Antennas Propag., Vol. 38, Aug. 1990

[11] C. Balanis, *Antenna Theory: Analysis and Design*, 2nd Ed, Wiley, 1997

[12] R. Rodriguez-Solis, Antenna Array Handout, Microstrip Antenna Design Course at UPRM

[13] R.J. Mailloux, *Phased Array Antenna Handbook*, 2nd Ed., Artech House 2005

[14] R.S. Elliot, *Microwave scanning Antennas*, Vol. 2, Academic Press, 1966

[15] G.Biffi Gentili and C. Salvador, “New serially fed Polarization-agile Linear Array of Patches”, IEE Proc. Microw. Antennas Propag., Vol. 145, No. 5, Oct 1998

[16] A.Vallecchi and B. Gentili, “On The Sysntesis of Uniformaly Spaced Dual Polarized Linear Series-fed Microstrip Arrays: A Partially Empirical Approach”, IEEE, 2004

[17] A.Vallecchi and B. Gentili, “Design of a Dual-Polarized Series-fed Microstrip Arrays with Low Losses and High Polarization Purity”, IEEE Trans. Antennas Propg., Vol. 53, No. 5, May 2005

[18] D.M. Pozar and D.H. Schaubert, “Comparison of three series fed microstrip array geometries”, IEEE Antennas Propag. Symp. Dig., 1993

[19] D.J. Lathrop and D.H. Schaubert, “Design of a series-fed, Aperture-coupled Microstrip Arrays”, IEEE, 1991

[20] A. Vallecchi, G.B. Gentili and M. Calamia, “Dual-band, dual Polarization Microstrip Antenna”, IEEE, 2003

[21] D.M. Pozar and S.M. Duffy, “A Dual-Band Circulary Polarized Aperture-Coupled Stacked Microstip Antenna for Global Positioning Satellite”, IEEE Trans. Antennas Propag, Vol. 45, No. 11, Nov. 1997

[22] Y.X. Guo,K.M. Luk and K.F.Lee, “Broadband Dual Polarization Patch element for Cellular-Phone Base Stations”, IEEE Trans. Antenna Propag., Vol. 50, No. 2, Feb 2002

[23] H.M. Chen, Y.F. Lin and T.W. Chiou, “Broadband Circularly Polarized Aperture-Coupled Microstrip Antenna in a 2.45 GHz Wireless communication system”, Microw. Optical Tech. Letters, Vol. 28, No. 2, Jan 2002

[24] G.P. Gunthier, J.P. Raskin, Linda P.B. Katehi and G.M. Rebeiz, “A 94 GHz Aperture-Coupled Micromachined Microstrip Antenna”, IEEE Trans. Antenna Propag., Vol. 47, No. 12, Dic 1999

[25] O. Lafond, M. Himdi and J.P. Daniel, “Thick Slot-coupled Printed Antenna Arrays for a 60 GHz indoors Communication System”, Microw. Optical Tech. Letters, Vol. 28, No. 2, Jan 2001

[26] K.S. Kim, T. Kim and J. Choi, “Dual-Frequency Aperture-Coupled Square Patch Antenna with Double Notches”, Microw. Optical Tech. Letters, Vol. 24, No. 24, March 2000

[27] R.B. Waterhouse, D. Novak, A. Nirmalathas and C. Lin, “Broadband Printed Antennas for Point-to-Point and Point-to-Multipoint Wireless Millimiter-wave Applications”, IEEE, 2000

[28] D. M. Pozar and S. D. Targonski, “ A shared-Aperture Dual-Band Dual-Polarized Microstrip Array”, IEEE Trans. Antenna Propag., Vol. 49, No. 2, Feb 2001

[29] Ansoft Corporation; www.ansoft.com

[30] Implementation of a Phased Array Antenna using Digital Beam Forming; MSEE Thesis, Juan A Torres, University of Puerto Rico Mayagüez Campus, Dec, 2005.

[31] Design and Implementation of a Transceiver and a Microstrip Corporate Feed for a Solid State X-Band Radar; MSEE Thesis, Mauricio Sánchez, University of Puerto Rico Mayagüez Campus, Dec. 2005